AD-A066 201 NAVAL RESEARCH LAB WASHINGTON D C F/G 20/3
ONR-NRL SUPERCONDUCTING MATERIALS SYMPOSIUM. A FORECAST.(U)
JAN 79 T L FRANCAVILLA, D U GUBSER, S A WOLF

UNCLASSIFIED NRL-MR-3906 SBIE-AD-E000 267 NL

1 OF 2
AD
AD66201

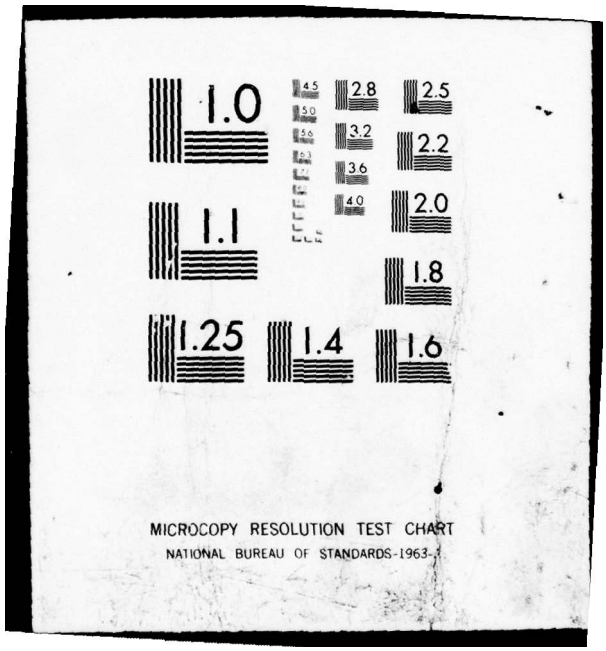
1.0
1.1
1.25
1.4
1.6
1.8
2.0
2.2
2.5
2.8
3.2
3.6
4.0
4.5
5.0
5.6
6.3
MICROCOPY RESOLUTION TEST CHART
NATIONAL BUREAU OF STANDARDS-1963-A

(12) LEVEL III

NRL Memorandum Report 3965

ONR-NRL Superconducting Materials Symposium — A Forecast

Edited by

T.L. FRANAVILLA, D.U. GUBSER AND S.A. WOLF

Material Science and Technology Division

January 10, 1979

NAVAL RESEARCH LABORATORY
Washington, D.C.

SECURITY CLASSIFICATION OF THIS PAGE (When Data Entered)

REPORT DOCUMENTATION PAGE

READ INSTRUCTIONS BEFORE COMPLETING FORM

1. REPORT NUMBER: NRL Memorandum Report 3906
2. GOVT ACCESSION NO.
3. RECIPIENT'S CATALOG NUMBER

4. TITLE (and Subtitle): ONR–NRL SUPERCONDUCTING MATERIALS SYMPOSIUM – A FORECAST
5. TYPE OF REPORT & PERIOD COVERED
6. PERFORMING ORG. REPORT NUMBER

7. AUTHOR(s): Edited by T. L. Francavilla, D. U. Gubser and S. A. Wolf
8. CONTRACT OR GRANT NUMBER(s)

9. PERFORMING ORGANIZATION NAME AND ADDRESS: Naval Research Laboratory, Washington, D.C. 20375
10. PROGRAM ELEMENT, PROJECT, TASK AREA & WORK UNIT NUMBERS: 61153N; NRL Problem P05-04A

11. CONTROLLING OFFICE NAME AND ADDRESS: Office of Naval Research, Arlington, Virginia 22217
12. REPORT DATE: January 10, 1979
13. NUMBER OF PAGES: 156

14. MONITORING AGENCY NAME & ADDRESS (if different from Controlling Office)
15. SECURITY CLASS. (of this report): UNCLASSIFIED
15a. DECLASSIFICATION/DOWNGRADING SCHEDULE

16. DISTRIBUTION STATEMENT (of this Report)

Approved for public release; distribution unlimited.

17. DISTRIBUTION STATEMENT (of the abstract entered in Block 20, if different from Report)

18. SUPPLEMENTARY NOTES

19. KEY WORDS (Continue on reverse side if necessary and identify by block number)

Superconducting materials	CuCL	Ion implantation synthesis (Nb_3Si)
Ternary compounds	Hydrides	Sputtering (Nb_3Si)
Granular superconductors	High Tc thin films	
$(SN)_x$	High pressure synthesis (Nb_3Si)	

20. ABSTRACT (Continue on reverse side if necessary and identify by block number)

This report is a compilation of short summaries of talks presented at a joint ONR-NRL symposium entitled Superconducting Materials - A Forecast, presented 29 September 1978.

DD FORM 1 JAN 73 1473 EDITION OF 1 NOV 65 IS OBSOLETE
S/N 0102-014-6601

SECURITY CLASSIFICATION OF THIS PAGE (When Data Entered)

251 950

CONTENTS

Partial Contents: ORDER OF PAPERS PRESENTED

FOREWORD

Superconducting materials research is entering an exciting period of development. The discovery of many new compounds and structures exhibiting superconductivity has renewed interest in a variety of fundamental phenomena. This conference has gathered together many scientists active in research on superconducting materials in order to review the current status of recent developments and to project their impact on future research. We asked the authors to prepare a brief summary of their presentations which are compiled into this report. While we were unable to include the rich exchanges which occurred during the question and answer periods, the essential points are covered so that the reader will have a better idea of the probable directions this research will take.

The editors gratefully acknowledge the assistance of many individuals who helped to make this symposium a success. In particular Lahni Blohm, Mark Skokan, Roy Carpenter and Dave Jones.

We sincerely appreciate the encouragement, support and advice of R. A. Hein and E. Edelsack during the planning and throughout the course of this Conference.

OPENING REMARKS

A. Berman

I welcome you to the ONR-NRL Superconducting Materials Symposium.

This symposium is indicative of the Navy's long term, continuing interest in the phenomena of superconductivity and its applications. From 1947 to 1950 - approximately 30 years ago - ONR sponsored seven different symposia involving cryogenics. 9 years ago in 1969, NRL hosted 4 smyposia on superconducting materials. The following year an ultar-low temperature conference was held at the Lab and in 1974 there was a workshop on superconducting applications also at NRL. It is clear from these joint ONR-NRL meetings that the Navy recognizes the potential importance of superconductivity and have made a large commitment to its eventual implementation.

For this conference, it is particularly interesting to reflect on the status of superconducting material research as it was in 1969 and as we perceive it today. In the 1969 symposia held at NRL, Professor B. Matthias opened the first meeting with a talk entitled "The Where and How to Obtain High Transition Temperatures". In 1969 there was much speculation about room temperature organic superconductors. Accordingly Professor Matthias, devoted most of his time telling the audience "where and how not to obtain high T_c". Organic superconductors - as predicted by Matthias - have not been found even though much time and effort have been devoted in its quest.

Today we have a similar situation with the speculations of 150 K superconductivity in CuCl. It is appropriate that this meeting in 1978 will address the CuCl speculations much as the 1969 meeting discussed the elusive organic superconductors. Will the verdict be similar or is there more hope that CuCl is a real superconductor? Some light will be shed on this subject later this morning by Dr. Earl F. Skelton of NRL.

In the 1969 symposia, considerable attention was given to new superconducting systems such as superconducting semiconductors, intercalated compounds, amorphous materials and thin films. At todays symposia there will be talks on granular super-

conductors and on metal hydride systems. While we see similarities between the two symposia, the cast of materials has changed.

In the 1969 symposia, - McMillian reviewed his then recently published theory of strong coupling superconductivity - an achievement which won for him and Rowell the Fritz London award at the recent Grenoble meeting this past summer. Over the past years, this theory has been successfully applied to many superconducting materials. Although the basic theory remains much the same as in 1969, many refinements in computational techniques have occurred. Dr. Papaconstantopoulus will enlighten us on some of these theoretical facets in his talk on metal hydride systems.

Finally, I return to the quest for high T_c materials. Here we note very definite differences today from the 1969 symposia. In 1969 investigators were concentrating their search for high T_c materials on bulk binary compounds. One talk at the earlier symposia entitled "Intermetallic Compounds - an Unlimited Source" discussed such binary systems exclusively. Certain well recognized empirical rules, such as the electron per atom ratios or the melting points, and known favorable crystal structures, such as the A15 compounds, served as valuable guides for the experimentalist.

Today, much has changed and the thrust of todays symposia reflects this fact. First, we are now entering the ternary compound era and all standard guides are not applicable to these compounds. Elemental superconductors have a maximum T_c of about 9 K. Binary materials have T_c values to 23 K. Predictions of T_c values for binary materials range up to 30 K in the elusive Nb_3Si compound which will be much discussed this afternoon. What can we expect for the T_c limit in ternary compounds? Perhaps the first speaker will provide this FORECAST.

Another major difference is in fabrication techniques. In 1969 most compounds were prepared with standard metallurgical techniques such as arc or induction melting. Today new fabrication methods are being used to create materials which could not be made before. Nb_3Ge with a T_c of 23 K is prepared only in thin film form using sput-

tering, e-beam evaporation or chemical vapor deposition techniques.

These and other new techniques which will be discussed this afternoon are being used in attempts to make Nb_3Si. Thus we see two main differences in superconducting materials research today vs 1969 1) the active exploration of ternary systems and 2) the use of new fabrication techniques to make selected compounds.

Let me conclude with some reflections on NRL's personal involvement in superconductivity. At NRL, we have supported basic research in the field of cryogenics and superconductivity over the past 30 years. Bob Hein, whom you will hear later today, joined the cryogenics Branch in 1951 and began studying properties of superconducting materials below 1 K. In 1971, a new group - the cryogenic and superconductivity branch - was formed to build and expand on early materials research with efforts given to superconducting applications. Bob was assigned the task of leading this group. The past 7 years - during the existence of the cryogenics and superconductivity branch - have been very successful in these pursuits. On the basic materials research, scientists at NRL have discovered superconductivity in a new crystal structure - the Ti_3P-type, have theoretically calculated the superconducting transition temperature for some 40 elements and compounds and most recently, have been investigating the nature of a unique phase transition in granular superconductors as well as investigated the famous or maybe infamous CuCl. Our fabrication facilities include ultra-high vacuun DC and RF sputterers and apparatus for high pressure synthesis. Characterization facilities include refrigeration systems to 0.01 K, magnetic fields to 20 T and pressures to 500 kbar. In the applied areas, we have developed a new technique for the formation of V_3Ga wire which has the highest measured critical current density values in magnetic fields to 20 T. In small scale applications we have been involved with many demonstartion tests using superconducting SQUID magnetometers as well as carrying on an active research program on the performance of high T_c refractory metal SQUID sensors.

At this symposium, we wish to explore those materials or material properties which are not necessarily related to immediate applications. We are addressing the question "What is the future for superconducting materials research"? Is the future one of acquiring a better understanding or known materials and enhancing their useful properties or might we expect to find new types of materials and fundamental phenomena. We hope this meeting will provide a FORECAST of things to come.

ONR - NRL SUPERCONDUCTING MATERIALS SYMPOSIUM-A FORECAST

September 29, 1978

ONR - NRL SUPERCONDUCTING MATERIALS SYMPOSIUM - A FORECAST

September 29, 1978

PROGRAM

Session A (Chairman - D.U. Gubser)			
9:00	A. BERMAN	Director of Research NRL	OPENING REMARKS
9:10	A.M. GOLDMAN	U. of Minn.	TERNARIES
9:40	P. LINDENFELD	Rutgers	GRANULAR SUPERCONDUCTORS
10:10		COFFEE	
Session B (Chairman - T.L. Francavilla)			
10:30	W. GILL	IBM	$(SN)_x$
11:00	E. SKELTON	NRL	CuCl
11:30	D. PAPACONSTANTOPOULUS	NRL	HYDRIDES
12:00		LUNCH	
Session C (Chairman - S.A. Wolf)			
1:30	R. HAMMOND	Stanford	HIGH T_C THIN FILMS
2:00	D. DEW HUGHES	Brookhaven	HIGH PRESSURE SYNTHESIS (Nb_3Si)
2:30		COFFEE	
Session D (Chairman - E.A. Edelsack)			
3:00	R. ROSE	MIT	ION IMPLANTATION SYNTHESIS (Nb_3Si)
3:30	R. SOMEKH	Cambridge	SPUTTERING (Nb_3Si)
4:00	R.A. HEIN	NSF	DISCUSSION AND CONCLUDING REMARKS
4:30		REFRESHMENTS	

SUPERCONDUCTING MATERIALS SYMPOSIUM

ALPERIN, Dr. Harvey
Naval Surface Weapons Ctr.
White Oak
Silver Sring, MD 20910

BEDARD, Fernand D.
Laboratory for Physical Sciences
4928 College Avenue
College Park, MD 20740

BERLINCOURT, T. Dr.
Office of Naval Research
800 N. Quincy St.
Arlington, VA 22217

BERMAN, Dr. A.
Code 1001
Naval Research Laboratory
Washington, DC 20375

BLOCH, Aaron N.
Dept. of Chemistry
Johns Hopkins University
Charles & 34th Sts.
Baltimore, MD 21218

BOYER, Larry L.
Code 5680
Naval Research Labortory
Washington, DC 20375

BRAVN, Hans
University of California
San Diego, CA 92093

BRYDEN, Wayne A.
Johns Hopkins University
Chemistry Dept.
Charles & 34th St.
Baltimore, MD 21218

BUCELOT, Thomas
Physics Dept.
University of Virginia
Charlottesville, VA 22901

CADIEU, F. J., Prof.
Dept. of Physics
Queens College of CUNY
Flushing, NY 11367

CAMPBELL, A. M.
Dept. of Engineering
Trumpington St.
Cambridge, England

CAPPELLETTI, Ronald
Ohio University
Dept. of Physics
Athens, OH 45701

CARTER, Forrest L., Dr.
Chemistry Division
Code 6132
Naval Research Laboratory
Washington, DC 20375

CARTER, G. C., Dr.
Numerical Data Advisory Board
2101 Constitution Ave.
Washington, DC 20418

CLAPP, M. T.
Massachusetts Institute of Technology
(4-132)
Cambridge, MA 02139

CLASSEN, John
Code 5263
Naval Research Laboratory
Washington, DC 20375

CLARKIN, P. A., Dr.
Office of Naval Research
619 Ballston Center Tower #1
800 N. Quincy St.
Arlington, VA 22217

CLINTON, W. L.
U.S. Department of Energy
Washington, DC 20545

CONNOLLY, John
National Science Foundation
1800 G St., N.W.
Washington, DC 20550

COX, John E.
Code 6320
Naval Research Laboratory
Washington, DC 20375

CUKAUSKAS, E. J.
Code 5263
Naval Research Laboratory
Washington, DC 20375

DALRYMPLE, Bruce
Becton Lab
Yale University
New Haven, CT 06520

DAS, B. N.
Code 6330
Naval Research Laboratory
Washington, DC 20375

DEAVER, Bascom S., Jr.
Department of Physics
University of Virginia
Charlottesville, VA 22901

DELONG, Lance
Department of Physics
University of Virginia
Charlottesville, VA 22901

DEW-HUGHES, D.
Brookhaven National Laboratory
Upton, NY 11973

DURVASULA, L. N.
Molecular Physics/INPST
University of Maryland
College Park, MD 20742

EASTON, D. S.
Metals & Ceramics Division
Oak Ridge National Laboratory
Oak Ridge, TN 37830

EDELSACK, E. A.
ONR 323
Ballston Centre Tower #1
800 N. Quincy St.
Arlington, VA 22217

EHRLICH, A. C., Dr.
Code 6331
Naval Research Laboratory
Washington, DC 20375

EVETTS, Jan E.
Dept. of Metallurgy and Material Science
Cambridge University
Pembroke Street
Cambridge, England

FARISS, Thomas
Physics Department
University of Virginia
Charlottesville, VA 22901

FELDMAN, Joseph
Code 6339
Naval Research Laboratory
Washington, DC 20375

FRADIN, Frank Y.
Materials Science Division
Argonne National Laboratory
Argonne, IL 60439

FRANCAVILLA, Thomas L.
Code 6338
Naval Research Laboratory
Washington, DC 20375

FRIEDBERG, Charles
Physics Department
University of Virginia
Charlottesville, VA 22901

GALFO, Christopher
Physics Dept.
University of Virginia
Charlottesville, VA 22901

Ganguly, A. K.
Code 5253
Naval Research Laboratory
Washington, DC 20375

GARDNER, Carl
DODNSA
Elkridge Landing Road
Linthicum, MD 20810

GHOSH, Arup K.
Brookhaven National Laboratory
Upton, NY 11973

GILL, W.
IBM Research Laboratory
5600 Cottle Road
San Jose, CA 95193

GOLDMAN, A. M.
University of Minnesota
School of Physics
Minneapolis, MN 55455

GUBSER, D. U.
Code 6338
Naval Research Laboratory
Washington, DC 20375

HALBRITTER, J.
Kernforschungszentrum
75 Karlsruhe, Germany

HALL, J. T.
National Bureau of Standards
Gaithersburg, MD 20234

HAMMOND, R.
Stanford University
Hansen Physics Laboratory
Stanford, CA 94305

HAWLEY, Marilyn
Johns Hopkins University
Chemistry Department
Charles & 34th St.
Baltimore, MD 21218

HEIDEN, C., Prof.
Institut Fur Angewandte Physik
der Justus - Liebig - Universitat Giessen
Heinrich Buff-Ring 16
D-6300 Giessen, Germany

HEIN, Robert A.
National Science Foundation
1800 G. St., N.W.
Washington, DC 20550

HOLDEMAN, Lou
National Bureau of Standards
Gaithersburg, MD 20234

HOLLENHORST, James
Stanford University
Hansen Physics Laboratory
Stanford, CA 94305

HOWE, David G.
Code 6320
Naval Research Laboratory
Washington, DC 20375

HUDAK, John J.
DODNSA
Elkridge Landing Road
Linthicum, MD 20810

HYUN, D. J.
Physics Department
University of Virginia
Charlottesville, VA 22901

KAHN, L. M.
University of Virginia
Charlottesville, VA 22901

KELLER, W. E.
Los Alamos Scientific Laboratory
P. O. Box 1663
Los Alamos, NM 87545

KELIN, Barry
Code 5680
Naval Research Laboratory
Washington, DC 20375

KOON, N. C.
Code 6332
Naval Research Laboratory
Washington, DC 20375

LEIBOWITZ, Jack R.
Dept. of Physics
Catholic University
Washington, DC 20064

LINDENFELD, P.
Physics Dept.
Rutgers University
New Brunswick, NJ 08903

LUO, H. L.
University of California
San Diego, CA 92093

LUTZ, Harry
Bldg. 480
Brookhaven National Laboratory
Upton, NYU 11973

LYNN, J. W., Dr.
Dept. of Physics
University of Maryland
College Park, MD 20742

MELNGAELIS, I.
Massachusetts Institute of Technology
Lincoln Labs
Cambridge, MA 02139

MERKLE, Larry, Dr.
Dept. of Chemical & Nuclear Engineering
University of Maryland
College Park, MD 20742

MUESSNER, R. A.
Code 6320
Naval Research Laboratory
Washington, DC 20375

MICHELSON, Peter
Stanford University
Hansen Physics Laboratory
Stanford, CA 94305

MOEHLECKE, Sergio
Brookhaven National Laboratory
Upton, NY 11973

MOULTON, William G.
Department of Physics
Florida State University
Tallahassee, FL 32306

NAGEL, David
Code 6682
Naval Research Laboratory
Washington, DC 20375

NISENOFF, M.
Code 5263
Naval Research Laboratory
Washington, DC 20375

NGAI, K. L.
Code 5277
Naval Research Laboratory
Washington, DC 20375

PAPACONSTANTOPOLUS, D.
Code 5680
Naval Research Laboratory
Washington, DC 20375

PAIK, Ho Jung
Dept. of Physics & Astronomy
University of Maryland
College Park, MD 20742

PARMENTER, Bob
University of Salerno,
Italy

PETERS, Robert
Physics Dept.
Catholic University
Washington, DC 20064

PICKART, Stanley J.
Condensed Matter Section
Division of Materials Research
National Science Foundation
Washington, DC 20550

PIERMARINI, G.T.
National Bureau of Standards
Gaithersberg, MD 20234

POTEMBER, Richard S.
Johns Hopkins University
Applied Physics Laboratory
Johns Hopkins Rd.
Laurel, MD 20810

PRASK, Henry J.
National Bureau of Standards
Bldg 235
Washington, DC 20234

PROBER, Dr. Daniel
Dept. of Engineering & Applied Science
Becton Center - Yale University
New Haven, CN 06520

ROBINSON, Arthur L.
Science Magazine
1515 Massachusetts Avenue, NW
Washington, DC 20005

ROTH, L.B.
Hughes Research Labs
3011 Malibu Cny.
Malibu, CA 90265

RUVALDS, J.
University of Virginia
Charlottesville, VA 22901

SAMARAS, D.G.
AFOSR
317 Architect Bldg.
1400 Wilson Blvd.
Arlington, VA 22209

SAUER, Prof. E.
Institut Fur Angewanite Physik
der Justus - Liebig-Universitat Giessen
Heinrich Buff-Ring 16
D-6300 Giessen, Germany

SCHINDLER, Dr. A.I.
Code 6000
Naval Research Laboratory
Washington, DC 20375

SCHRIEMPF, Thomas
Code 6330
Naval Research Laboratory
Washington, DC 20375

SEKULA, S.T.
Oak Ridge National Lab
P.O. Box X
Oak Ridge, TN 37830

SIEWICK, Joseph T.
Physics Department
Georgetown University
Washington, DC 20057

SKOKAN, Mark R.
Code 5263
Naval Research Laboratory
Washington, DC 20375

SOUKOULIS, C.
University of Virginia
Charlottesville, VA 22901

SOULEN, ROBERT
National Bureau of Standards
Gaithersburg, MD 20234

SPAIN, Dr. Ian L.
Chemical & Nuclear Engr. Dept.
University of Maryland
College Park, MD 20742

SPENCER, Cary
AIRCO Superconductor Manufacturing Group
100 Mountain Avenue
Murray Hill, NJ 07974

STEINER, Richard
Physics Department
University of Virginia
Charlottsville, VA 22901

STOKES, James P.
Johns Hopkins University
Chemistry Dept.
Charles & 34th St.,
Baltimore, MD 21218

STRONGIN, Myron
Brookhaven National Laboratory
Upton, NY 11973

SWEEDLER, A
California State University
Dept. of Physics
Fullerton, CA 92634

TOTH, Louis
University of Minnesota
School of Physics
Minneapolis, MN 55455

VAUGHAN, W.H.
Code 8438
Naval Research Laboratory
Washington, DC 20375

WANG, Frederick E.
Naval LSurface Weapons Center
White Oak Laboratory
Silver Spring, MD 20910

WANG, Li Kong
Physics Dept.
University of Virginia
Charlottesville, VA 22901

WARREN, Dr. John L.
U.S. Dept. of Energy
Mail Stop J-309
Washington, DC 20545

WEBB, Alan W.
Code 6339
Naval Research Laboratory
Washington, DC 20375

WEBB, George W.
Univ. of California-San Diego
B019 La Jolla, CA 92093

WEINMAN, Dr. Leslie S.
Code 6313
Naval Research Laboratory
Washington, DC 20375

WELKER, Nancy K.
Laboratory for Physical Sciences
4928 College Avenue
College Park, MD 20740

WIESMANN, Bud
Brookhaven National Lab
Upton, NY 11973

WOLF, S.A.
Code 6338
Naval Research Laboratory
Washington, DC 20375

WOLF, S.M.
U.S. Dept. of Energy
Washington, DC 20545

YODER, Max
Office of Naval Research
323 Ballston Center Tower #1
800 N. Quincy St.
Arlington, VA 22217

YOUNG, Charles
Code 5253
Naval Research Laboratory
Washington, DC 20375

YU, Shu-Cheng
University of Maryland
College Park, MD 20782

Ternary Compounds

A. M. Goldman
School of Physics and Astronomy
University of Minnesota
Minneapolis, Minn. 55455

Two classes of ternary compounds have emerged in the last few years which exhibit promising superconducting properties. These are the ternary molybdenum sulfides and selenides, which are known as the Chevrel phase compounds, and the rare earth rhodium borides.

The Chevrel phase compounds have the general formula $M_xMo_6S_8$ where M stands for a large number of metals. The quantity x varies from 1 to 4 depending upon M, and of course S can be replaced by Se. These compounds have a rhombohedral crystal structure. They have high T_c's, exceptionally large values of H_{c2}, and in some instances exhibit either re-entrant superconductivity or the coexistence with superconductivity of long-range antiferromagnetic order. Thus the Chevrel phase compounds are of great technical and scientific importance.

The rare earth rhodium borides have the general formula $(RE)Rh_4B_4$ where RE = Y, Er, Tm and Lu are superconducting. These compounds have a tetragonal lattice and are not as technically interesting as the Chevrel phase compounds as their T_c's are only moderately high and H_{c2}'s are low. On the other hand, re-entrant superconductivity has been observed in $ErRh_4B_4$ and there is a possibility that superconductivity and ferromagnetism coexist over some limited range of temperature in this compound. Thus $ErRh_4B_4$ is of extremely high scientific interest.

Note: Manuscript submitted November 21, 1978.

The high upper critical fields of the Chevrel phases are a consequence of the materials being dirty Type-II superconductors with paramagnetic limiting being reduced by spin-orbit scattering of the two states forming a Cooper pair. A most remarkable feature of these compounds is the fact that the additions of substantial concentrations of rare earth ions do not reduce T_c and H_{c2} as in binary and psuedobinary compounds. The addition of such ions may even raise H_{c2}. The latter is a consequence of the rare earth ions polarizing s-electrons in a manner that the internal field at the Mo sites cancels the external field. The d-electrons from the Mo sites are responsible for the superconductivity.

The high critical fields make the Chevrel phases technically very important. A serious question is whether ductile material with high critical current density and large H_{c2} can be made. The production of thin films on flexible substrates is one way to obtain a ductile material. Possibly such films can be made either by sputtering, or by multiple source vapor deposition onto heated substrates.

Better samples of all materials are needed in all experiments in order to understand in detail the delicate effects which may be involved in the coexistence of superconductivity and magnetic order.

Details of the mechanism for superconductivity in these compounds would be revealed if $\alpha^2F(\omega)$ could be determined by quantitative electron tunneling. Unfortunately such experiments are made difficult by the short coherence lengths of the materials and by the fact that high quality films or bulk materials are not yet available. Point contact experiments may produce misleading results because of the extreme pressure sensitivity of the superconducting properties of these compounds.

An important area of work which should not be overlooked is the search for additional ternary systems with unusual properties. Such work has intrinsic scientific merit.

The possible coexistence of ferromagnetism and superconductivity in $ErRh_4B_4$ which is a suggested interpretation of detailed heat capacity experiments is extremely important. The statistical mechanics of systems of coupled order parameters already has a substantial literature. The coexistence problem in the specific instance of superconductivity and ferromagnetism has many important aspects. First, is re-entrant superconducting behavior general? Secondly, is the magnetic ordering temperature affected by the fact that the material is superconducting? There is a thermal hysteresis associated with the lower transition in $ErRh_4B_4$ which may possibly be explained by a difference in the ordering temperatures between the normal and superconducting states.

The character of the coexistence is also of interest. Long ago Suhl and Anderson predicted that ferromagnetic spin alignment in superconductors would occur in small domains rather than in a homogeneous fashion. There may be evidence of what they called "cryptoferromagnetism" in some recent neutron scattering work. On the other hand, a Landau-Ginzburg model of the coupled order parameters suggests that the coupled magnetic-superconducting system may consist of alternating magnetic and superconducting domains of a characteristic size the order of the geometric mean of the superconducting and magnetic coherence lengths. A combination of neutron scattering experiments and Josephson tunneling experiments, which can measure the spatial variation of the superconducting order parameter, may be needed to unravel this problem and distinguish between the two possibilities. It is clear that if there is coexistence the dynamics as well as the statistical mechanics of the coupled order parameters will be an incredibly rich field with many unexpected phenomena.

The author would like to thank M. B. Maple, F. Fradin, W. Thomlinson, C. Varma and M. Ishikawa for their assistance in preparing this lecture.

Ternary Compounds

A. Introduction

B. High Upper Critical Fields

C. Lattice-Properties, Superconductivity

D. Magnetic Interactions - Effects on T_c and H_{c2}.

E. Superconductivity and Long-Range Magnetic Order

Antiferromagnetism

Ferromagnetism - reentrant superconductivity

F. Future Trends

General References

1. Ø. Fischer , Appl. Phys. 16, 1 (1978).

2. M. B. Maple, Superconductivity and Magnetic Order, to be published in the Proceedings of the 15th International Conference on Low Temperature Physics, Grenoble, France, August 23-29, 1978.

3. M. Ishikawa, Ø. Fischer and J. Muller, Long Range Order in the Superconducting State of Heavy Rare Earth Molybdenum Sulfides and Their Psuedoternary Compounds, to be published in the Proceedings of the 15th International Conference on Low Temperature Physics.

4. M. B. Maple, in The Rare Earths in Modern Science and Technology ed. by Gregory J. McCarthy and J. J. Rhyne, Plenum Publishing Corporation (New York, 1978), p 381.

Ternary Compounds with Promising Superconducting Properties

A. Introduction

1. Ternary molybdenum sulfides and selenides-chevrel phase compounds.

   General formula: $M_xMo_6S_8$ where M stands for a large number of metals -- e.g., Sn, Dy, Eu, Er, etc. and x varies from 1 to 4 depending on M.

   Rhombohedral crystal structure with the angle close to 90^o

   High T_c

   Exceptionally large H_{c2} values

   Coexistence of long-range magnetic order and superconductivity

   Re-entrant superconductivity in $Ho_{1.2}Mo_6S_8$

2. $RERh_4B_4$, where RE = Y, Er, Tm, and Lu

   Tetragonal lattice

   Moderately high T_c

   Low H_{c2}

   Re-entrant superconductivity in $ErRh_4B_4$ (T_{c1} = 8.5 K, T_{c2} = 0.95 K)

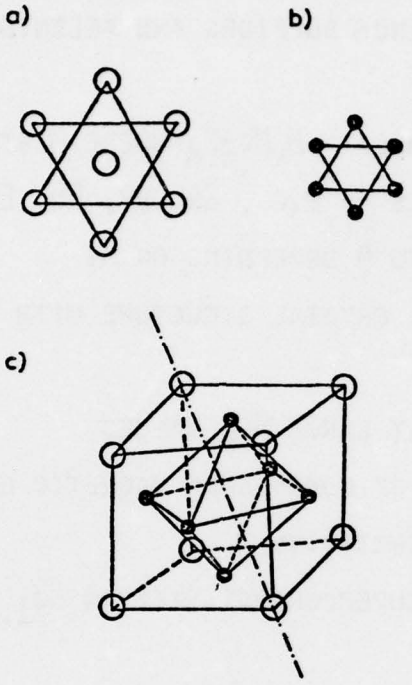

The unit Mo_6X_8 in the compounds $M_xMo_6S_8$. (a) Projection of the X positions along the ternary axis (b) Projection of the Mo positions along the ternary axis. (c) View of a Mo_6X_8 unit. The dot-dashed line indicates the ternary axis

R. CHEVREL: THESIS, UNIVERSITY OF RENNES (1974)

STRUCTURE OF YRh_4B_4. Rh_4 TETRAHEDRA ARE LOCATED AT THE ORIGIN AND CENTER OF THE UNIT CELL. ONLY ONE OF THE FOUR B_2 PAIRS IS SHOWN.

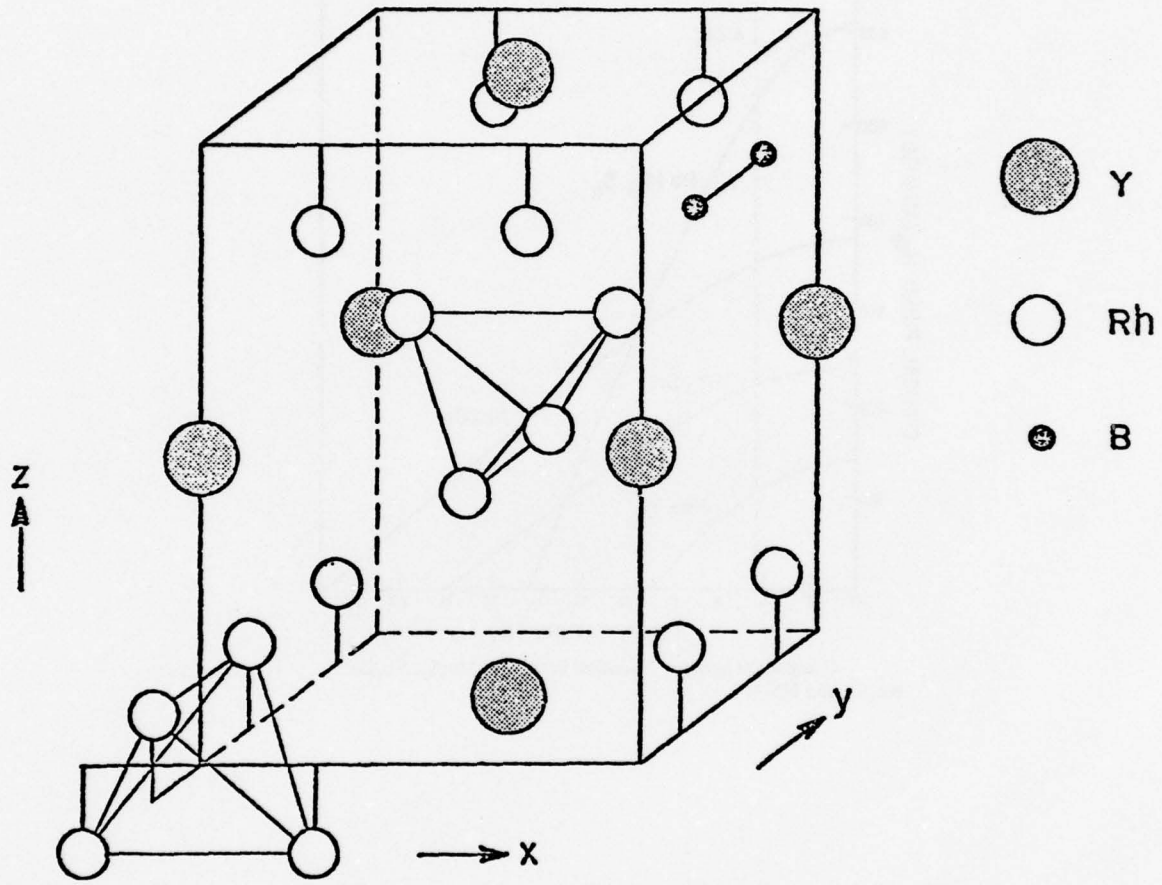

J. M. VANDENBERG AND B. T. MATTHIAS, PROC. NAT. ACAD. SCI. USA 74, 1336 (1977).

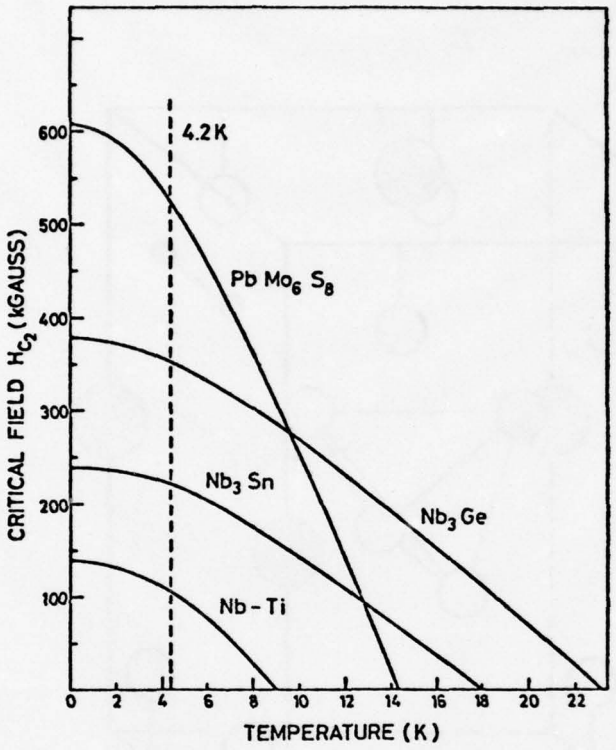

Comparison between the critical fields of $PbMo_6S_8$, Nb_3Ge, Nb_3Sn, and Nb–Ti

Ø. FISCHER, APPLIED PHYS. 16, 1 (1978)

B. High Upper Critical Fields of the Chevrel Phases

External fields interact with electrons in two ways:

1. with orbital motion through $e\vec{p}\cdot\vec{A}/m$
2. with spin through $g\mu_B\vec{H}\cdot\vec{\sigma}$

The latter limits H_{c2} to 18.4 T_c (kG) by the so-called Clogston-Chandresekhar mechanism.

For Chevrel phases $H_{c2} = \dfrac{\phi_0}{2\pi\xi^2(T)}$

consistent with $\xi(0)$ of a dirty, Type-II superconductor.
But $H_{c2}(0) > 18.4\ T_c$ $(2.5 \times H_p(0)$

Explanation is in strong spin-orbit scattering

$$\lambda_{so} = 2\hbar/2\pi\tau_{so}k_B T_c$$

when $\lambda_{so} >> 1$; $H_p = 1.33\sqrt{\lambda_{so}}\ H_{p0}$

C. Lattice Properties - Superconductivity

1. Specific heat measurements and inelastic neutron scattering in Chevrel phases imply low frequency modes compatible with molecular crystal model with Mo_6X_8 "molecules".

2. Mössbauer studies of $SnMo_6Se_8$ (T_c = 6.5 K) and $SnMo_6S_8$ (T_c = 13 K) are consistent with Sn-phonons softening in the S-compound (high-T_c) and not in Se (low-T_c). Other evidence not so clear and it is not certain as to details of the connection T_c and the phonon spectrum. $\alpha^2F(\omega)$ studies are required.

3. Low temperature lattice phase transitions occur in Chevrel phases.

4. T_c is not correlated with M in MMo_6S_8. The relevant conduction electrons are 4d electrons of Mo. M influences T_c indirectly.

5. Large pressure dependence of T_c.

6. Isotope effect in Chevrel phase Mo_6Se_8. Either Mo or Se replacement has same effect. T_c seems to be determined by Mo_6Se_8 clusters.

D. Magnetic Interactions in Chevrel Phases - Effects on T_c and H_{c2}

1. In binary psuedobinaries, T_c and H_{c2} are lowered by magnetic impurities.

2. Chevrel phases are unusual, e.g., $Sn_{1-x}\,Eu_x\,Mo_6\,Se_8$. Eu^{2+} ions have $\mu = 7\,\mu_B$, but T_c is unchanged up to $x = 0.5$. Also H_{c2} increases from 275 kG ($x = 0$) up to 390 kG ($x = 0.4$).

T_c is not changed because it is determined by d-electrons of Mo which are shielded from the pair-breaking of Eu^{2+} spins by a sulfur cage - small J_{DF} coupling.

Eu^{2+} spins polarize s-electrons parallel to $H_{EXTERNAL}$ at Eu site, but antiparallel at Mo site. Thus the internal field can cancel the external field!

This picture was determined using Mossbauer (^{151}Eu) and NMR (^{95}Mo).

F. Y. Fradin, G. K. Shenoy, B. D. Dunlap, A. T. Aldred and C. W. Kimball, Phys. Rev. Lett. 38, 719 (1977).

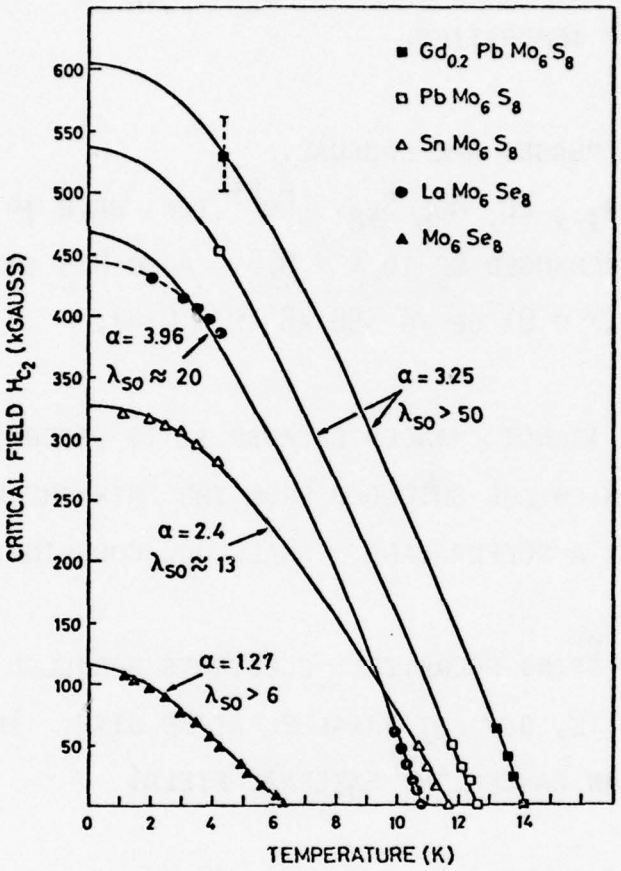

Upper critical field H_{c_2} versus temperature for several $M_xMo_6X_8$ compounds

Ø. FISCHER, H. JONES, G. BONGI, M. SARGENT, R. CHEVREL: J. PHYS. CZ, L450 (1974).

E. Superconductivity and Long-Range Magnetic Order in $RE_xA_xB_z$

PERIODIC DISTRIBUTION OF RE IONS WITH MOMENTS FROM PARTIALLY FILLED 4F SHELLS

RARE EARTHS INTERACT VIA RKKY MECHANISM

MAGNETIC ORDER IS LONG-RANGE

SHARP ORDERING TEMPERATURE T_M

λ ANOMALY IN C(T) AT T_M

CUSP IN $\chi(T)$ AT T_M

THE EXCHANGE INTERACTION IS WEAK

$|J| \sim 0.01\,eV$

$$\mathcal{H}_{int} = -2\mathcal{J}(g_J - 1)\,\underset{\sim}{J}\cdot\underset{\sim}{S}$$

SUPERCONDUCTIVITY IS RETAINED EVEN IN THE PRESENCE OF LARGE CONCENTRATIONS OF RARE EARTHS, $T_M \sim T_c$.

Important Results

1. Development of long-range magnetic order in the superconducting state.

2. Certain coexistence of antiferromagnetism and superconductivity.

3. Possibility of ferromagnetic order destroying superconductivity at a second transition temperature $T_{c2} \sim T_M$

4. Possibility of coexistence of superconductivity and ferromagnetic order at T_{c2}.

   specific heat anomaly at T_{c2}

   neutron scattering

These systems are not dilute substitutional alloy systems. Order is long-range, not cluster or spin-glass like.

Coexistence of Superconductivity and Long-Range Antiferromagnetic Order

$RE_xMo_6S_8$ or $RE_xMo_6Se_8$ ($x = 1.0$ or 1.2)

1. All superconducting except Ce and Eu which are normal down to 50 mK because of Kondo effect.

2. Variation of T_c with RE can be accounted for by electron depairing via an exchange interaction between conduction electrons and rare earth moment.

3. $|J| \sim 0.01$ eV
   $T_M \sim n B N(E_F) J^2 (g_J - 1)^2 J(J+1)$
   obeyed qualitatively.

4. $RE_{1.2}Mo_6S_8$; RE = Gd, Tb, Dy and Er
   feature in $H_{c2}(T)$ at T_M

5. $RE_1Mo_6Se_8$; RE = Gd, Tb, Er
   λ-anomaly in $C(T)$ at T_M
   cusp in $\chi(T)$ at T_M.

6. Neutron scattering
   $ErMo_6Se_8$ (powders)
   $Dy_{1.2}Mo_6S_8$

T_M, T_c, - T_G, DEGENNES FACTOR G, $G^{2/3}$ FOR $REMo_6S_8$ AS A FUNCTION OF RE.

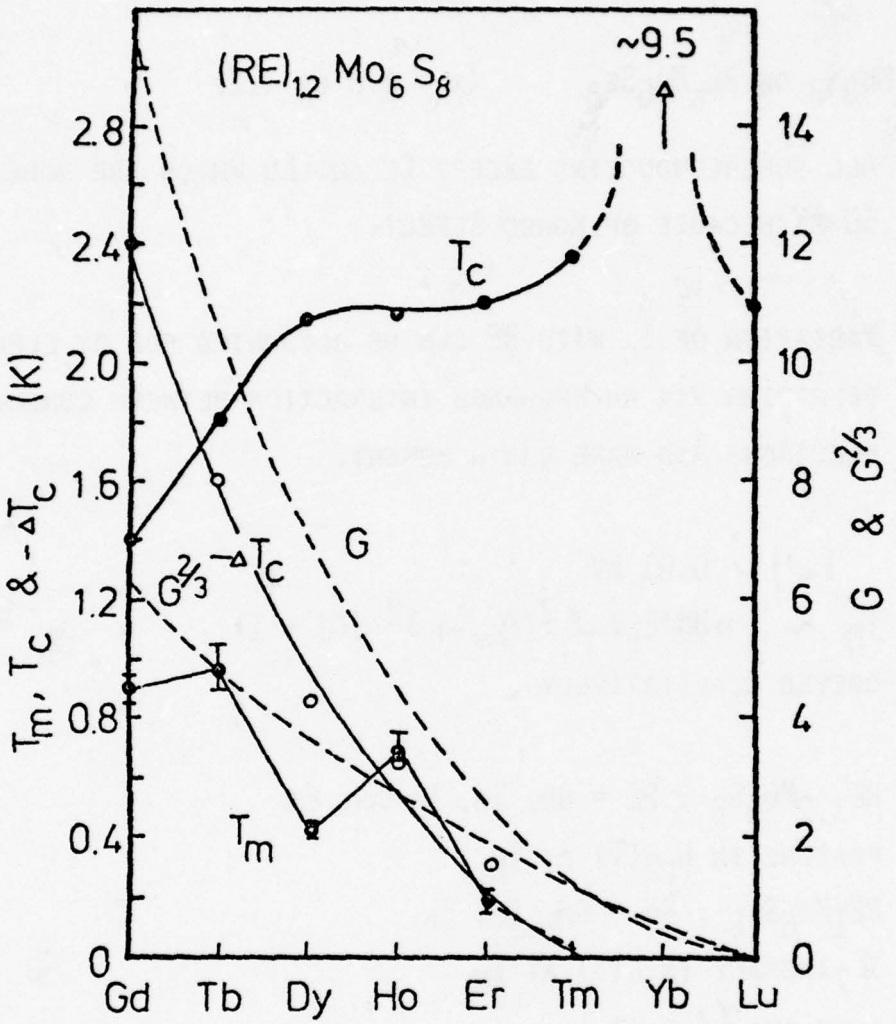

$$G = (g-1)^2 J(J+1)$$

$$k_B T_m = \frac{c N \chi_0}{12 \mu_B^2} G \Gamma^2$$

M. ISHIKAWA AND J. MULLER, SOLID STATE COMMUN. (TO BE PUBLISHED).

RESISTANCE VS. T.

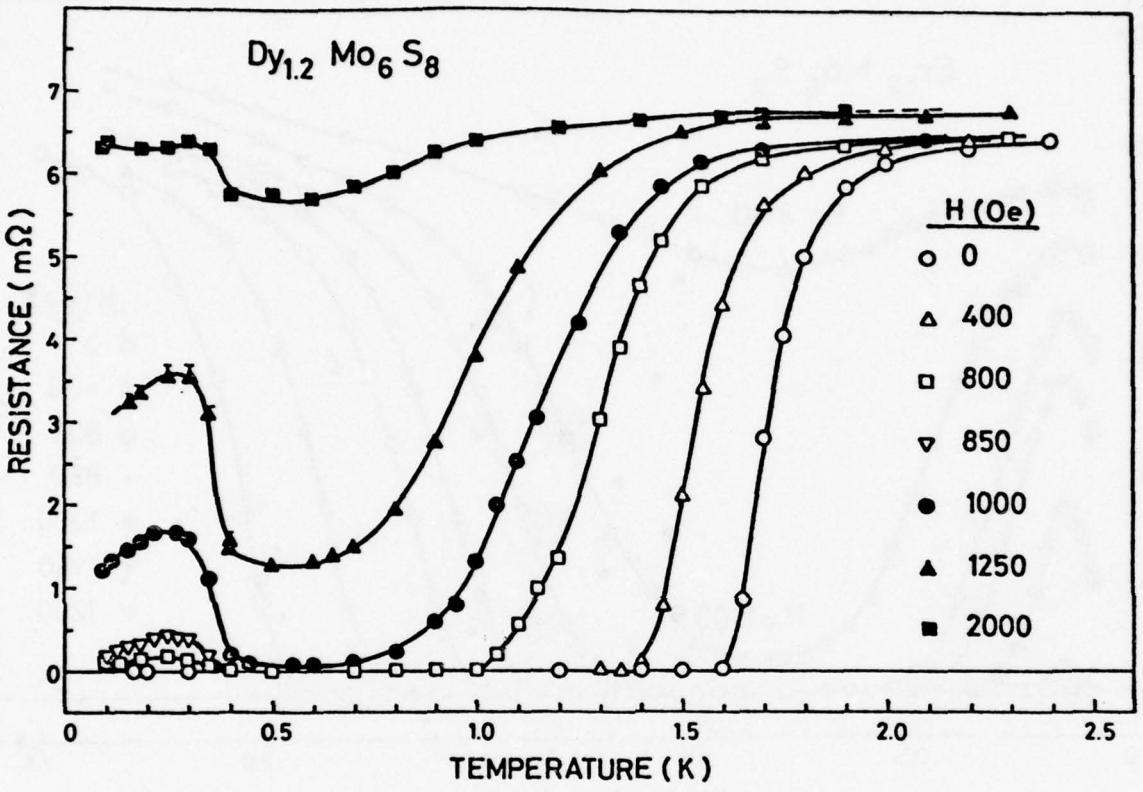

M. ISHIKAWA AND Ø. FISCHER, SOLID STATE COMMUN. 24, 747 (1977)

RESISTANCE VS. T

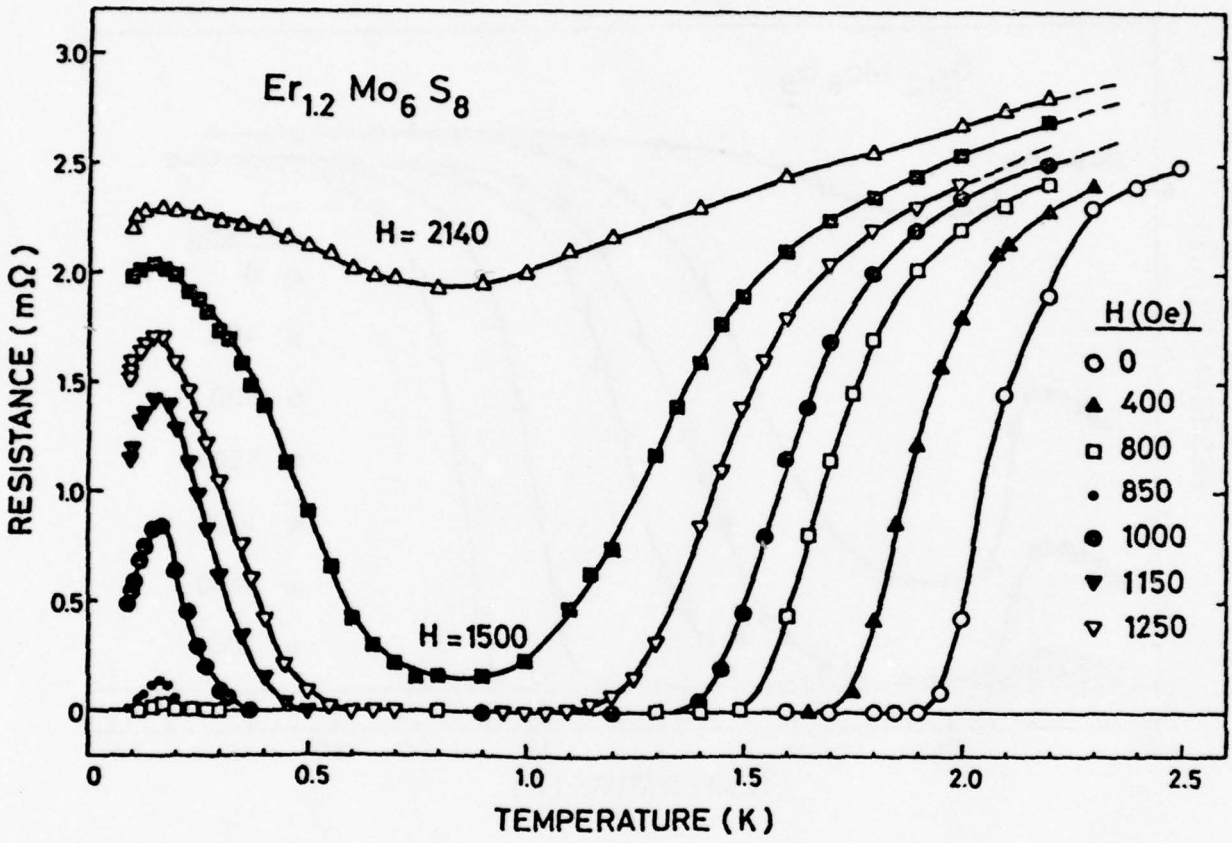

M. ISHIKAWA AND Ø. FISCHER, SOLID STATE COMMUN. 24, 747 (1977)

POWDER NEUTRON DIFFRACTION SPECTRA ABOVE (T = 0.7 K) AND BELOW (T = 0.05) THE MAGNETIC TRANSITION. THE INSET GIVES THE ANTIFERROMAGNETIC ARRANGEMENT OF MOMENTS ALONG THE TERNARY AXIS.

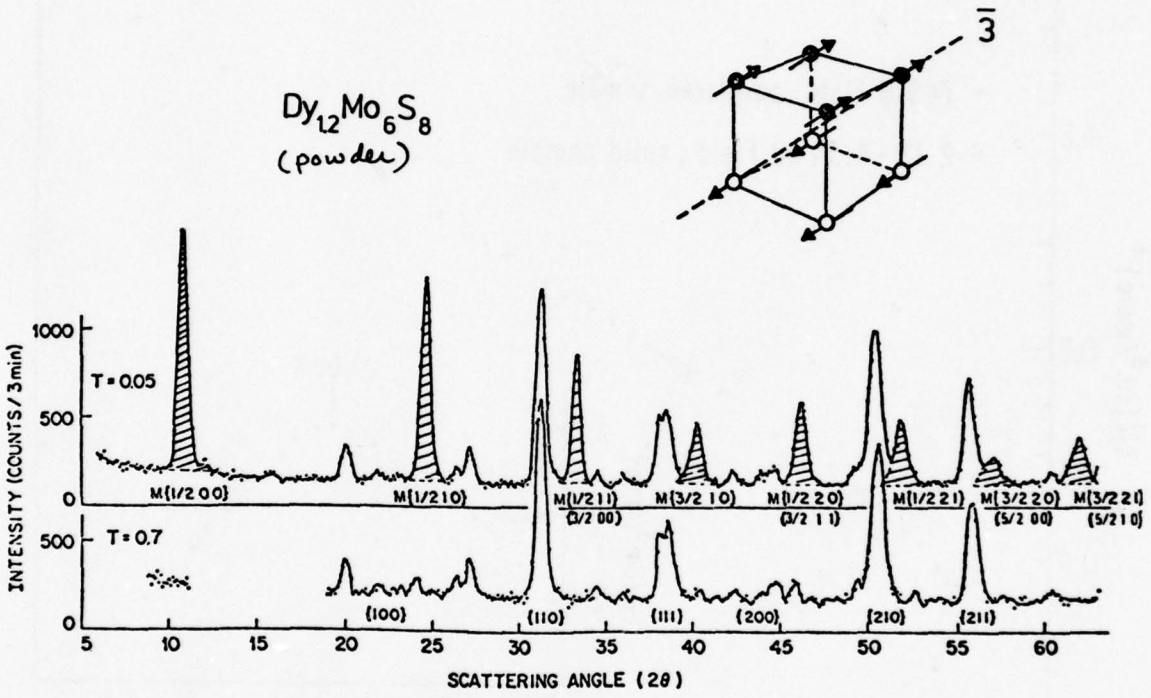

Fig. 4

D. E. MONCTON, G. SHIRANE, W. THOMLINSON, M. ISHIKAWA AND Ø. FISCHER, TO BE PUBLISHED.

INVERSE SUSCEPTIBILITY VS. T BETWEEN 0.8 K AND 12 K. THE INSET CONTAINS M VS. T NEAR THE NEEL TEMPERATURE AT 1.05 K.

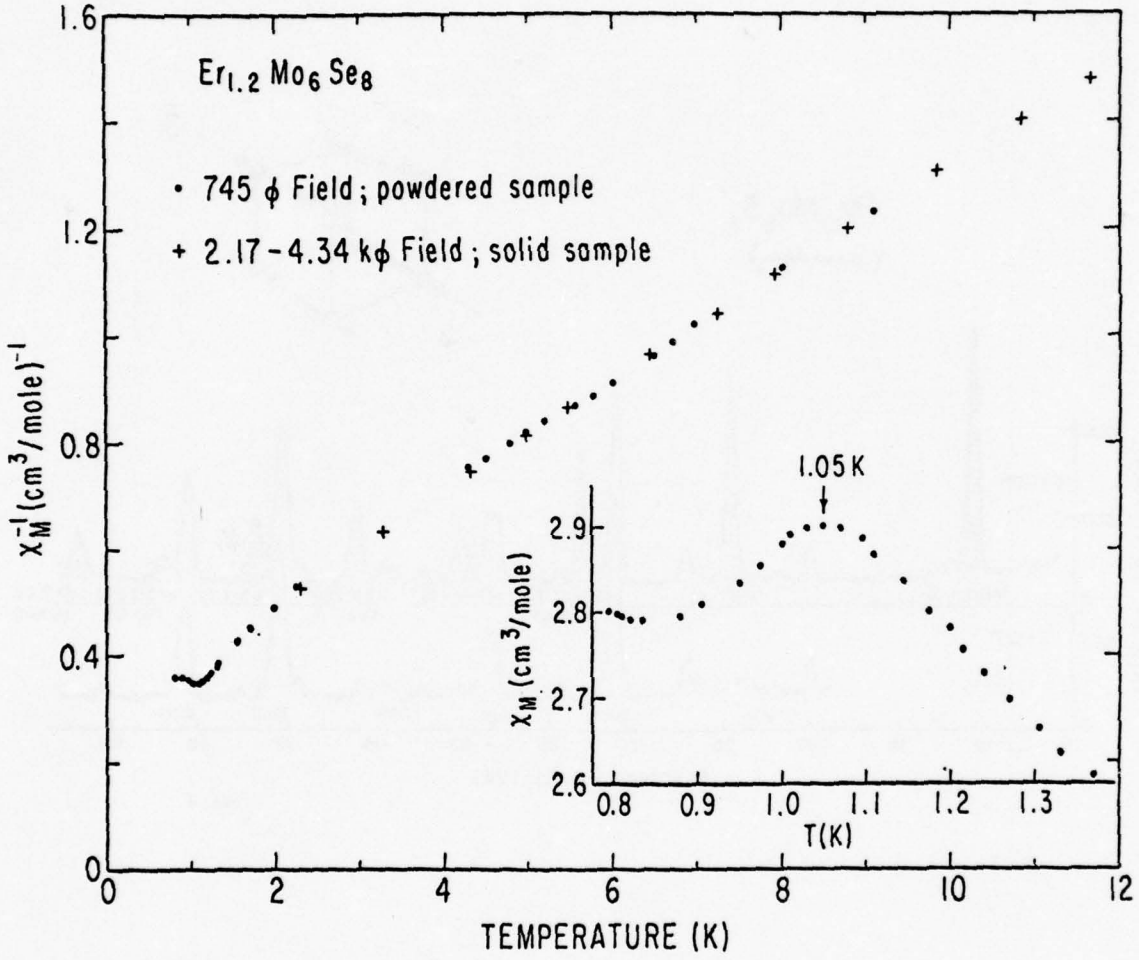

A. W. MCCALLUM, D. C. JOHNSTON, R. N. SHELTON, W. A. FERTIG AND M. B. MAPLE, SOLID STATE COMMUN. 24, 501 (1977).

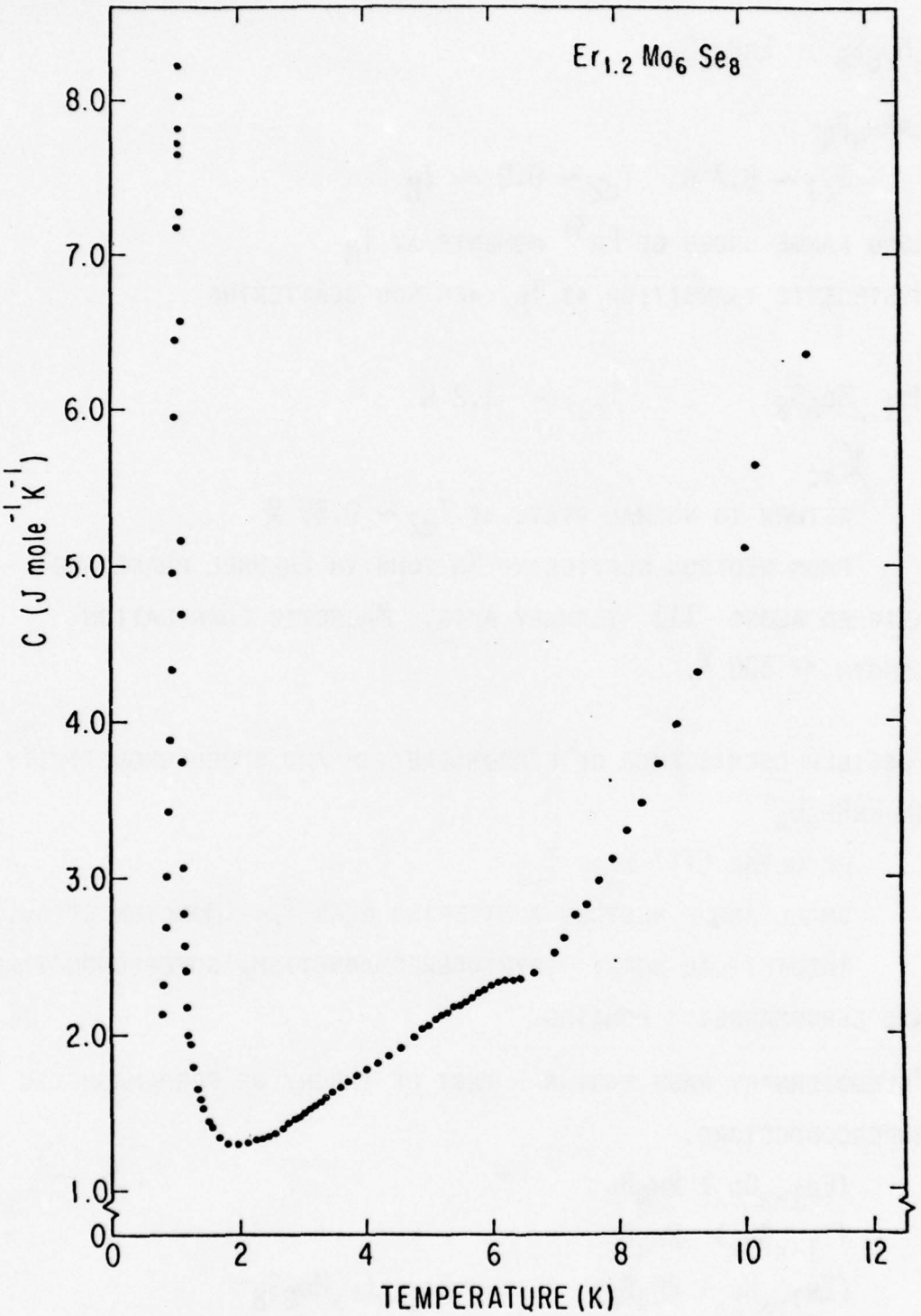

R. W. McCallum, D. C. Johnston, R. N. Shelton, W. A. Fertig and M. B. Maple: Solid State Commun. 24, 501 (1977).

Re-entrant Superconductivity Due to Ferromagnetic Order

$Ho_{1.2}Mo_6S_8$, $ErRh_4B_4$

1. $ErRh_4B_4$

   $T_{c1} \sim 8.7$ K, $T_{c2} \sim 0.9 \sim T_M$

   Long range order of Er^{3+} moments at T_M

   Hysteretic transition at T_M, neutron scattering

2. $Ho_{1.2}Mo_6S_8$ $T_{c1} \sim 1.2$ K

   χ_{AC}

   return to normal state at $T_{c2} \sim 0.65$ K

   From neutron scattering Ho ions in Chevrel phase are aligned along 111 ternary axis. Magnetic correlation length ~ 300 Å.

3. Possible coexistence of ferromagnetism and superconductivity in $ErRh_4B_4$

   peculiar C(T) near T_{c2}

   small angle neutron scattering near T_{c2} (Moncton et al.).

   Theoretical work: cryptoferromagnetism, superconducting and ferromagnetic domains.

4. Psuedoternary rare earths - test of theory of ferromagnetic superconductors.

   $(Er_{1-x}Gd_x)\ Rh_4B_4$
   $(Y_{1-x}Gd_x)\ Rh_4B_4$
   $(Er_{1-x}Ho_x)\ Rh_4B_4$ $\qquad Ho_{1-x}Lu_xMo_6S_8$
   $(Lu_{1-x}Ho_x)\ Rh_4B_4$
   $(Er_{1-x}Tm_x)\ Rh_4B_4$

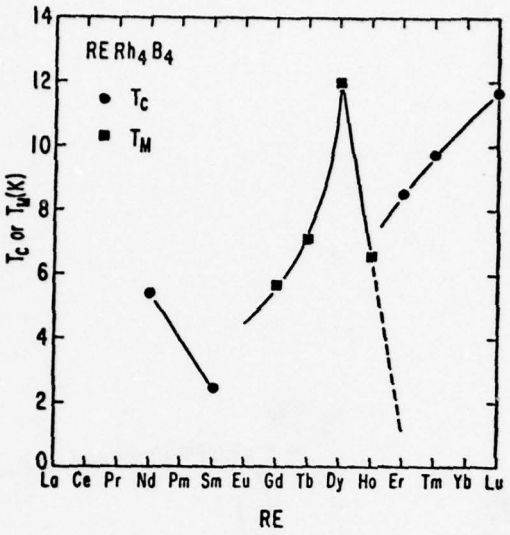

Superconducting transition temperatures T_c and magnetic ordering temperatures of $RERh_4B_4$ compounds (4). The dashed line represents a linear extrapolation of the Curie temperatures of the $DyRh_4B_4$ and $HoRh_4B_4$ compounds to the $ErRh_4B_4$ compound.

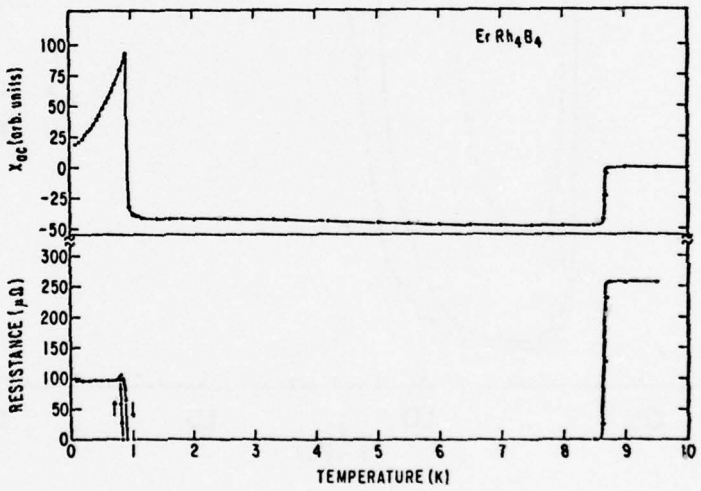

ac magnetic susceptibility χ_{ac} and ac electrical resistance vs temperature for $ErRh_4B_4$ in zero applied magnetic field

M. B. MAPLE IN THE RARE EARTHS IN MODERN SCIENCE AND TECHNOLOGY ED. BY G. J. MCCARTHY AND J. J. RHYNE (PLENUM PRESS, NEW YORK) 1978, P. 381.

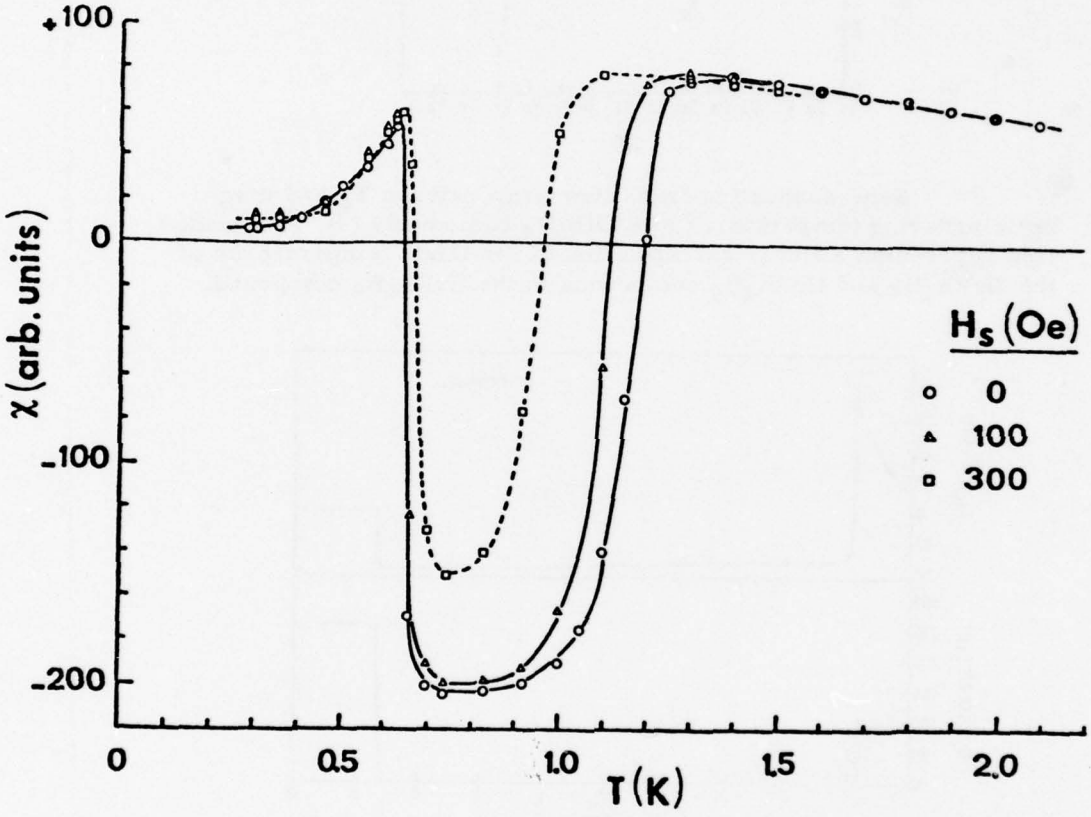

AC MAGNETIC SUSCEPTIBILITY AS A FUNCTION OF TEMPERATURE FOR $Ho_{1.2}Mo_6S_8$, FROM ISHIKAWA AND FISCHER, SOLID STATE COMMUN. 23, 37 (1977).

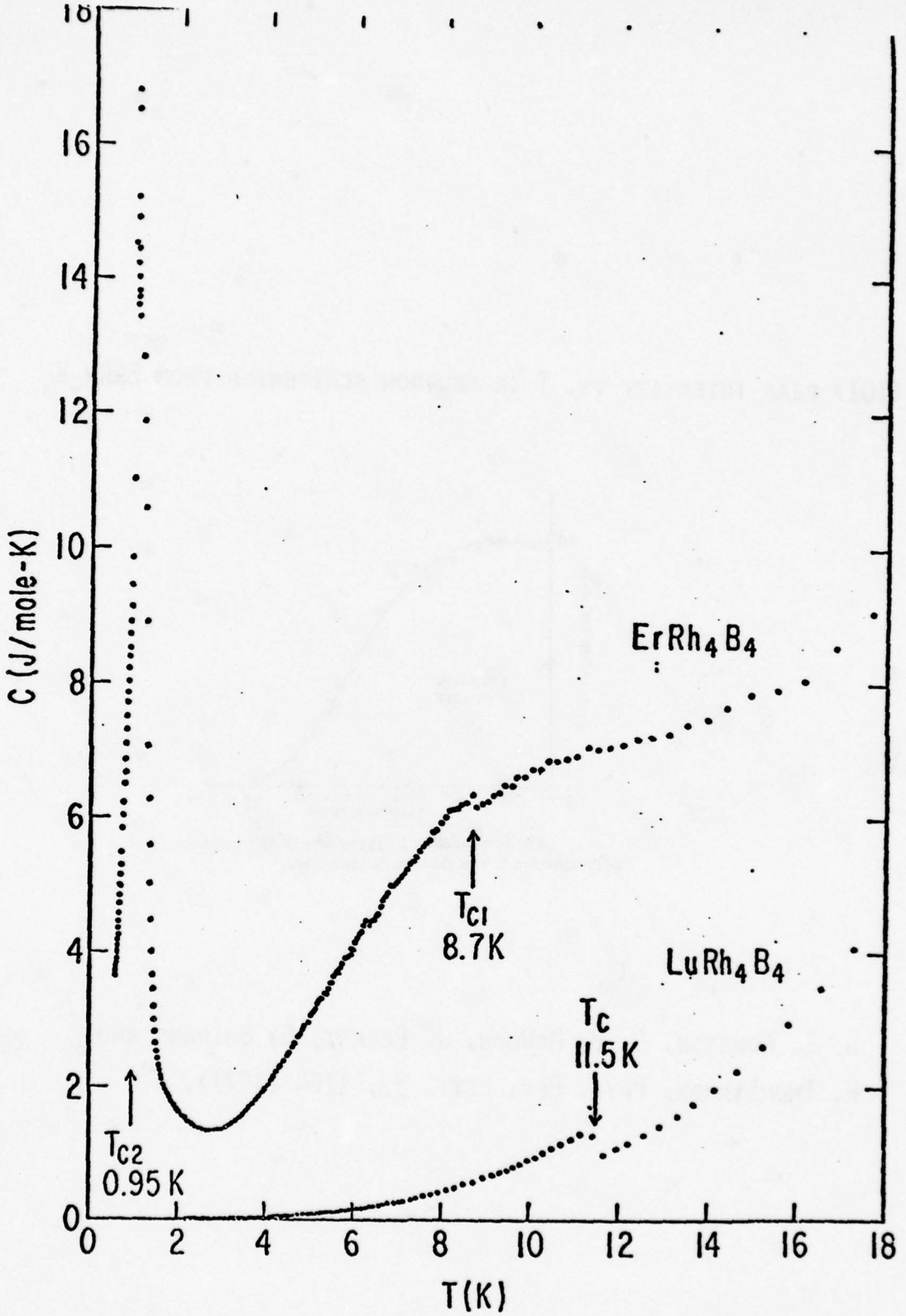

L. D. WOOLF, H. B. MACKAY, R. W. MCCALLUM, D. C. JOHNSTON AND M. B. MAPLE, TO BE PUBLISHED.

(101) PEAK INTENSITY VS. T IN NEUTRON SCATTERING FROM $ErRh_4B_4$

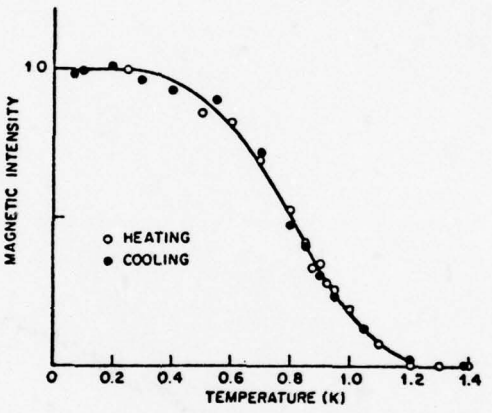

The temperatures dependence of the magnetic contribution to the (101) peak intensity.

D. E. MONCTON, D. B. MCWHAN, J. ECKERT, G. SHIRANE AND W. THOMLINSON, PHYS. REV. LETT. 39, 1164 (1977).

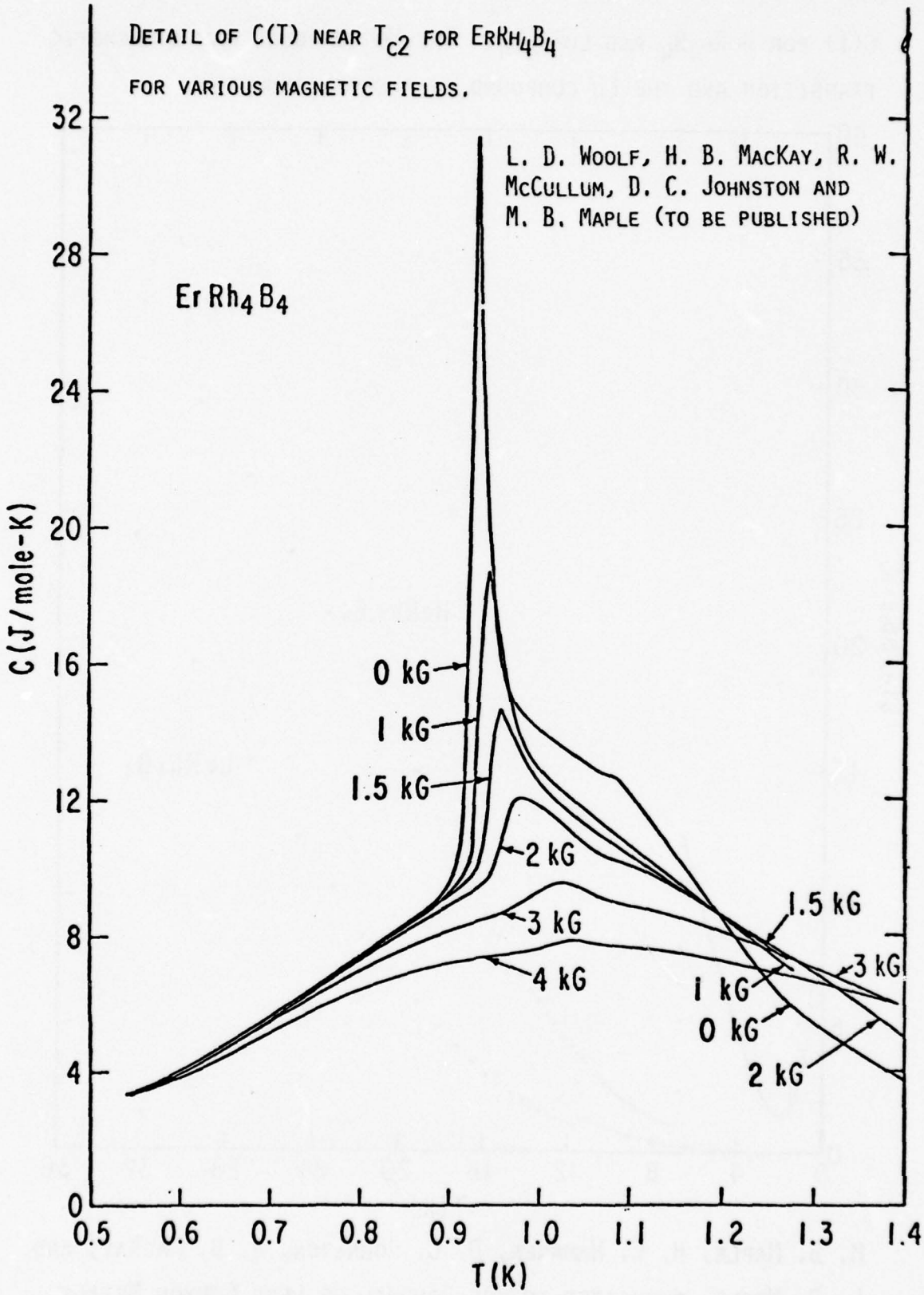
DETAIL OF C(T) NEAR T_{c2} FOR $ErRh_4B_4$
FOR VARIOUS MAGNETIC FIELDS.
L. D. WOOLF, H. B. MACKAY, R. W. McCULLUM, D. C. JOHNSTON AND M. B. MAPLE (TO BE PUBLISHED)
$ErRh_4B_4$
C(J/mole-K)
T(K)
0 kG
1 kG
1.5 kG
2 kG
3 kG
4 kG
1.5 kG
3 kG
1 kG
0 kG
2 kG
0
4
8
12
16
20
24
28
32
0.5
0.6
0.7
0.8
0.9
1.0
1.1
1.2
1.3
1.4

C(T) FOR $HoRh_4B_4$ AND $LuRh_4B_4$. THE Ho COMPOUND HAS A MAGNETIC TRANSITION AND THE Lu COMPOUND IS A SUPERCONDUCTOR;

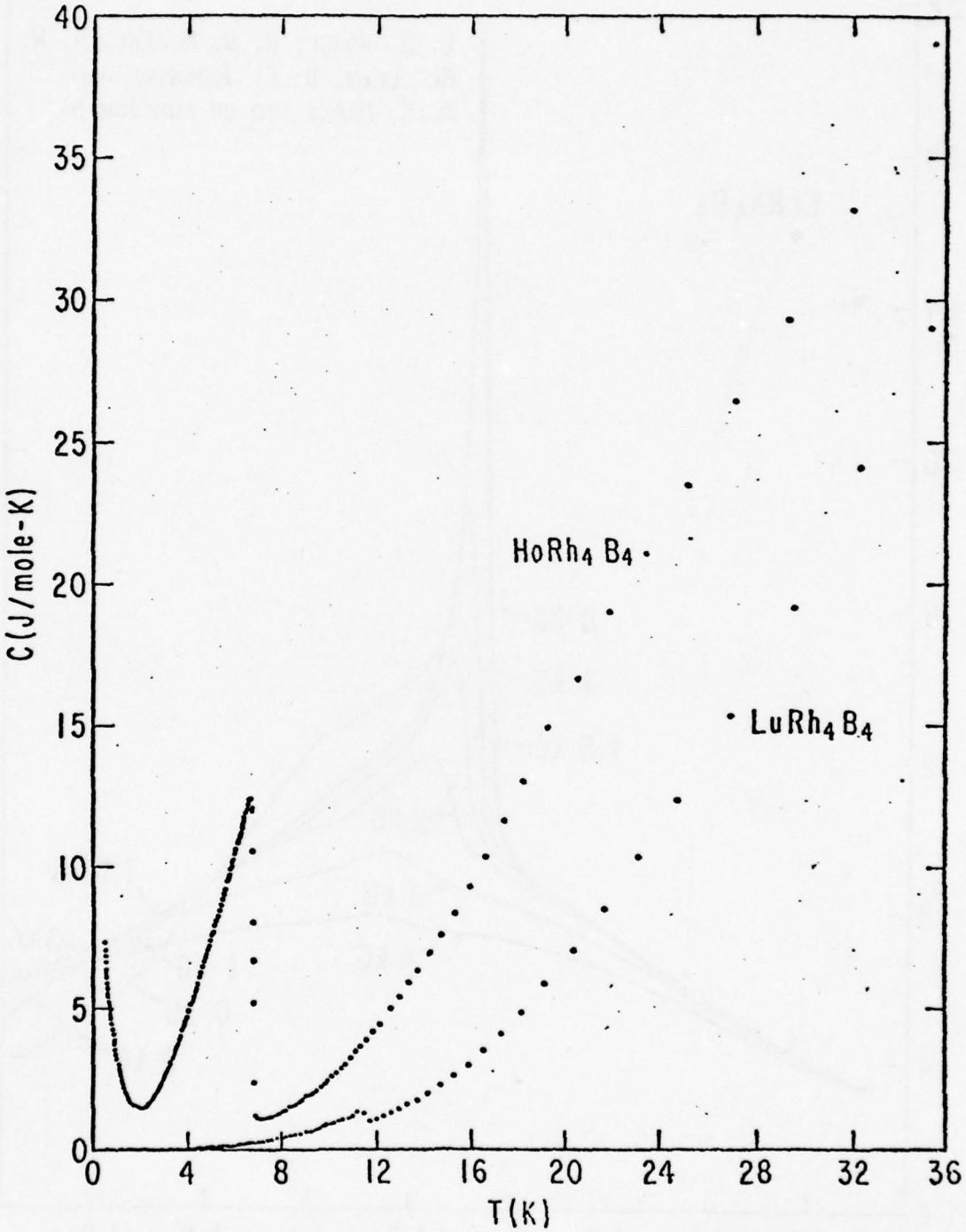

M. B. MAPLE, H. C. HAMAKER, D. C. JOHNSTON, H. B. MACKAY, AND L. D. WOOLF, SUBMITTED TO THE JOURNAL OF LESS COMMON METALS.

PHASE DIAGRAM OF THE PSUEDOTERNARY DETERMINED FROM AC SUSCEPTIBILITY MEASUREMENTS.

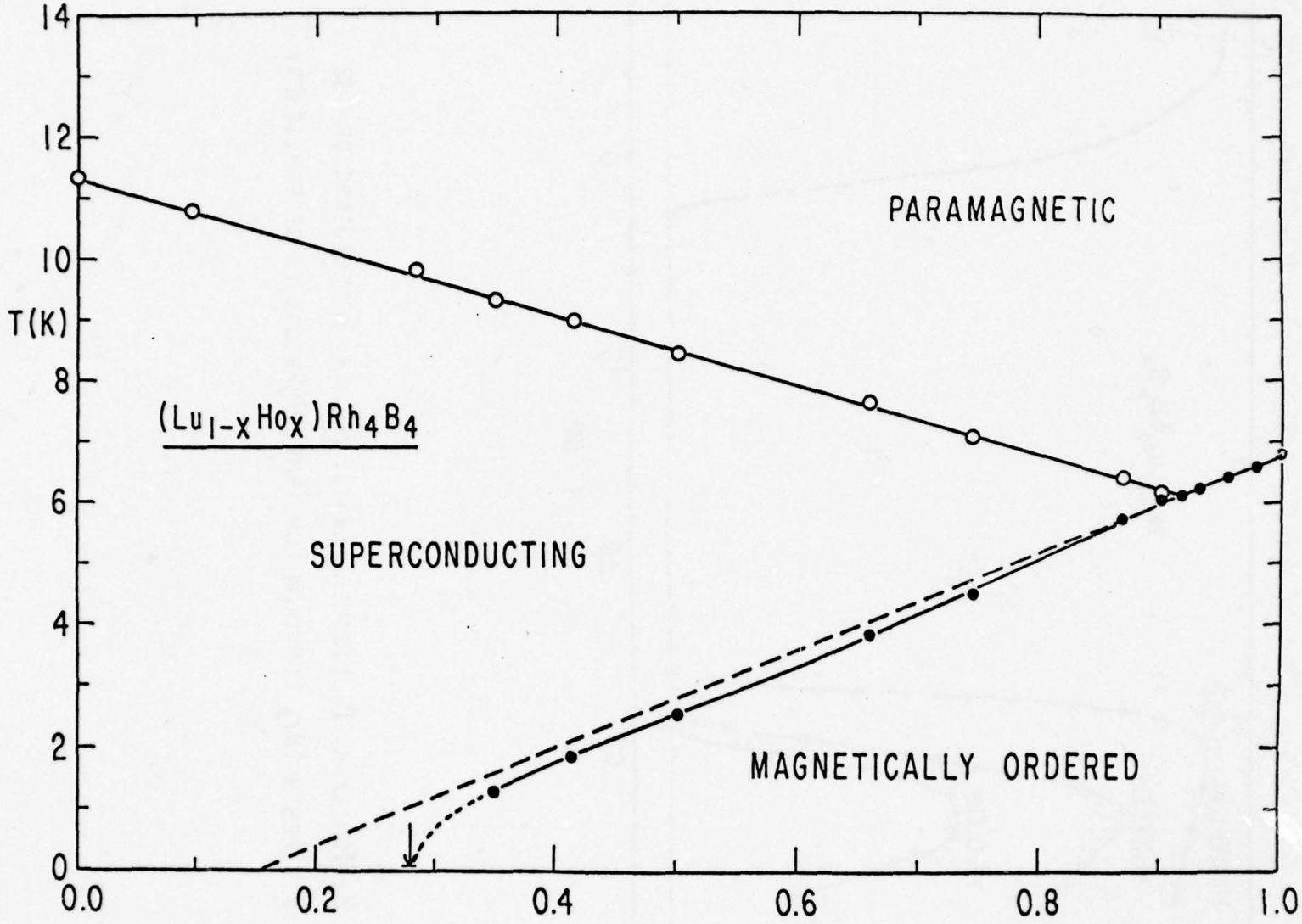

M. B. MAPLE ET AL., SUBMITTED TO THE JOURNAL OF LESS COMMON METALS.

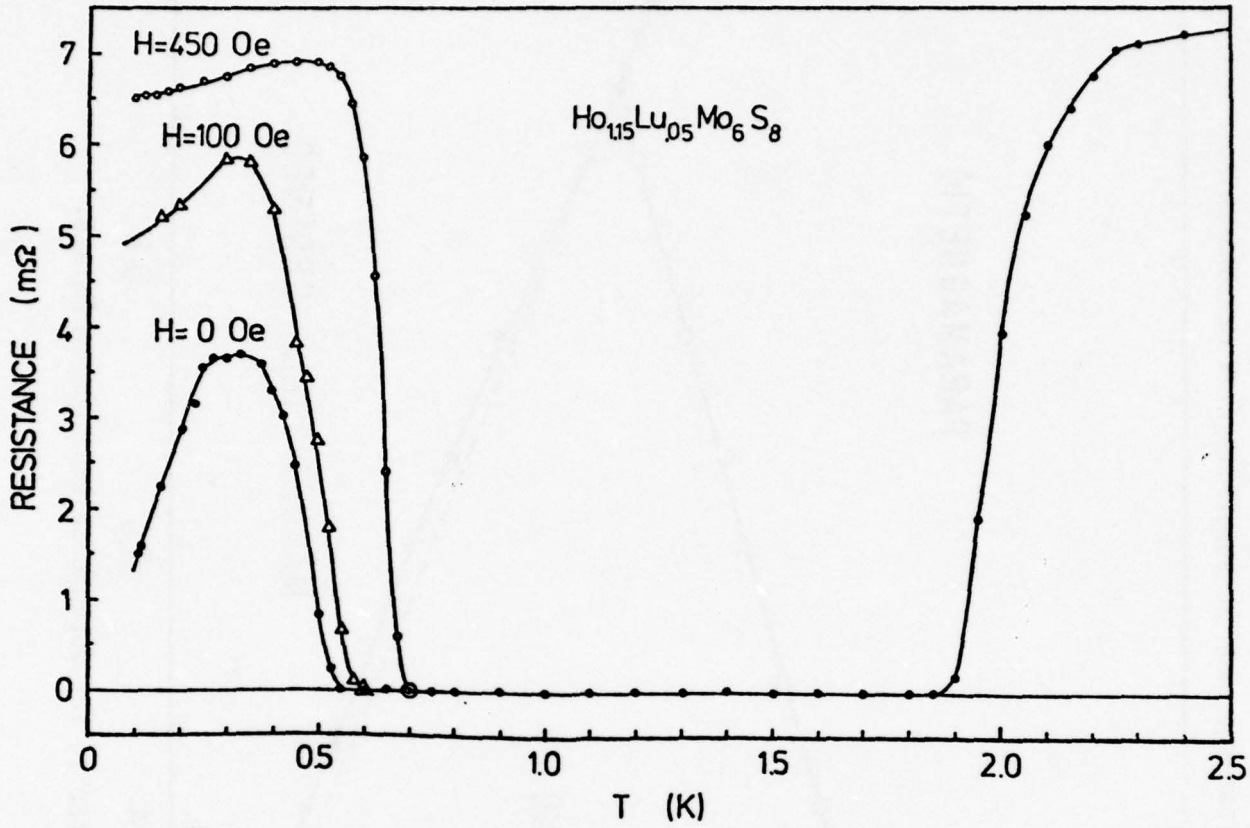

M. Ishikawa, Ø. Fischer, and J. Muller, Proceedings of the Fifteenth Int. Conf. on Low Temp. Physics, to be published.

F. Future Trends

1. High critical fields of tremendous importance. Can ductile materials with high critical currents be made? Possibly good thin films, made by sputtering or by using multiple source vapor deposition techniques are a route to ductile, useful material.
   See: C. K. Banks, L. Kammerdiner and H. L. Luo, J. Solid State Chem. 15, 271 (1975).

2. Better samples are needed for all experiments in order to better understand coexistence of long-range order and superconductivity. So far most experiments have been done on sintered materials.

3. More work on mechanisms of superconductivity - $\alpha^2 F(\omega)$ determined by tunneling or other techniques. Are there triplet pairs or other mechanisms?

4. More study of crystalline electric field around RE ions. Systematics of variation of T_c and T_M with rare earth ions needs study. Disparate results on magnetic moment of Er^{3+} in $ErRh_4B_4$ as measured by Mössbauer effect and by neutron scattering need further study.

5. Are there other ternary systems with such rich properties? A systematic search for them has high scientific interest.

6. COEXISTENCE OF FERROMAGNETISM AND SUPERCONDUCTIVITY IN $ErRh_4B_4$.

A. GENERALITY OF RE-ENTRANT BEHAVIOR?

B. IS T_M IN THE SUPERCONDUCTING STATE SMALLER THAN T_M IN THE NORMAL STATE?

C. WHY IS TRANSITION AT T_{c2} HYSTERETIC?

D. CHARACTER OF COEXISTENCE. IS THERE CRYPTO-FERROMAGNETISM OR ARE THERE ALTERNATING DOMAINS? WHAT ARE THE DYNAMICAL PROPERTIES OF THE COUPLED SUPERCONDUCTING AND MAGNETIC ORDER PARAMETERS? PERHAPS A COMBINATION OF NEUTRON SCATTERING AND JOSEPHSON TUNNELING CAN BE USED TO STUDY THESE QUESTIONS. THE DYNAMICS AND STATISTICAL MECHANICS OF THE COUPLED ORDER PARAMETERS COULD BE A VERY RICH SUBJECT OF HIGH SCIENTIFIC INTEREST.

SEE FOR EXAMPLE: YOSEPH IMRY, J. PHYS. C8, 567 (1975).

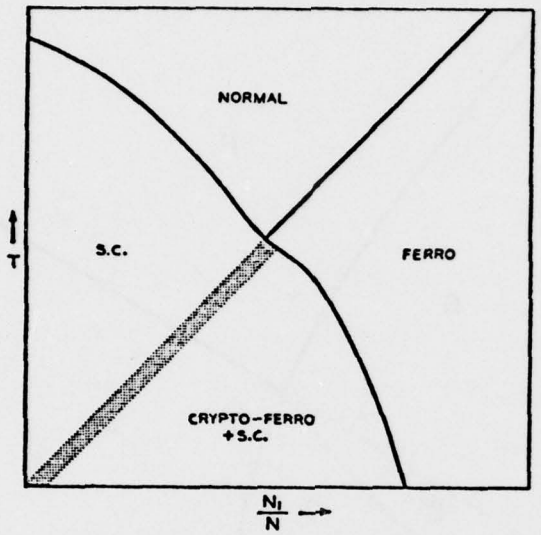

Phase diagram for ferromagnetism, superconductivity, and cryptoferromagnetism.

P. W. ANDERSON AND H. SUHL, PHYS. REV. 116, 898 (1959)

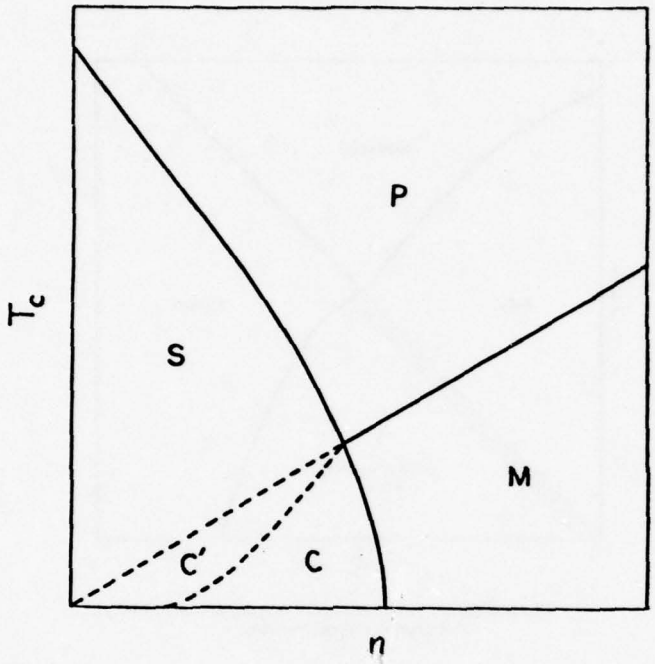

Phase diagram exhibiting superconducting D, paramagnetic P, magnetically ordered M, and S-M coexistence (C and C') phases

L. P. Gor'kov and A. I. Rusinov, JETP 19, 922 (1964)

Granular Superconductors

P. Lindenfeld, Rutgers University

The granular metals are mixtures of metals and insulators, usually prepared by sputtering or evaporation. They can have a wide range of electrical properties, from metallic through semiconducting to insulating. In some cases they are superconductors, and can then have transition temperatures which are much higher than those of their constituents.[1]

Until recently there was a good deal of uncertainty, and even controversy, about their structure. This seems now to have been resolved with the realization that there can be two quite different kinds of material with entirely different properties.[2] On the one hand there are random mixtures which are well described by percolation theory of non-interacting mixtures. On the other hand there may be a true granular structure, consisting of more or less uniform metal crystallites surrounded by amorphous insulator. (Figs. 1 and 2.)

The example of the second category which has been studied in greatest detail is Al-Al_2O_3, and this system will be used to illustrate some of the interesting properties of this class of materials.

The granular metals are sometimes called "cermets" or ceramic metals. They can have the characteristic mechanical properties of other kinds of ceramic materials, namely hardness and stability. In part this is expected because the granular structure prevents the existence of mobile dislocations. In addition the amorphous insulator in the true granular materials acts as a glue to hold the metal grains together and is therefore presumably responsible for the remarkable thermal and mechanical stability of this class of substances.

The main properties of Al-Al_2O_3 are illustrated on Figs. 3 and 4. The metallic region extends to about 10^{-4} Ωcm, and is characterized by an increasing transition temperature and a

decreasing grain size as the resistivity increases. For higher resistivities the grain size remains at about 30 Å, the temperature coefficient of resistance becomes negative, and T_c is roughly constant. With higher oxide content the grains separate, the material becomes increasingly insulating, and superconductivity disappears.[3,4] In the region near the metal-insulator transition the resistivity changes rapidly with only small changes in composition.

The excellent homogeneity and the resulting regular behavior which can be achieved are illustrated on Figs. 5 and 6 which show the transition to superconductivity in the heat capacity and the thermal conductivity of two specimens in the metallic region, together with the relevant theoretical curves.[5,6]

For higher resistivities the heat-capacity transition disappears (Fig. 7) since the grain size is too small to make superconductivity possible when the grains are isolated.[5] Fig. 8 shows the expected behavior of isolated grains of different size[7] and Fig. 9 the experimental curves of Ref. 5 which are seen to follow the curves of Ref. 7 and which can therefore be interpreted in terms of an effective size which characterizes the intergrain coupling.

In materials in which the grain size is large enough one can observe two transitions, one when the individual grains undergo a transition, and a second one when coupling between the grains causes coherent superconductivity in the whole specimen.[8]

The remaining figures show measurements[9] on a specimen of 0.04 Ωcm on which the heat-capacity transition was too small to be observed in our experiment, and on a similar specimen of 0.02 Ωcm. Both specimens exhibit a regular electrical transition (Figs. 10,12,13). It may be seen on Fig. 11 that superconducting fluctuations persist at 3 K to a magnetic field of over 5T, followed by a remarkably regular negative quadratic magneto-resistance. The variation of the extrapolated normal-state resistance in zero field, R_N, with temperature is shown on Fig. 14, together with theoretical curves expected for hopping conductivity. There still seem to be some partial metallic paths in these specimens, which may be responsible for the electrical transitions.

It remains to be explored whether superconductivity is still possible when the electron states tend to be truly localized.

It is interesting to note that the most interesting question, namely that of the enhanced transition temperature, remains unresolved. A great deal of speculation has centered on the possibility that the large surface-to-volume ratio of the grains causes the average phonon frequency to be decreased. The other possibility which has been discussed is that the presence of the insulator leads to an enhanced electron-electron interaction, either via phonons, or conceivably through an electron-mediated ("exciton") mechanism. It would therefore be particularly interesting to determine whether the presence of the insulator is essential for the enhancement of T_c. It has been pointed out[10] that in very thin films enhanced T_c's have been observed in layered structures which were entirely metallic.[11]

It is clear that a rich field remains for the investigation and application of granular superconductors.

1. For a comprehensive review see B. Abeles, Applied Solid State Science (Academic Press, New York, 1976) vol. 6, p. 1.

2. G. Deutscher, M. L. Rappaport, and Z. Ovadyahu, to be published.

3. G. Deutscher, H. Fenichel, M. Gershenson, E. Grünbaum, and Z. Ovadyahu, J. Low Temp. Phys. 10, 231 (1973).

4. G. Deutscher, M. Gershenson, E. Grünbaum, and Y. Imry, J. Vac. Sci. Technol. 10, 697 (1973).

5. T. Worthington, P. Lindenfeld, and G. Deutscher, Phys. Rev. Lett. 41, 316 (1978).

6. Y. H. Hsu, Ph.D. Thesis, Rutgers University, 1978, unpublished.

7. B. Mühlschlegel, D. J. Scalapino, and R. Denton, Phys. Rev. B 6, 1767 (1972).

8. G. Deutscher and M. L. Rappaport, J. de Physique, 39, C6-581 (1978).

9. W. L. McLean, P. Lindenfeld, and T. Worthington, in Electrical Transport and Optical Properties of Inhomogeneous Media, AIP Conference Proceedings No. 40, edited by J. C. Garland and D. B. Tanner (American Institute of Physics, New York 1978) p. 403.

10. M. Strongin, O. F. Kammerer, J. E. Crow, R. D. Parks, D. H. Douglass, and M. A. Jensen, Phys. Rev. Lett. 21, 1320 (1968).

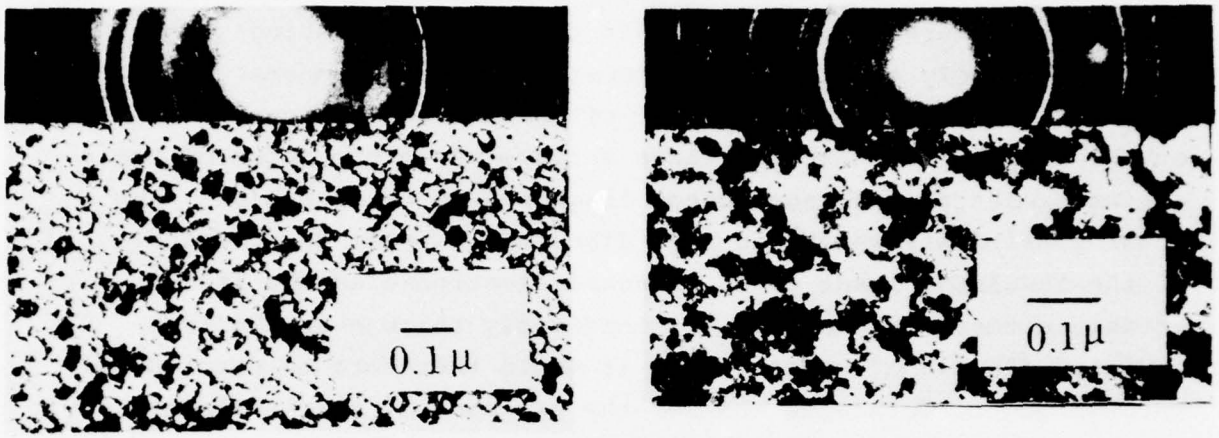

Fig. 1. Transmission electron micrographs and diffraction patterns for the two types of structures. Al-Ge (left) has a true granular arrangement; In-Ge (right) shows the pattern characteristic of random mixtures near the percolation threshold. (From Ref. 2.)

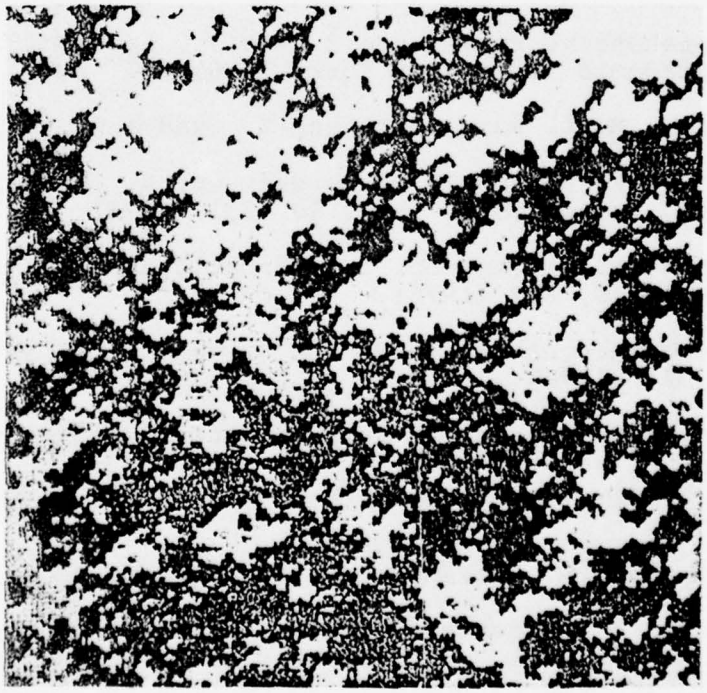

Fig. 2. Computer simulation of a mixture of two non-interacting materials near the percolation threshold. (From Matsubara et al.)

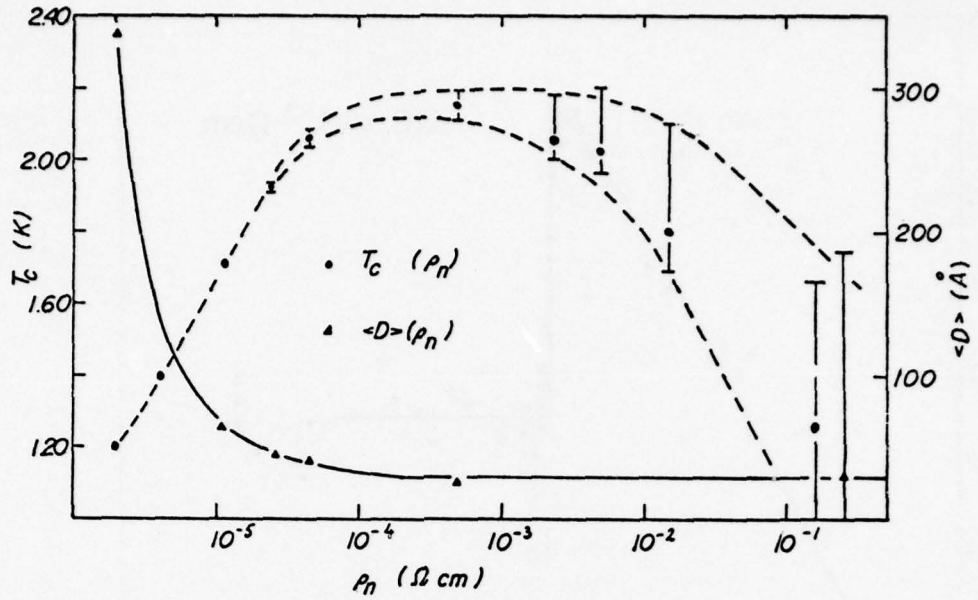

Fig. 3. The transition temperature and average grain size of Al-Al_2O_3 specimens deposited on uncooled substrates. The separation between the two dashed curves indicates the width of the transition. (From Ref. 3.)

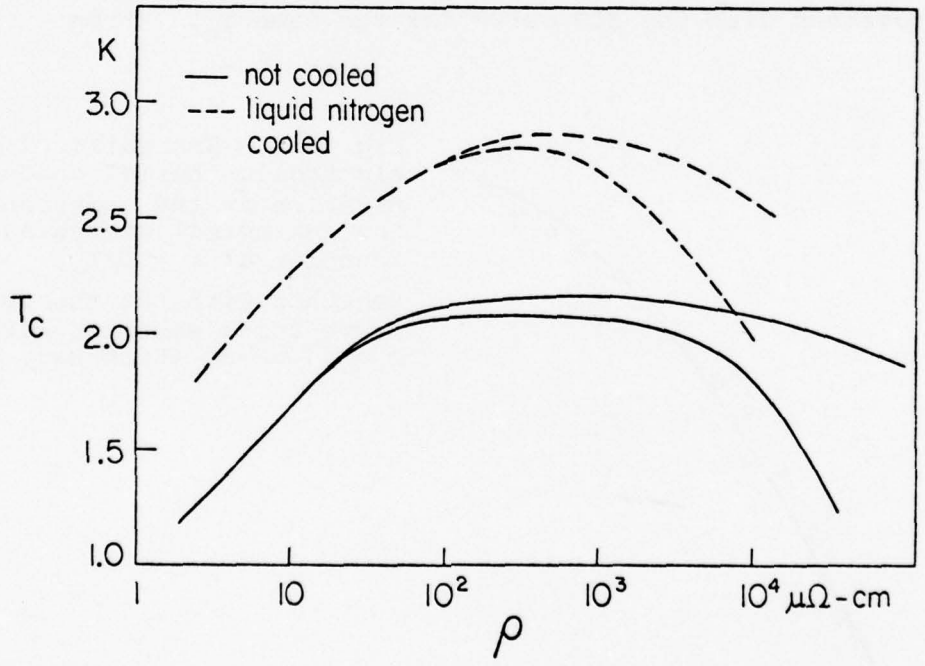

Fig. 4. The influence of the deposition temperature on the transition temperature. The grain size of the specimens deposited at liquid-nitrogen temperature is about 20 Å, compared to 30 Å (see Fig. 3) for room-temperature deposition. (Adapted from Ref. 4.)

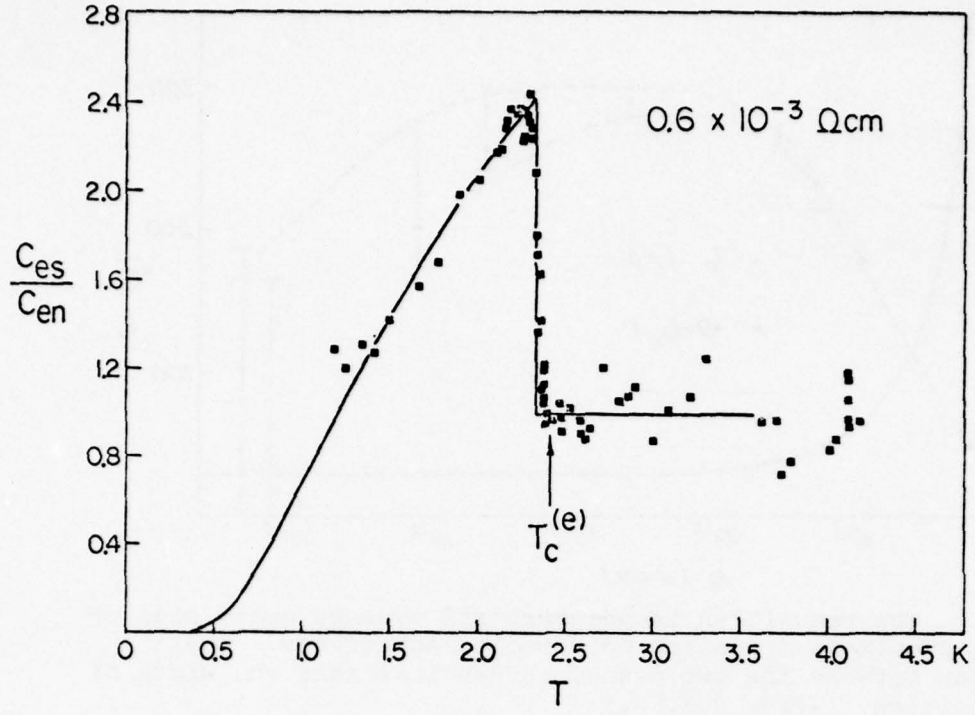

Fig. 5. The heat-capacity transition of a 0.6 x 10^{-3} Ωcm specimen, together with the BCS curve for the same T_c. (From Ref. 5.)

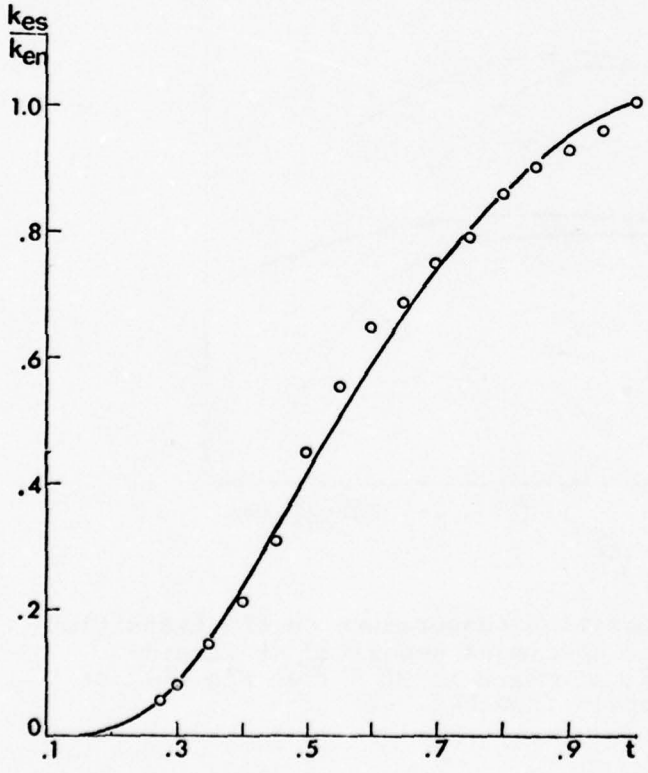

Fig. 6. The ratio of the electronic thermal conductivities in the superconducting and normal states as a function of $t = T/T_c$, together with the theoretical curve, for a specimen with $\rho = 44\ \mu\Omega$-cm (From Ref. 6.)

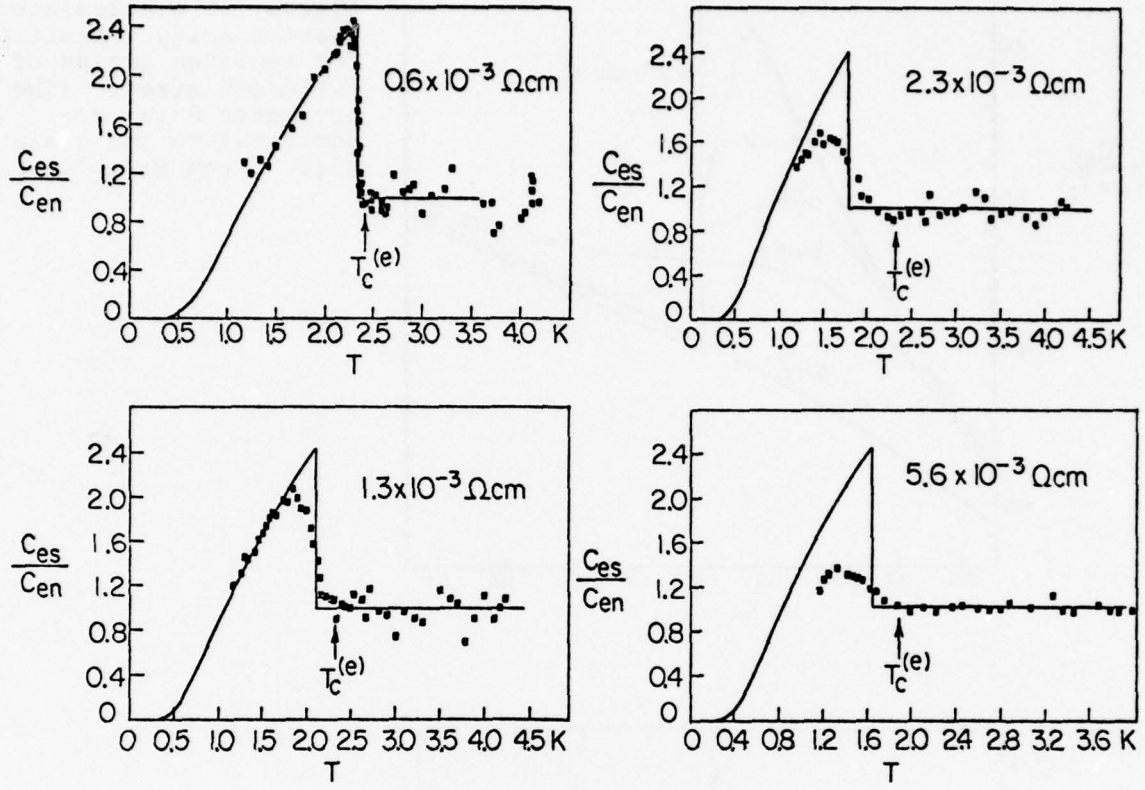

Fig. 7. The heat-capacity transition of four specimens with increasing resistivity. (From Ref. 5.)

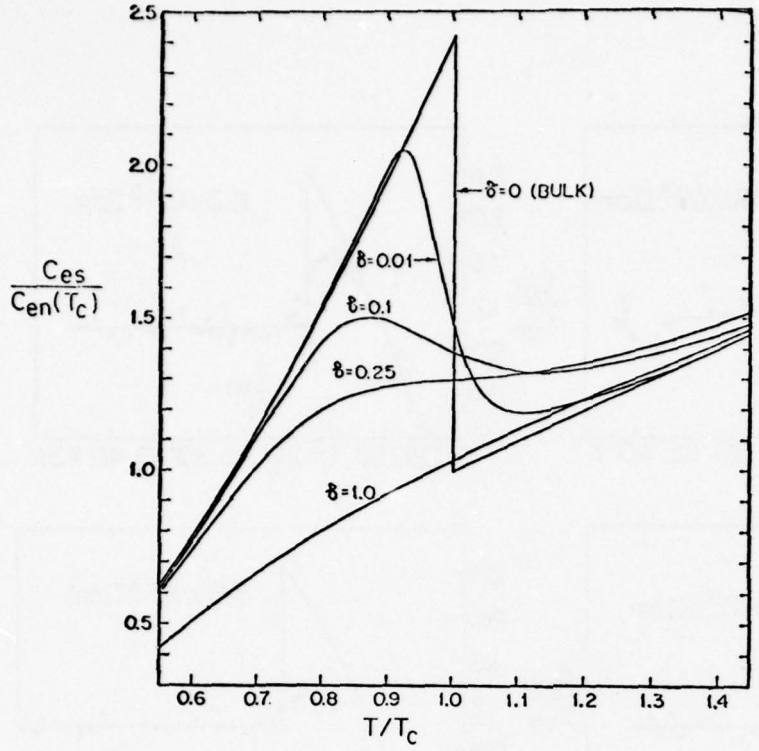

Fig. 8. The calculated heat-capacity transitions for isolated grains of different sizes. (The parameter δ is proportional to the grain size. From Ref. 7.)

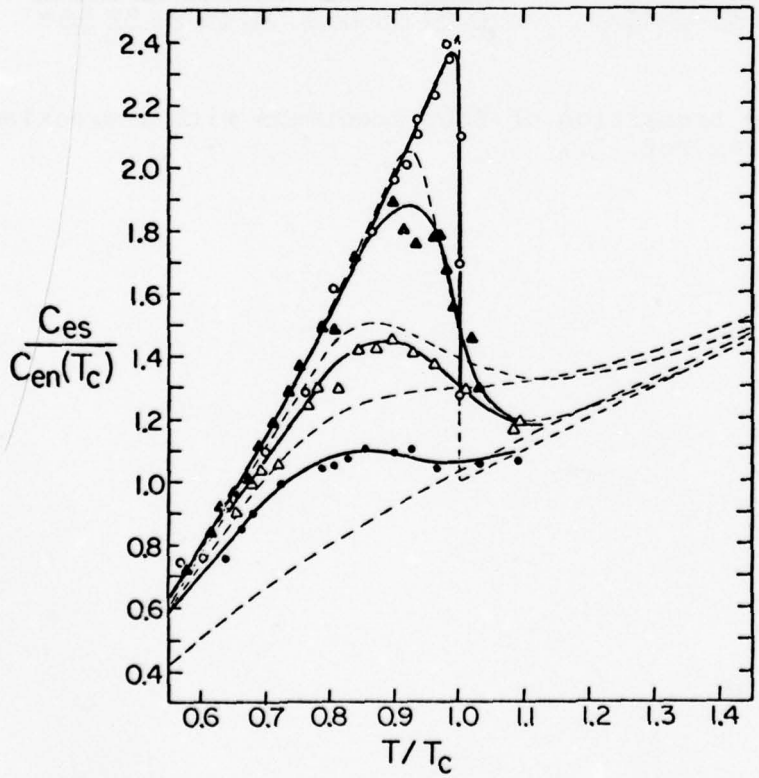

Fig. 9. The data of Fig. 7 plotted together with the theoretical curves (dashed lines) of Ref. 7.

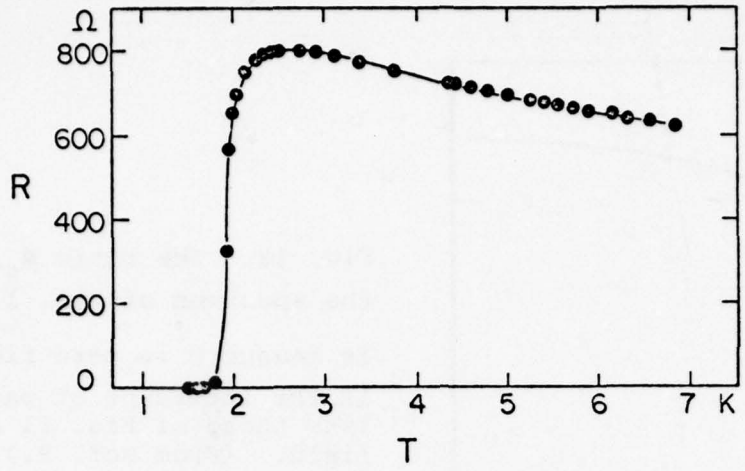

Fig. 10. The resistance as a function of temperature for a specimen of 0.04 Ωcm.

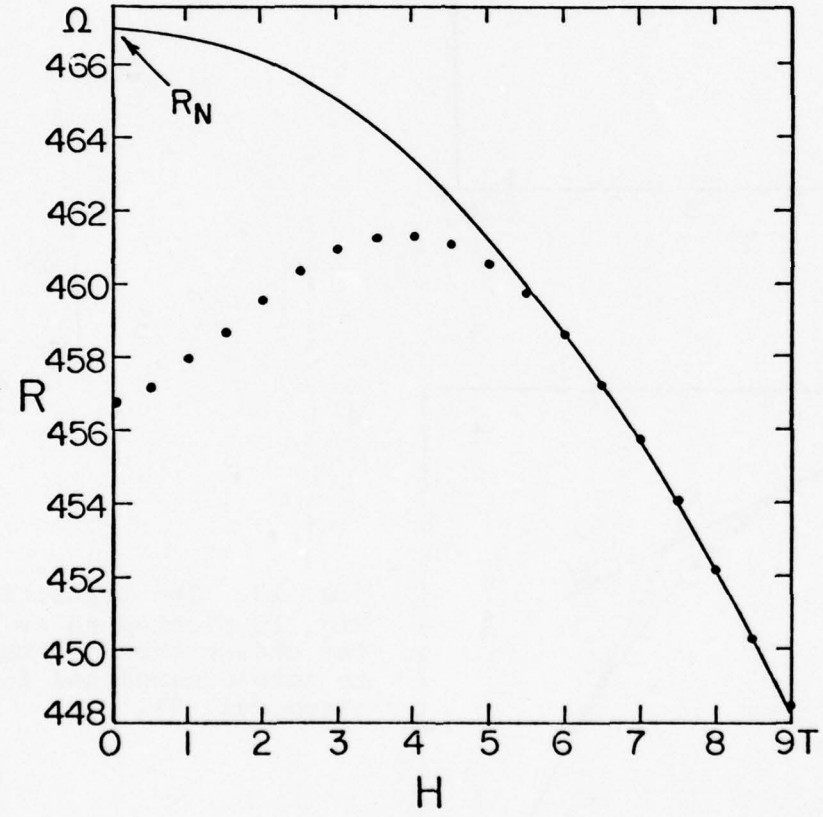

Fig. 11. The resistance as a function of magnetic field for a specimen whose room-temperature resistivity is 0.02 Ωcm. The solid line is a parabola fitted to the high-field data. (From Ref. 9.)

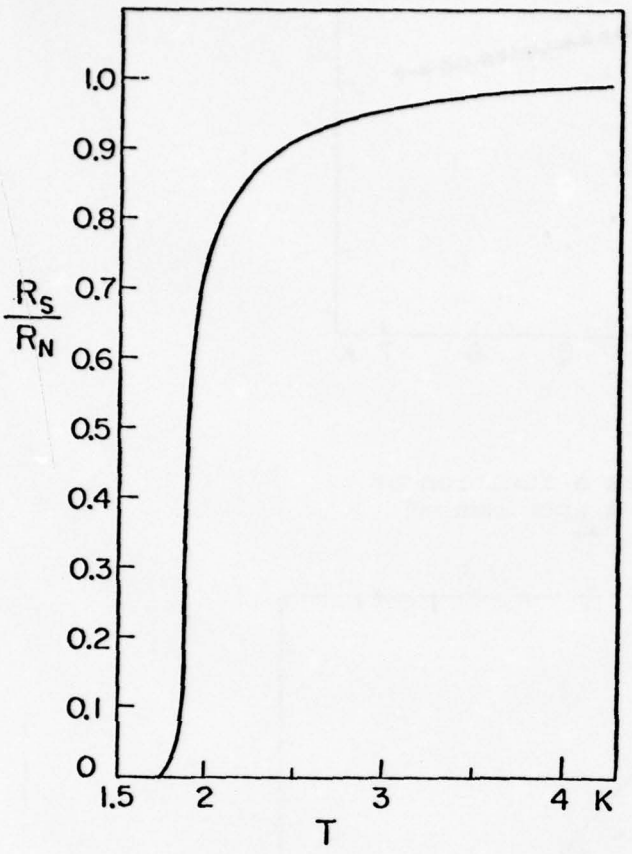

Fig. 12. The ratio R_s/R_N for the specimen of Fig. 11. R_s is measured in zero field, R_N is the intercept of parabolas like those of Fig. 11 at zero field. (From Ref. 9.)

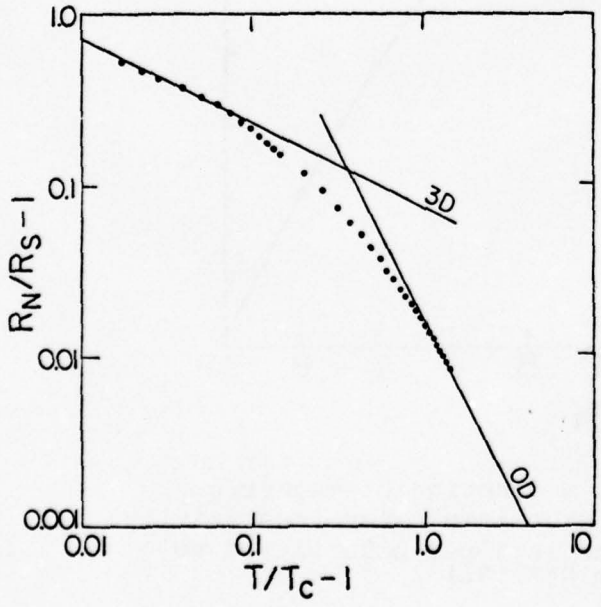

Fig. 13. The transition of Fig. 12 plotted so as to show the change from 3-dimensional to zero-dimensional fluctuations, (From Ref. 9).

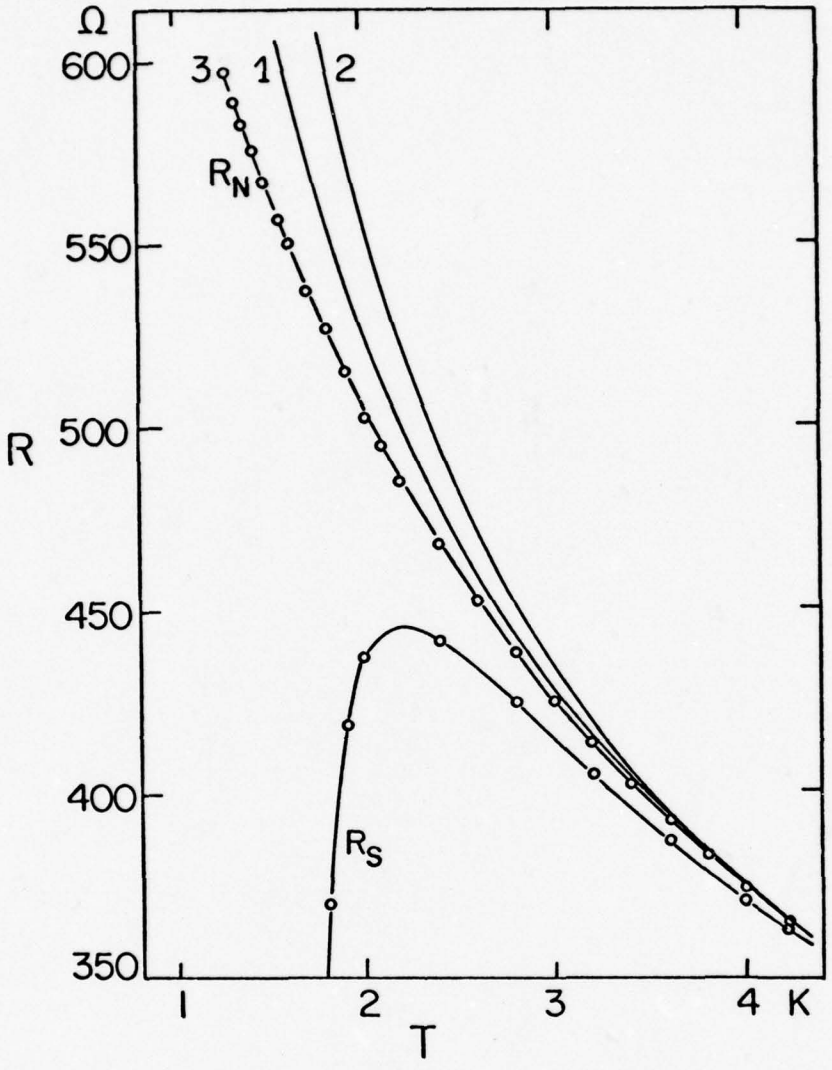

Fig. 14. The resistance of the specimen of Ref. 9 as a function of temperature. Curve 1 is calculated for the Mott hopping conduction formula $\sigma = \sigma_o e^{-(T_o/T)^{1/4}}$ and curve 2 for the relation $\sigma = \sigma_o e^{-(T_o/T)^{1/2}}$ of P. Sheng et al. (Phys. Rev. Lett. 31, 44, 1973).

SUPERCONDUCTIVITY IN $(SN)_x$ AND ITS HALOGEN DERIVATIVE $(SNBr_{0.4})_x$

W. D. Gill
IBM Research Laboratory
San Jose, California 95193

The electronic properties of polysulfur nitride $(SN)_x$ have been of considerable interest since Walatka et al. [1] showed that it is a metal and Greene et al. [2] found that $(SN)_x$ superconducts below 0.3K. Initially $(SN)_x$ was believed to be a quasi 1-D metal, an inorganic analogue of the 1-D organic metals such as TTF-TCNQ [3]. However 1-D metallic systems are inherently unstable, undergoing a metal-insulator transition at finite temperature. The persistence of metallic conductivity to very low temperature and the observed superconductivity indicated that $(SN)_x$ had sufficient interchain coupling to stabilize its metallic properties. Detailed band structure calculations (Fig. 1) and a variety of experiments have confirmed that $(SN)_x$ is a highly anisotropic rather than 1-D metal [4]. However $(SN)_x$ remains of considerable interest as a prototype polymeric and metal-atom-free superconductor. Its anisotropic properties are also of considerable interest in understanding the role of interchain coupling in stabilizing the metallic and superconducting properties of quasi 1-D systems.

Since the discovery of superconductivity in $(SN)_x$ many unsuccessful attempts have been made to synthesize analogous compounds. Recently the first chemical modifications of $(SN)_x$ have been synthesized by reaction with halogens [5]. The most extensively studied of these $(SN)_x$ derivatives is $(SNBr_{0.4})_x$ [6]. On bromination $(SN)_x$ crystals change color from gold to blue/black and swell extensively perpendicular to the chain axis but maintain their fibrous nature. Structural studies with x-rays and particularly transmission electron microscopy (TEM) show only small changes in the $(SN)_x$ lattice parameters and indicate that most of the bromine is located at the periphery of ~20 A diameter $(SN)_x$ fibers (Fig. 2). A commensurate superlattice structure with period 2b is observed in the TEM diffraction patterns (Fig. 3) suggesting that the bromine is ordered along the $(SN)_x$ chains.

In this talk we will compare the electronic properties (Figs. 4 to 7) and especially the superconducting properties (Figs. 8 to 11) of $(SN)_x$ and its halogen derivative $(SNBr_{0.4})_x$. A model involving suppression of electron-hole scattering processes is presented to explain the dramatic changes in the electronic properties on bromination of $(SN)_x$. Assuming charge transfer of approximately 0.1 electrons/SN unit from the conduction band, the Fermi level is lowered about 1eV. This lowering of E_F expands the hole pockets and shrinks or even eliminates the electron pockets suppressing electron-hole scattering.

The decreased width of the superconducting transition in $(SNBr_{0.4})_x$ [6,7], the change to a well-behaved perpendicular critical field [7] and the observation of a complete Meissner effect [8] are indicative of increased interfiber coupling in the superconducting sense, i.e., $(SNBr_{0.4})_x$ is more representative of bulk three-dimensional superconductivity than is $(SN)_x$.

REFERENCES

1. V. V. Walatka, M. M. Labes and J. H. Perlstein, Phys. Rev. Lett. 31, 1139 (1973).

2. R. L. Greene, G. B. Street and L. J. Suter, Phys. Rev. Lett. 34, 557 (1975).

3. See review by A. J. Berlinsky, Contemp. Phys. 17, 331 (1976).

4. See review by H. P. Geserich and L. Pintschovius, Feskörperprobleme XVI, Advances in Solid State Physics, Vol. XVI (J. Treusch, ed.) Vieweg and Sohn, Braunscheig, Germany (1976) p. 65.

5. C. Bernard, A. Herold, M. Lelauren and G. Robert, C. R. Acad. Sci. C283, 625 (1976); G. B. Street, W. D. Gill, R. H. Geiss, R. L. Greene, J. J. Mayerle, JCS Chem. Commun., 407, (1977).

6. W. D. Gill, W. Bludau, R. H. Geiss, P. M. Grant, R. L. Greene, J. J. Mayerle and G. B. Street, Phys. Rev. Lett. 38, 1305 (1977); C. K. Chiang, M. J. Cohen, D. L. Peebles, A. J. Heeger, M. Akhtar, J. Kleppinger, A. G. MacDiarmid, J. Milliken and M. J. Moran, Solid State Commun. 23, 609 (1977).

7. J. F. Kwak, R. L. Greene and W. W. Fuller, to be published in Phys. Rev. B.

8. R. H. Dee, D. H. Dollard, J. F. Carolan, B. G. Turrell, R. L. Greene and G. B. Street, Bull. Amer. Phys. Soc. 23, 384 (1978).

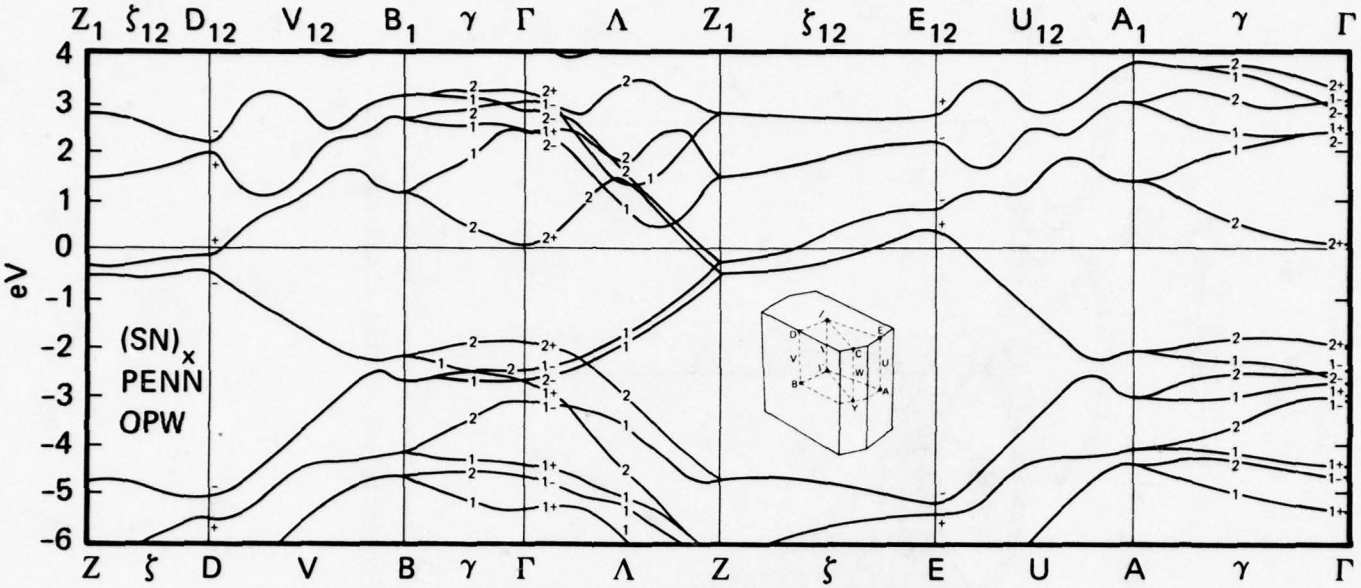

Figure 1. Band Structure of $(SN)_x$ (W. E. Rudge and P. M. Grant, Phys. Rev. Lett. 35, 1799 (1975).

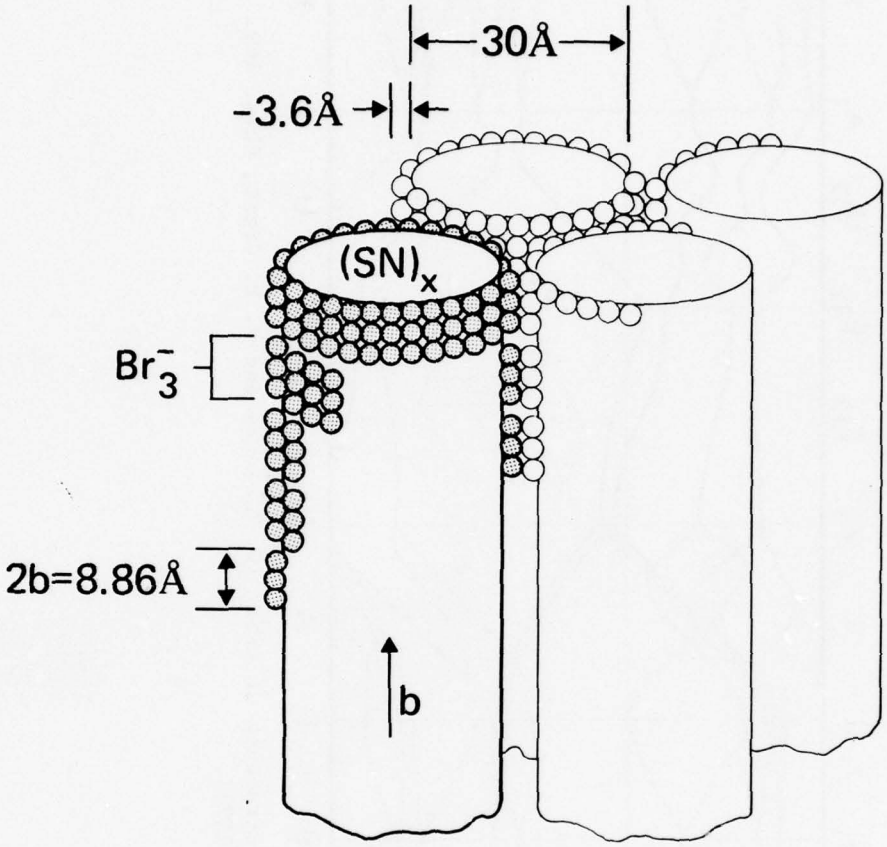

Figure 2. Schematic of bromine cladding model.

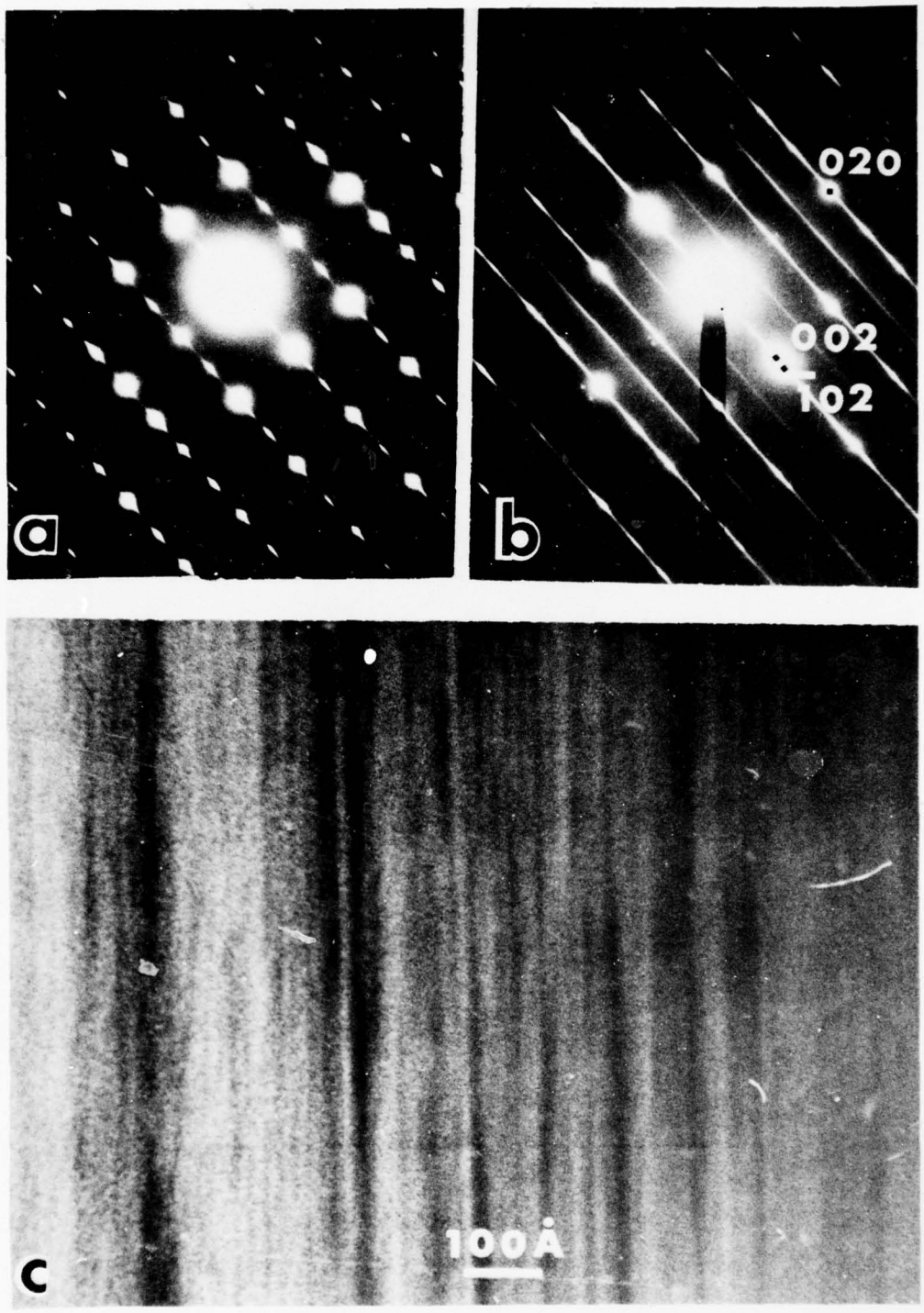

Figure 3. (a) Electron diffraction pattern from a bundle of $(SN)_x$ fibers showing the b*c* reciprocal lattice net. Streaking perpendicular to the b* direction is caused by the small lateral dimensions of the fiber. (b) Electron diffraction pattern from a bundle of $(SNBr_{0.4})_x$ fibers oriented similarly to (a). The simultaneous occurrence of (002) and $(\bar{1}02)$ reflections and the larger streaks are attributed to extensive twinning of the $(SN)_x$. (c) Electron micrograph of $(SNBr_{0.4})_x$ twinned fibers with 20A dimensions.

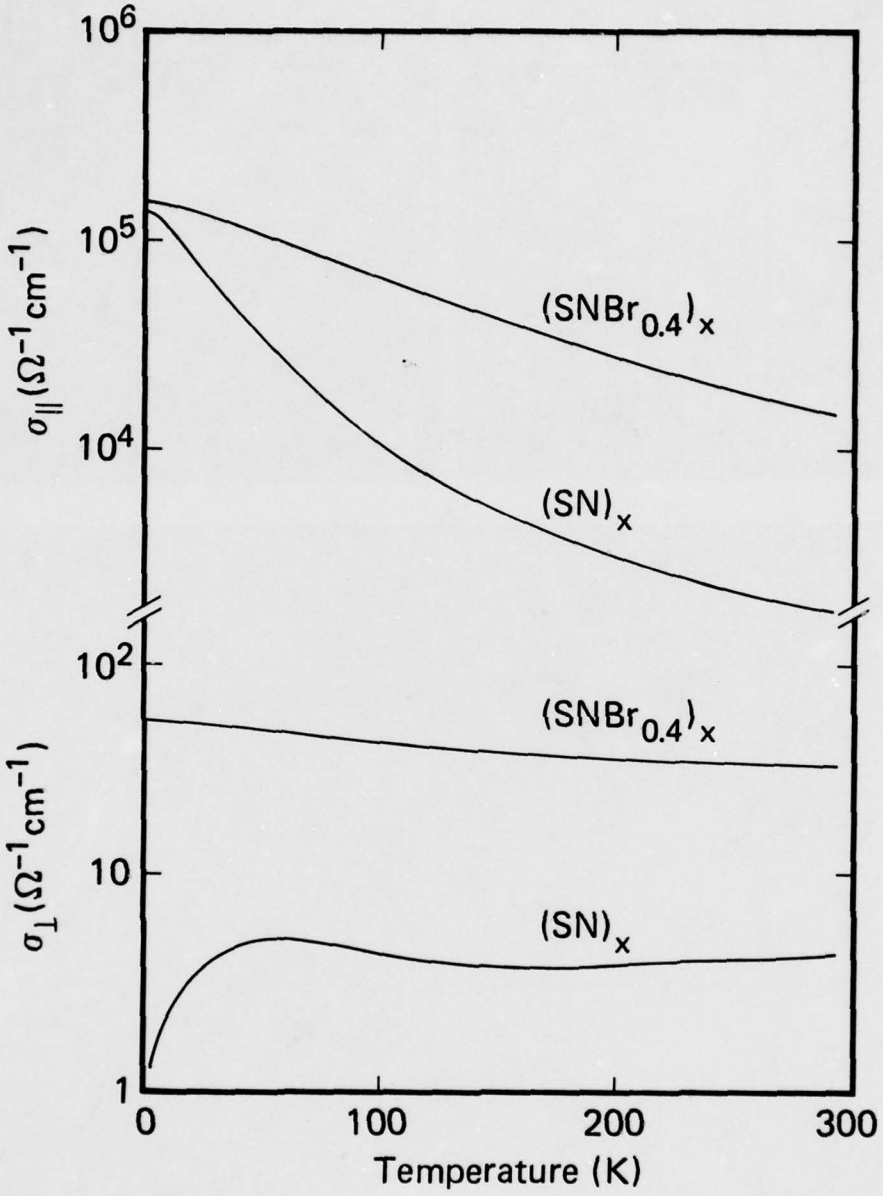

Figure 4. Comparison of conductivity data for $(SN)_x$ and $(SNBr_{0.4})_x$.

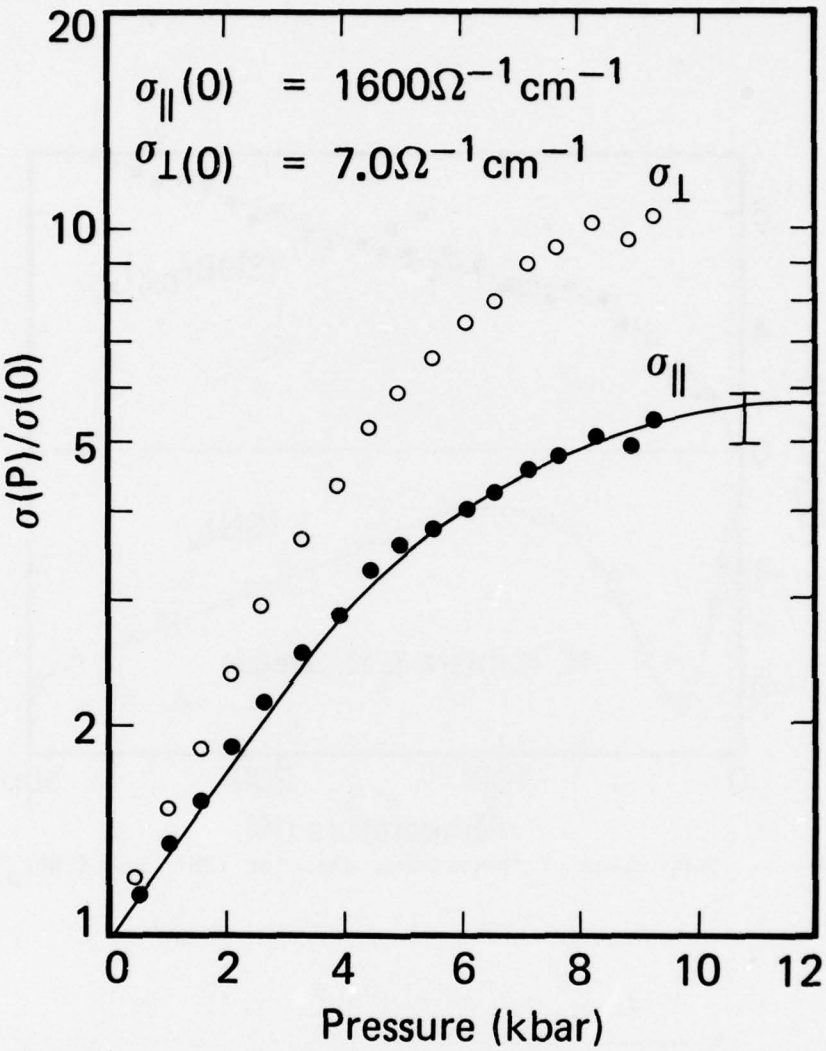

Figure 5. Pressure dependence of normal conductivity in $(SN)_x$. In $(SNBr_{0.4})_x$ conductivity increases by only ~20% under 10 kbar hydrostatic pressure.

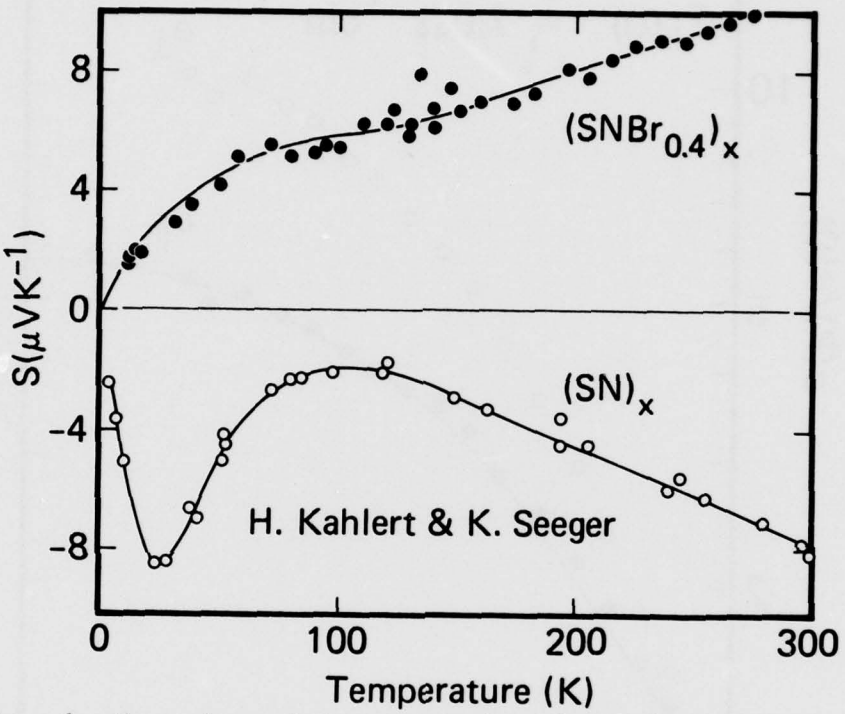

Figure 6. Comparison of thermopower data for $(SN)_x$ and $(SNBr_{0.4})_x$.

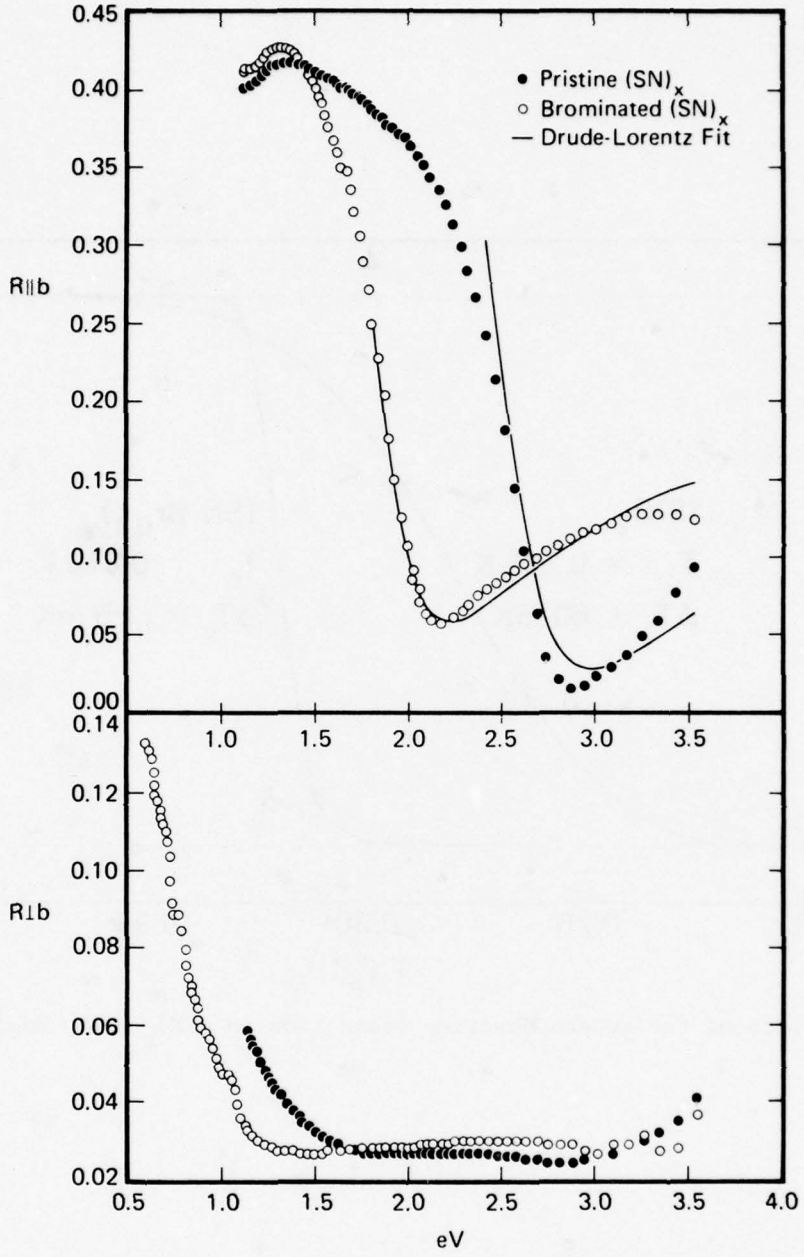

Figure 7. Optical reflectivity of an $(SN)_x$ crystal before and after bromination.

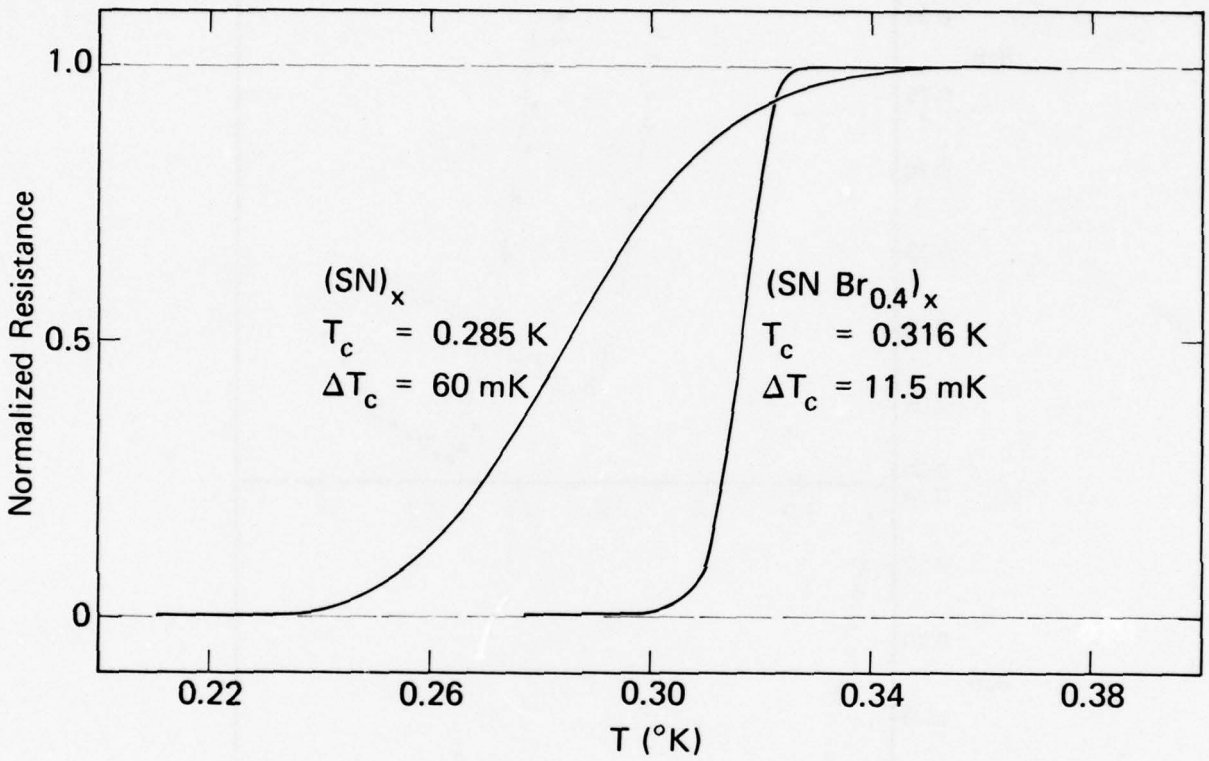

Figure 8. Width of the superconducting transition in $(SN)_x$ and $(SNBr_{0.4})_x$ [7].

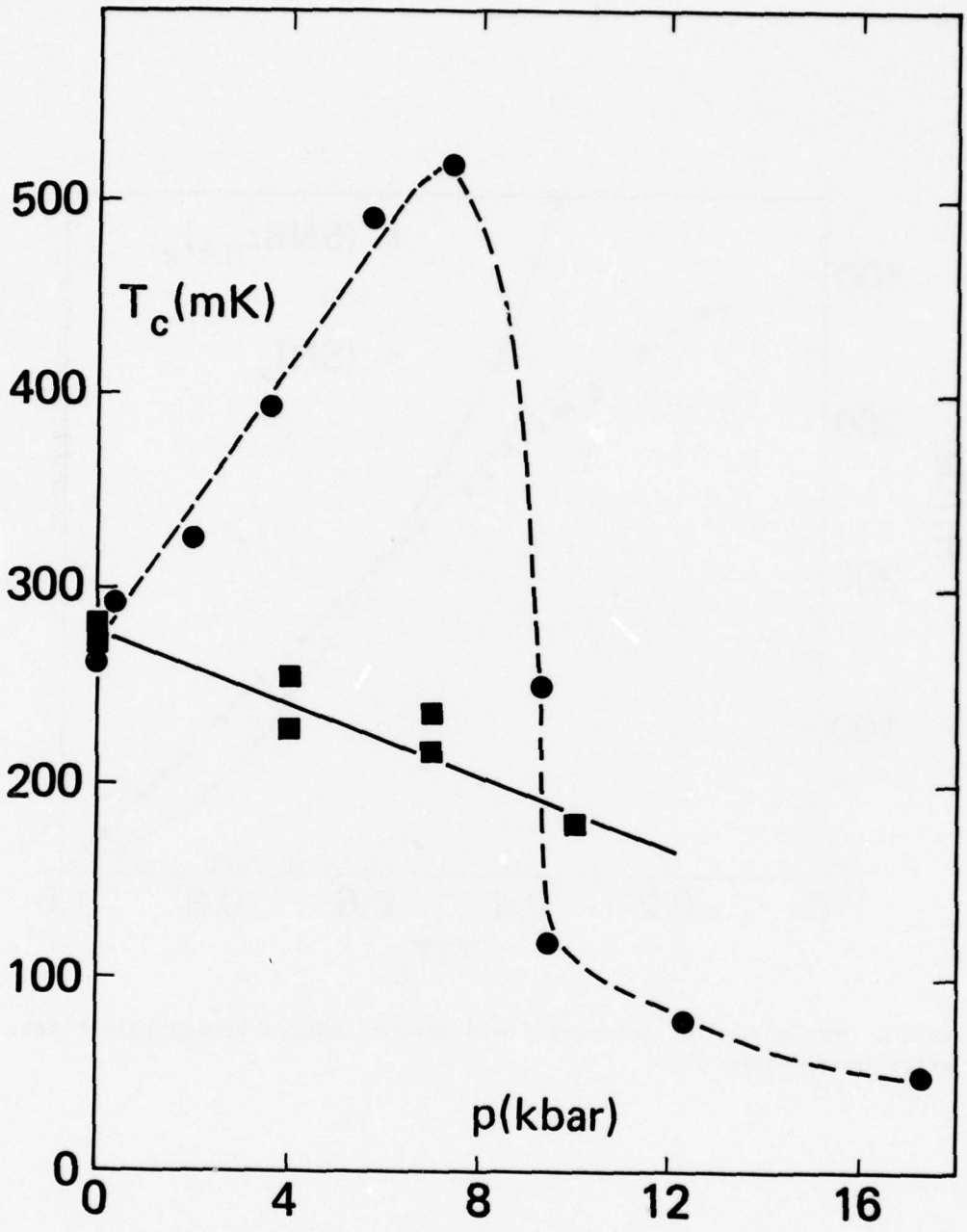

Figure 9. T_c versus pressure for $(SN)_x$ and $(SNBr_{0.4})_x$.

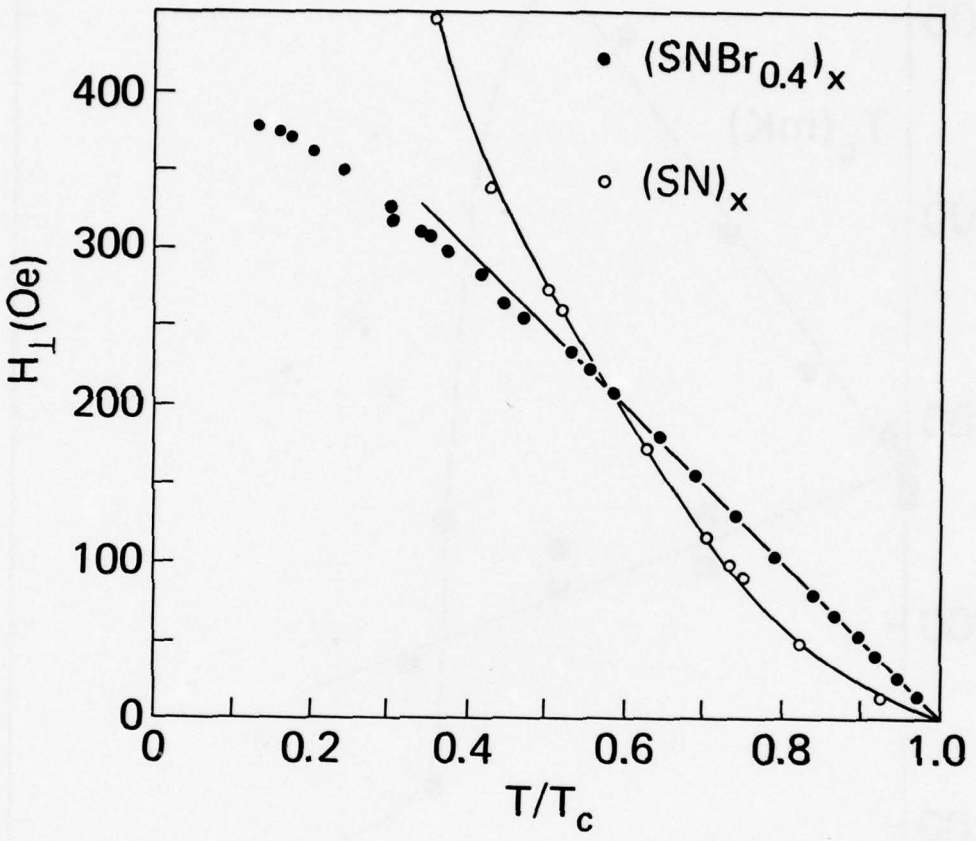

Figure 10. Perpendicular critical field versus reduced temperature before and after bromination [7].

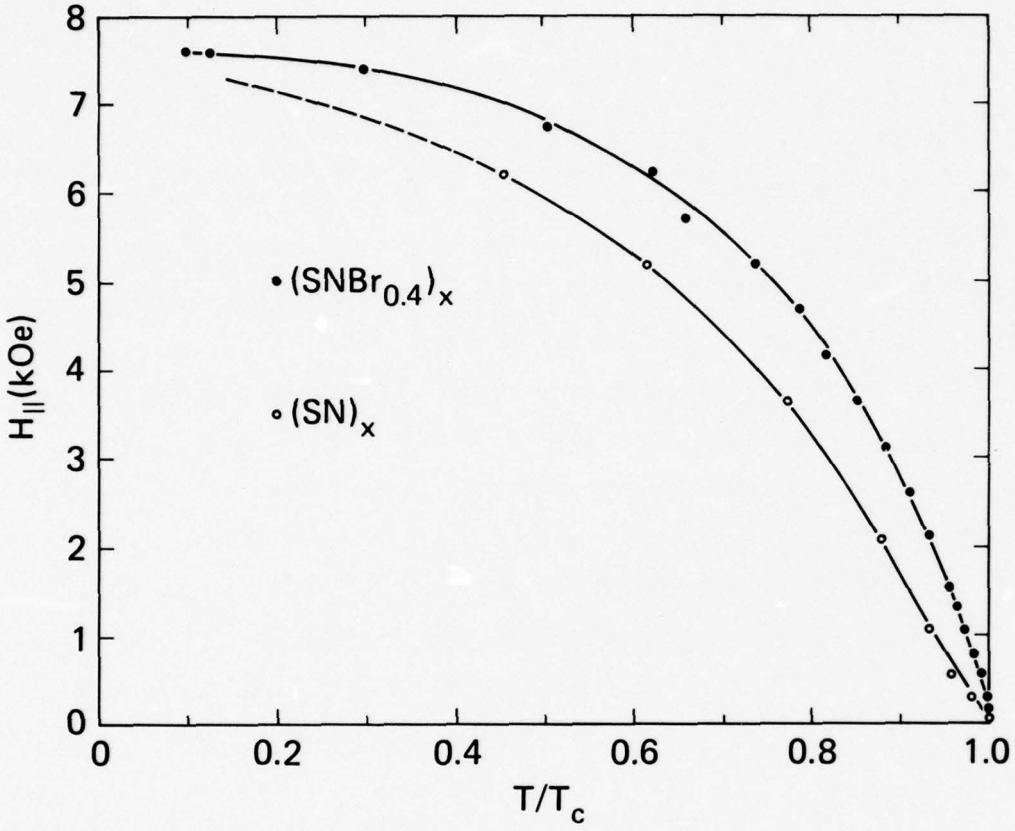

Figure 11. Parallel critical field versus reduced temperature before and after bromination [7].

STUDIES OF CuCl at ELEVATED PRESSURES

E. F. Skelton*
Naval Research Laboratory

Considerable international attention has recently been focused on CuCl because of reports by Soviet scientists of an extremely large diamagnetic anomaly at 5 kbar pressure and at temperatures above 100 K (Fig. 1) [1]. Brandt, Kuvschinnikov, Rusakov, and Semenov have interpreted their experimental observations as evidence of a state of "perfect" diamagnetism which they identify as a Meissner effect [2]. They further suggest that this may be an example of high temperature "excitonic" superconductivity. Preliminary reports of anomalous diamagnetic susceptibilities have also been made by I. Lefkowitz and co-workers and by C. W. Chu and his colleagues [1]. In all cases, the effects appear to be associated with non-equilibrium conditions, as they are observed only under conditions of very rapid cooling or warming and only in "certain" samples.

Another unusual phenomena observed in CuCl is the pressure dependence of the room temperature resistivity. Originally Serebryanaya, Popova, and Rusakov[3] and, subsequent to that Chu, Early, Geballe, Rusakov and Schwall [4], reported a precipitous drop in the resistivity of more than six-orders of magnitude at about 40 kbar, followed by an equally large rise at higher pressures. Serebryanaya et al. report a resistivity above 100 kbar of about 10^3 ohm-cm, slightly greater than the ambient pressure value [3]. The phase diagram of CuCl is rather complex and not yet completely understood; a summary of the available data is presented in Fig. 2.

Several months ago, studies were undertaken at NRL with the objective of providing additional information on some of the unusual properties of this material. All samples used in this work were freshly prepared within days of the various measurements by first forming a saturated solution of CuCl in 5N-HCl. The solution was then diluted 9:1 with distilled water, the CuCl filtered out, and subsequently washed in glacial acetic acid, ethanol, and finally, dry ether. The product was dried in an oven at about 90 C and stored in a desiccator under vacuum.

High pressure x-ray diffraction measurements were performed in a diamond-anvil pressure cell to confirm the observations of Serebryanaya et al. [3] of a zinc blende-to-tetragonal phase transformation at room temperature and about 60 kbar, as well as a tetragonal-to-NaCl transition at higher pressures. Specifically, our preliminary data show approximately a 14% volume reduction at 60 ± 2 kbar and less than an 1% volume change at 108 ± 3 kbar at the tetragonal-to-NaCl transition. We also find the NaCl-structure stable to 225 ± 6 kbar. This information is summarized in terms of the compressibility data plotted in Fig. 3.

---

*Other researchers contributing to the results reported here include F. L. Carter, C. T. Ewing, F. J. Rachford, and A. W. Webb from NRL, I. L. Spain and S. C. Yu from the University of Maryland, and R. A. Hein from NSF.

We have also monitored the optical properties of the samples in transmitted white light in a manner similar to that employed by VanValkenburg [5] in his earlier studies of selected silver and cuprous halides. Contrary to our aforementioned high pressure techniques, the optical properties of CuCl were examined in an ungasketed diamond-cell. Thus the sample is observed throughout a pronounced pressure gradient ranging from ambient at the periphery, to a maximum value near the center of the cell. The cell was clamped to a pressure estimated to be in excess of 100 kbar and a series of four microphotographs were recorded (Fig. 4). The dark ring seen in all frames was observed immediately after pressurization. The opacity in the central region was observed to grow with time; approximately twelve hours were required to achieve the condition in frame 4 of Fig. 4, after which no further changes were detected. These observations were readily repeated on several samples and are similar to the results reported earlier by VanValkenburg [5]. It was observed however that the sluggishness of the central, opaque transition did appear to increase with increased age of the samples. Upon release of pressure, the material was observed to transform back to its original transparent form. The central, opaque region generally passed through an intermediate brownish stage as the pressure was lowered. Samples similar to those shown in Fig. 4 were also cooled to L-He temperatures; it was found that after cryogenic cooling, the reverse transformation was extremely sluggish -- in one instance, the opacity remained for seven days after release of the pressure, thereby suggesting a thermally driven reaction. Based on our x-ray measurements, we believe the central, opaque form to be the NaCl-structure.

In a separate, but similar experiment, the relative magnetic susceptibility of CuCl was monitored with an a.c. mutual inductance bridge. It was found that the growing opacity discussed above was accompanied by a strong change in the relative magnetic susceptibility (Fig. 5). Once the optical properties of the sample reached a stationary state, the susceptibility stabilized, as evidenced by the relatively small variation of the signal 24-hours after pressurization. A similar phenomenon was observed in what is believed to be the first example of microwave absorption measurements in a diamond anvil pressure cell [6]. In this case the CuCl filled pressure cavity was contained in the inductive leg of a microwave resonance circuit. Again, immediately after pressurization, there was a significant and continued increase in the Q of the circuit and an accompanying shift in the resonance frequency. As the growth of the opaque phase waned, both the Q and the resonance frequency stabilized. All indications are that the transformation involved is to a more conductive or metal-like phase. This is inconsistent with the observed increase in the resistivity in this pressure region reported in Ref. [3] and [4].

Several mechanisms have been proposed to explain the aforementioned anomalous diamagnetic susceptibility. Brandt et al. [2] have suggested that this may be the first example of electron pairing through excitonic states, as originally proposed by Ginsburg [7]. The idea of Allender, Bray, and Bardeen [8] that this mechanism may be enhanced by the close interaction of a metal with a Fermi energy inside the semi-conductor band gap, thereby providing an ample source of electrons for the excitonic coupling has also been cited in this regard.*

---

*We are grateful to Dr. Feldman of NRL for pointing out that the predictions of potentially very high superconducting transition temperatures in these models, e.g., $T_c > 100$ K (cf. [9]) has been criticized by Phillips [10].

Abrikosov [11] has suggested that the anamolous properties may be the result of the formation of "metallic excitonium," i.e., a Wigner-hole lattice, and that the electron pairing can couple through phonons in the Wigner lattice. Finally, Blount and Phillips have proposed that much of the pecular behavior of CuCl may be due to a Guinier-Preston transitional precipitate occurring through the disproportionation reaction: $2CuCl \rightarrow CuCl_2 + Cu$.

We have undertaken a series of experiments to assess the extent to which the aforementioned disproportionation is enhanced by elevated pressures. A CuCl sample was pressurized in the NRL tetrahedral press to 60 kbar and held at that pressure for about 20-hours; before releasing the pressure, the sample was quenched to L-N_2 temperatures. The specimen was then quickly transferred to the sample chamber of an ESCA facility. Scans were made to identify the presence of Cu, Cu^+, and Cu^{2+}. In Cu, the ESCA cross-section is greatest for the 2p-3/2 electron for which the binding energies are 932.4, 931.9, and 935.5 eV for Cu, Cu^+, and Cu^{2+}, respectively. Three ESCA scans in the energy range of interest are shown in Fig. 6. The scans for both the unpressed sample and the interior bulk of the pressed sample (24 hours after release of pressure) show no signs of any cupric ions. The surface of the pressed sample however (middle curve) does show a cupric signal at about 935 eV. The poor quality of the scan in this case is due to the presence of carbon also found on the surface which is predominately caused by the graphite electrical contacts used in this particular run. It is at present unclear whether the absence of a cupric signal from the interior of the pressed sample is due to the fact that the disproportionation is a surface effect or a retransformation back to the cuprous form. In any event, the data are not yet conclusive and additional studies involving, inter alia, extended ESR and compressibility measurements of $CuCl_2$ are presently underway.

References:

1. Phys. Today, Sept., 1978; pp. 17-19.

2. N. B. Brandt, S. V. Kuvschinnikov, A. P. Rusakov, and M. V. Semenov, Pis'ma. Zh. Eksp. Theo. Fiz. 27, 37 (05 Jan. 78); Sov. Phys. JETP Lett. 27, 33 (1978).

3. N. R. Serebryanaya, S. V. Popova, and A. P. Rusakov, Fiz. Tverd. Tela 17, 2772 (1975); Sov. Phys. Solid State 17, 1843 (1976).

4. C. W. Chu, S. Early, T. H. Geballe, A. Rusakov, and R. E. Schwall, J. Phys. C: Solid State Phys. 8, L241 (1975).

5. A. VanValkenburg, J. Res. NBS 68A, 97 (1964).

6. F. J. Rachford, I. L. Spain, and E. F. Skelton - to be published.

7. V. L. Ginsburg, Usp. Fiz. Nauk 101, 185 (1970); Sov. Phys. Usp. 13, 355 (1970).

8. D. Allender, J. Bray and J. Bardeen, Phys. Rev. B7, 1020 (1973).

9. A. P. Rusakov, Phys. Stat. Sol.(b) 72, 503 (1975).

10. J. C. Phillips, Phys. kev. Lett. 29, 1551 (1972).

11. A. P. Rusakov, Pis'ma. Zh. Eksp. Theo. Fiz. 27, (1978); Sov. Phys. JETP 27, (1978).

12. E. I. Blount and J. C. Phillips - unpublished, (1978).

13. E. Rapport and C. W. F. T. Pistorious, Phys. Rev. 172, 838 (1968).

14. V. Meisalo and M. Kalliomäki, High Temp.-High Press. 5, 663 (1973).

15. A. L. Edwards and H. G. Drickamer, Phys. Rev. 122, 1149 (1961).

16. R. S. Bradley, D. C. Munro, and P. N. Spencer, Trans. Faraday Soc 65, 1912 (1969).

17. A. P. Rusakov, S. G. Grigoryan, A. V. Omel'chenko, and A. E. Kadyshevich, Zh. Eksp. Theo. Fiz. 72, 726 (1977); Sov. Phys. JETP 45, 380 (1977).

18. A. P. Rusakov, A. V. Omel'chenko, V. N. Laukhin, and S. G.Grigoryan, Fiz. Tverd. Tela (Leningrad) 19, 1167 (1977); Sov. Phys.-Solid State 19, 680 (1977).

19. P. W. Bridgman, Proc. Am. Acad. Arts and Sci. 67, 345 (1932).

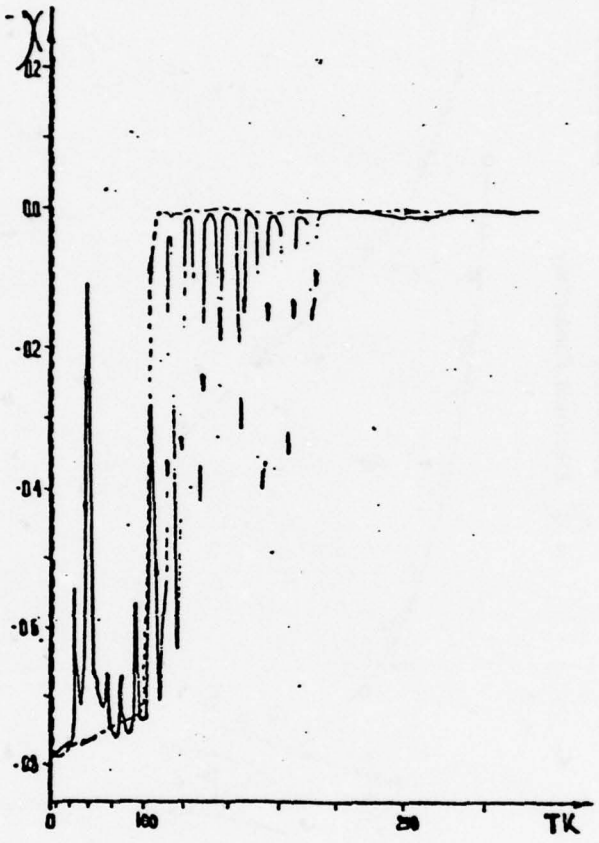

Figure 1

Temperature dependence of the diamagnetic susceptibility of CuCl at 5 kbar on cooling (solid curve) and warming (dashed curve). (Taken from Ref. [2].)

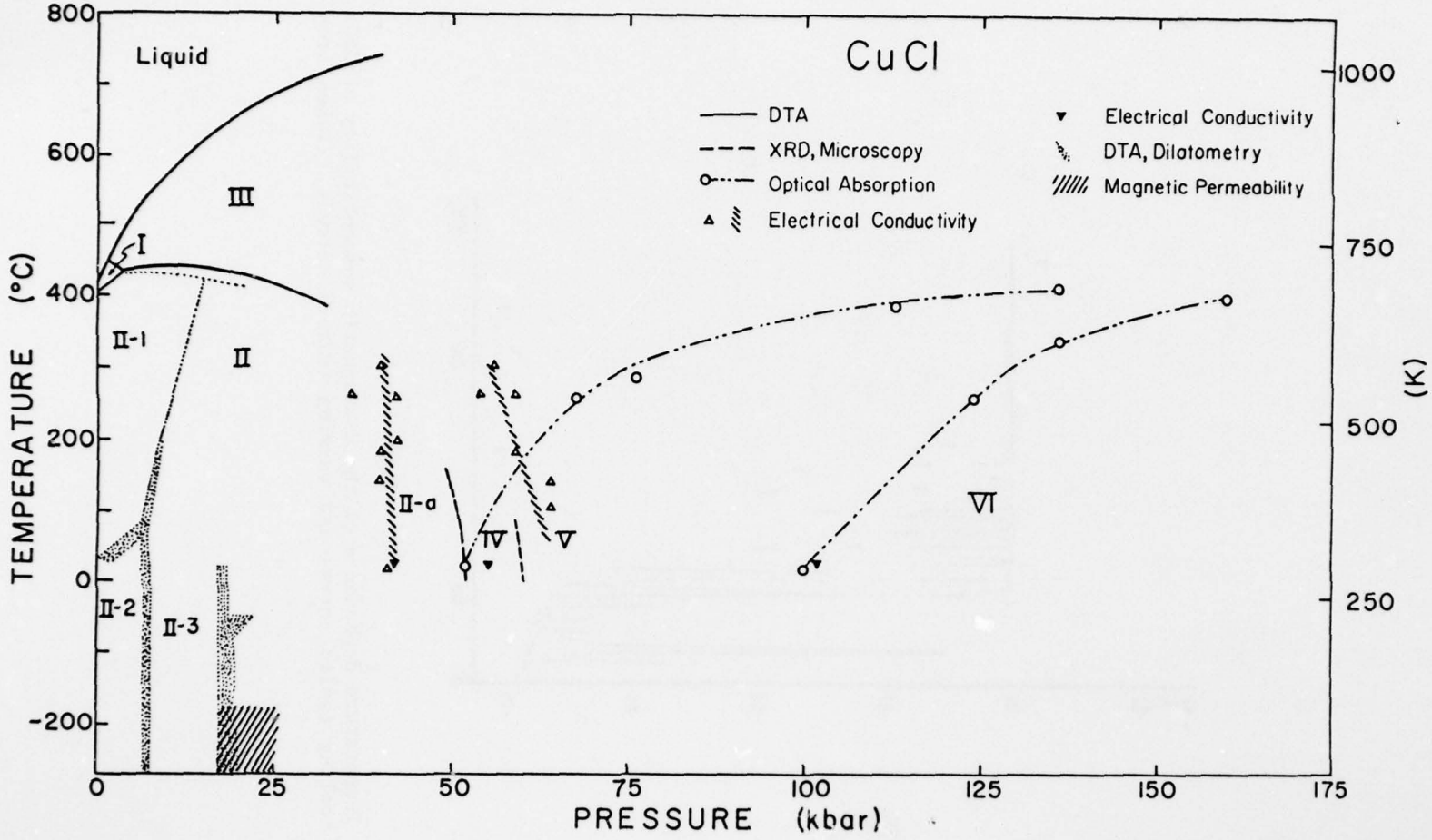

Figure 2

Composite phase diagram for CuCl based on published DTA [13], XRD & microscopy [14], optical absorption [15], electrical conductivity [3 & 16], DTA & dilatometry [16 & 17], and magnetic permeability [16 & 17] data.

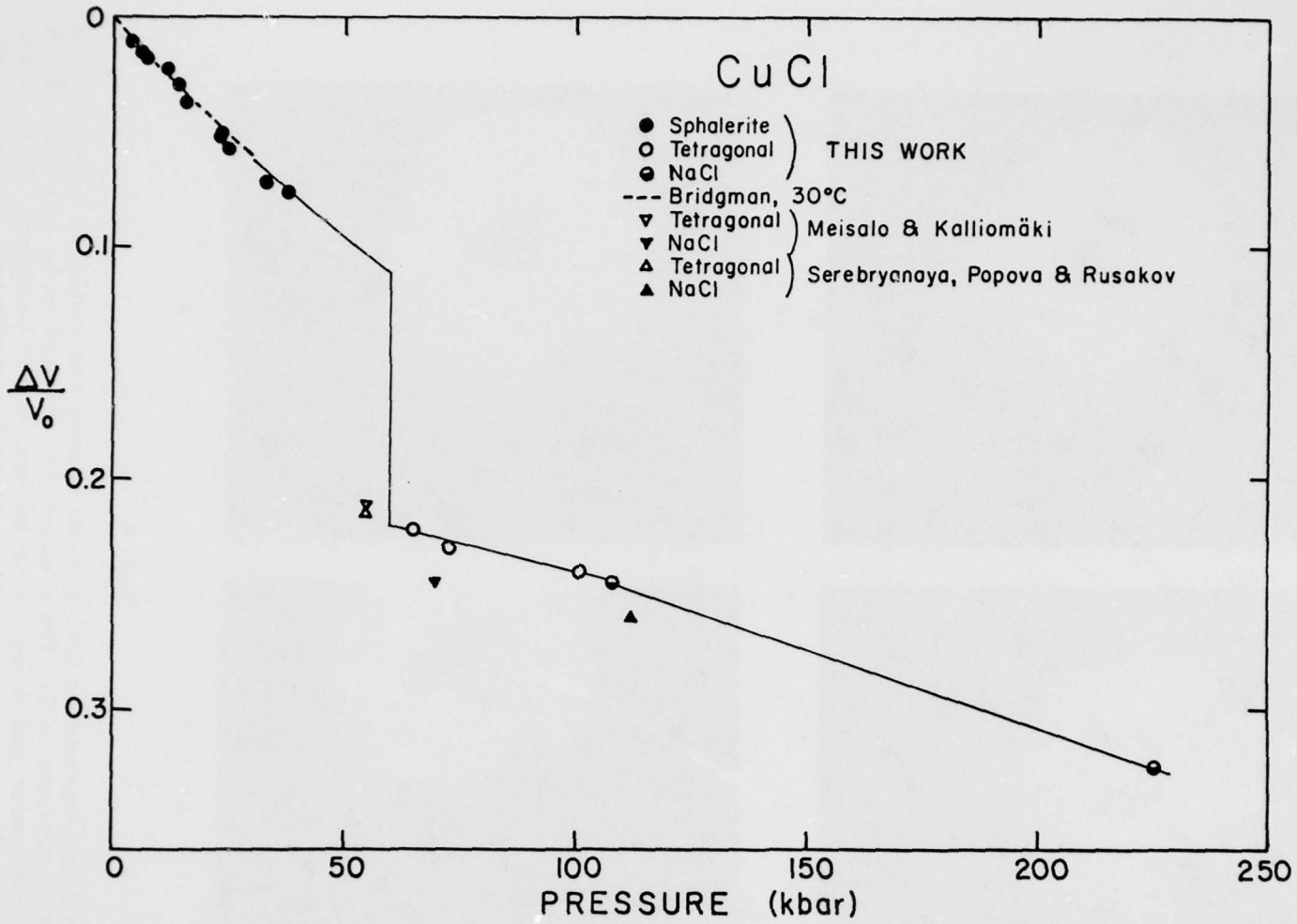

Figure 3

3. Compressibility and structure of CuCl based on room temperature x-ray diffraction measurements (this work) and compared with earlier measurements by Bridgman [19], Meisalo and Kalliomäki [14], and Serebryanaya et al. [3].

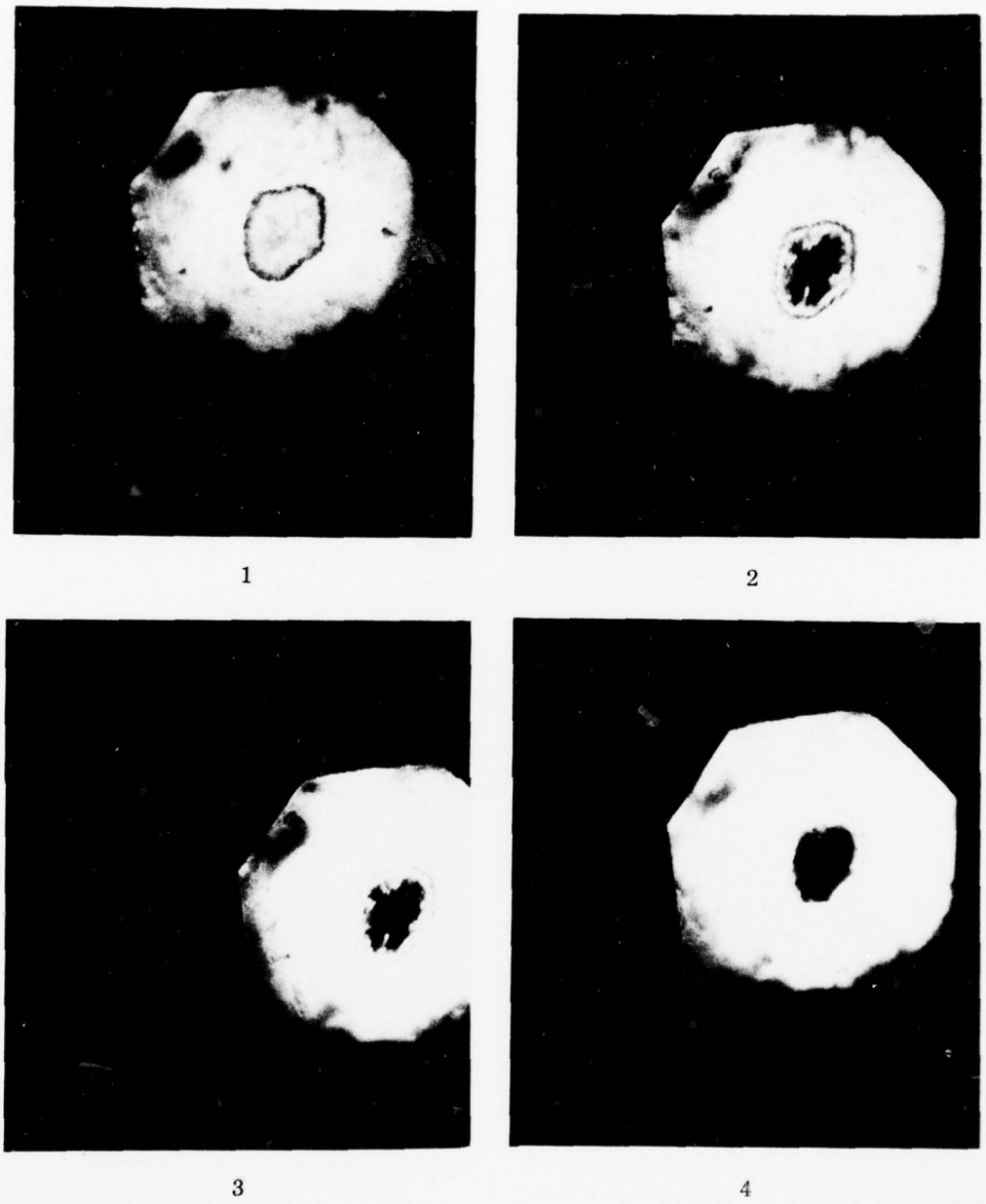

Figure 4

Microphotographs of CuCl pressed between the anvils of a non-gasketed diamond-anvil pressure cell. The pressure is estimated to be in excess of 100 kbar near the center and drops off to ambient at the periphery. Frame 1 was taken immediately after pressurization, frame 2 approximately one hour later, frame 3 several hours later, and frame 4 approximately 12 hours later. See text for additional details.

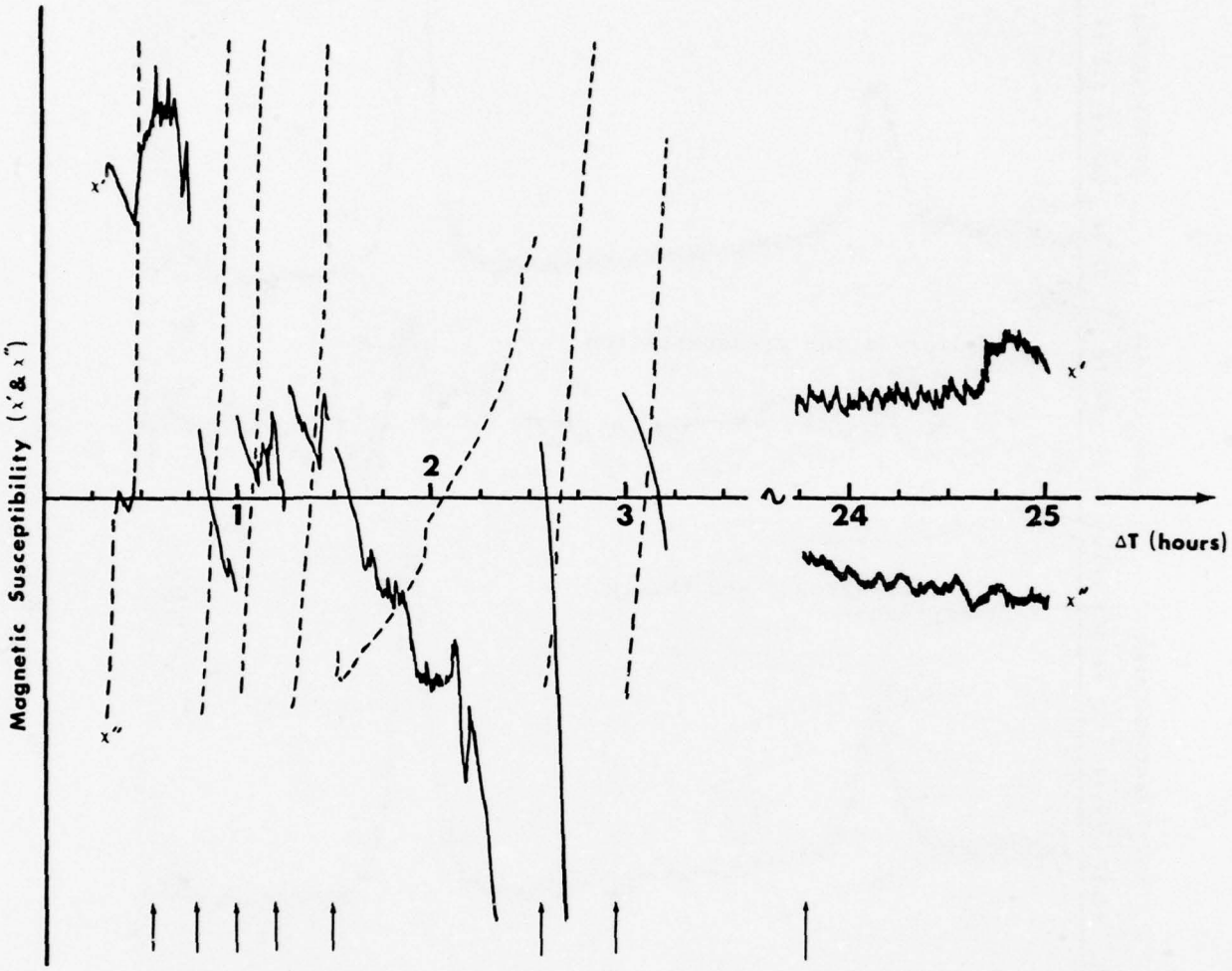

Figure 5

Time dependence of the in-phase (solid line) and out-of-phase (dashed line) components of the relative magnetic susceptibility of CuCl in an ungasketed diamond-anvil pressure cell versus the time after pressurization. The growing opacity shown in the central regions in Fig. 4 is accompanied by the strong, continued changed in the relative susceptibility. The bridge was rebalanced throughout the run to bring the signal back on scale; these points are identified by arrows in the lower portion of the figure.

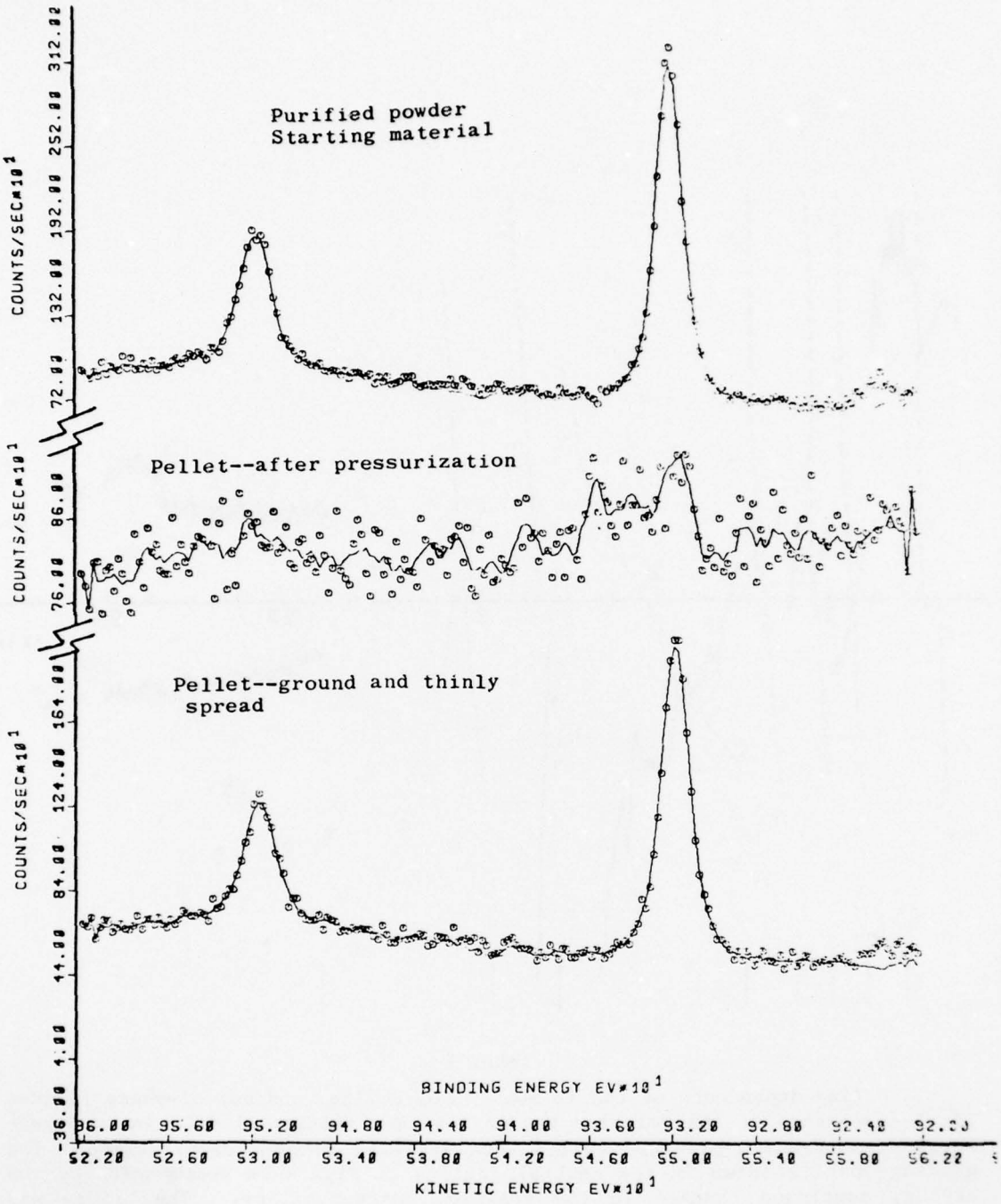

Figure 6

ESCA scan of several CuCl samples. The top curve is from an unpressed sample and shows strong cuprous peaks at 951.6 eV (2p-1/2) and 932 eV (2p-3/2). The middle curve was recorded after the sample had been pressed to 60 kbar for about 20-hours and quenched to L-N_2 temperatures; indications of both cuprous and cupric (935 eV) peaks are present. The bottom curve is from the interior of the pressed material and about 24-hours after removal from the press. See text for additional details.

Superconducting Properties of Hydride Systems

D. A. Papaconstantopoulos, B. M. Klein and L. L. Boyer

We are concerned here with the phenomenon of superconductivity in metal hydrides. We present a summary of the experimental situation and an outline of the theoretical interpretation given by the Naval Research Laboratory (NRL) group in the case of palladium-based hydrides.

Hydrogen added in metals usually occupies the octahedral site in fcc lattices and the tetrahedral site in bcc lattices. The physical and chemical properties of these hydrides are often quite different from those of the host metal. An understanding of these differences has been attempted in the past via two simple models. The proton model which has the hydrogen electrons filling up the empty upper states of the host metal, and the anion model which adds a low-lying hydrogen state to the states of the host metal. Since the first works of Switendick[1] appeared, it has been recognized that the band theory picture — which accounts for both the proton and anion models — is the most reliable method to provide the foundations for interpreting the experiments in metal hydrides.

The first example of enhancement of the superconducting temperature T_c due to the presence of hydrogen, was reported in 1970 by Satterthwaite and Toepke[2] for Th_4H_{15}. In 1972

Skoskiewicz[3] discovered superconductivity in PdH, and shortly after Stritzker and Buckel[4] using ion-implanation confirmed this result and also found that replacement of H by D increases T_c even further (inverse isotope effect). Several measurements of T_c in PdH followed these discoveries and many theories were proposed to explain these phenomena.

We present here the theoretical interpretation offered by the NRL group and co-workers.[5-8] This theory is based on elaborate band structure calculations, neutron scattering data and on an application to compounds of ideas put forward by McMillan,[9] Hopfield[10] and Gaspari-Gyorffy.[11] The results show that the high value of T_c in PdH(D) is mainly due to the softness of the optic mode phonon frequencies which are associated with local hydrogen vibrations. This is a quantitative verification of an earlier suggestion by Ganguly.[12] Ganguly[12] also proposed that the observed inverse isotope effect is caused by the effective increase of the Pd-H force constant over the Pd-D force constant, due to enhanced anharmonicity of the H motion. Using our band structure results and neutron scattering data[13] for both PdD and PdH, we have again confirmed quantitatively Ganguly's idea. We have also calculated the x-dependence of T_c for PdH_x and PdD_x. In this calculation we employed first the rigid band approximation (RBA),[6,7] which allowed us to use the band structure of the stoichiometric case (x=1.0). We then confirmed the validity of the RBA, for a narrow energy range around the Fermi

level, by performing coherent-potential-approximation (CPA) calculations.[8] The physical picture which emerged from both the RBA and the CPA approaches regarding the x-dependence of T_c, is that the strong hydrogen dependence is mostly due to the fact that the wavefunctions at the Fermi level acquire more and more hydrogen s-character with increasing x.

Higher superconducting transition temperatures have been observed by Stritzker[14] in Pd-(Cu,Ag,Au)-H alloys, while lower T_cs have been measured for Pd-(Rh,Ni)-H alloys. We have performed calculations[15] of the electron-phonon interaction and T_c for $Pd_{1-y}Ag_yH_x$ and $Pd_{1-y}Rh_yH_x$ as a function of both y and x, using the virtual crystal approximation to allustrate the y variation and both the RBA and the CPA to treat the x-dependence. We have found that addition of Rh to PdH decreases the hydrogen site electron-phonon interaction η_H, while addition of Ag to PdH increases η_H. Due to the fact that there are no neutron-scattering data available for a wide range of concentrations in these alloys, we cannot make a precise determination of T_c. However, the above variation of η_H strongly indicates decrease of T_c by the addition of Rh and enhancement of T_c by the addition of Ag.

References

1. A. C. Switendick, Ber. Bunsenges. Phys. Chem. 76, 535 (1972).
2. C. B. Satterthwaite and I. L. Toepke, Phys. Rev. Lett. 25 741 (1970).
3. T. Skoskiewicz, Phys. Status Solidi A 11, K123 (1972).
4. B. Stritzker and W. Buckel, Z. Phys. 257, 1 (1972).
5. D. A. Papaconstantopoulos and B. M. Klein, Phys. Rev. Lett. 35, 110 (1975).
6. B. M. Klein, E. N. Economou and D. A. Papaconstantopoulos, Phys. Rev. Lett. 39, 574 (1977).
7. D. A. Papaconstantopoulos, B. M. Klein, E. N. Economou and L. L. Boyer, Phys. Rev. B 17, 141 (1978).
8. D. A. Papaconstantopoulos, B. M. Klein, J. S. Faulkner and L. L. Boyer, Phys. Rev. Sept. (1978).
9. W. L. McMillan, Phys. Rev. 167, 331 (1968).
10. J. J. Hopfield, Phys. Rev. 186, 443 (1969).
11. G. D. Gaspari and B. L. Gyorffy, Phys. Rev. Lett. 28, 801 (1972).
12. B. N. Ganguly, Z. Phys. 265, 433 (1973); Z. Phys. B 22, 127 (1975).
13. J. M. Rowe, J. J. Rush, H. G. Smith, M. Mostoller and H. E. Flotow, Phys. Rev. Lett. 33, 1297 (1974); A. Rahman, K. Skold, C. Pelizzari and S. K. Sinha, Phys. Rev. B 14, 3630 (1976).
14. B. Stritzker, Z. Phys. 268, 261 (1974); B. Stritzker, Proc. of 14th Intern. Confer. on Low Temperature Physics, Ed. Krusius and Vuorio, Vol. 2, p. 32 (1975).
15. D. A. Papaconstantopoulos, E. N. Economou, B. K. Klein and L. L. Boyer, Journal de Physique Suppl. 6, Vol. 1, p. C6-435 (1978).

Pd-H

Macklet, Schindler, Gillespie		Specific Heat
Skoskiewicz (Pd-Ni-H)		H loaded by electrolysis
Stritzker and Buckel		Ion implanation
Harper et al.		Electrolytic charging
Miller and Satterthwaite		" "
Sansores and Glover		PdH films by quench condensation
Schirber and Northrup		Prepared by H_2-gas pressure
McLachlan et al.		Resistivity-Optical phonons
Rowe et al.	Pd-D	Coherent neutron scattering
Rahman et al.	Pd-H	Anharmonicity
Ganguly		"
Eichler et al.		
Dynes and Garno		Tunneling

Th_4H_{15}(D) AND ThH_2

SATTERTHWAITE AND TOEPKE	$T_c = 8.3^o$ K
	NO ISOTOPE EFFECT
WINTER AND RIES	CLUSTER CALCULATIONS
LAU ET AL.	NMR STUDY
WEAVER ET AL.	PHOTOELECTRON SPECTRA
	NARROW OCCUPIED CONDUCTION BAND 1 eV
	LARGE GAP FROM BONDING STATES 2 eV

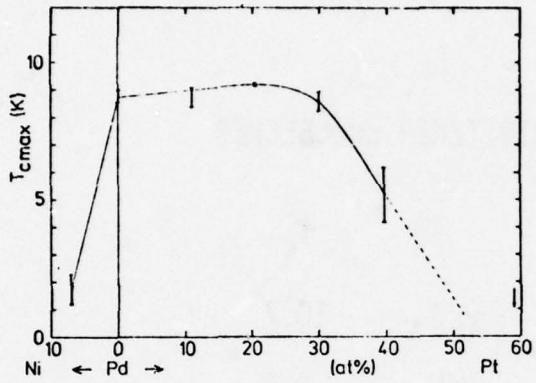

Fig. 1: Maximum T_c in the (Ni-Pd-Pt)-H system

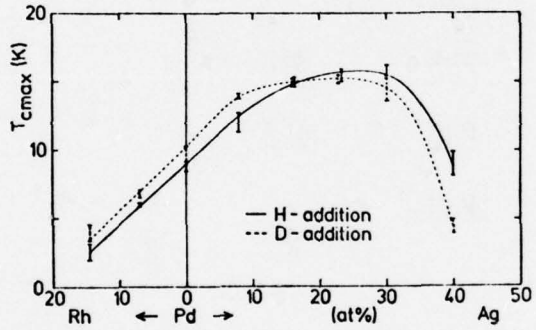

FIG. 2: MAXIMUM T_c IN THE (Rh-Pd-Ag)-(H,D) SYSTEMS

	Pd-Cu-H	Pd-Ag-H	Pd-Au-H
T_c	16.6	15.6	13.6
NOBLE METAL (AT %)	45	30	16
$H/_{MET.}$-RATIO	0.7	0.8	0.9

STRITZKER AND BECKER

	T_c
PaD	10.7
PaH	8.8
PaLI	-
PaB	3.8
PaC	1.3
PaN	-

Nb-H

WELTER AND JOHNEN: T_c AND RESISTIVITY

FOR $x > 0.7$ HYDRIDE PHASE $T_c < 1.3^{o}$ K

FOR $0 < x < 0.7$ TWO-PHASE REGION $T_c = 9.4$ K

RESIDUAL RESISTIVITY EXHIBITS A MAXIMUM AT $x \approx 0.69$

WEAVER ET AL. OPTICAL ABSORPTIVITY SPECTRA

Nb-D

ROWE ET AL. NEUTRON SCATTERING

ACOUSTIC MODES ONLY

V-H

HAUCK VH_2 $T_c = 3.9^{o}$ K

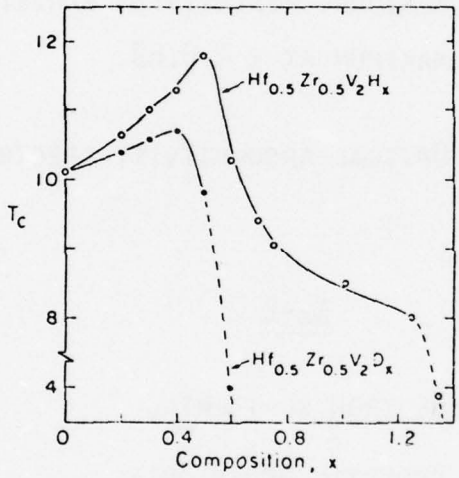

Fig. 1. Variation of T_c with composition, χ, in the alloys $Hf_{0.5}\ Zr_{0.5}V_2H(D)_\chi$

AD-A066 201 NAVAL RESEARCH LAB WASHINGTON D C F/G 20/3
ONR-NRL SUPERCONDUCTING MATERIALS SYMPOSIUM. A FORECAST.(U)
JAN 79 T L FRANCAVILLA, D U GUBSER, S A WOLF

UNCLASSIFIED NRL-MR-3906 SBIE-AD-E000 267 NL

2 OF 2
AD
A066201

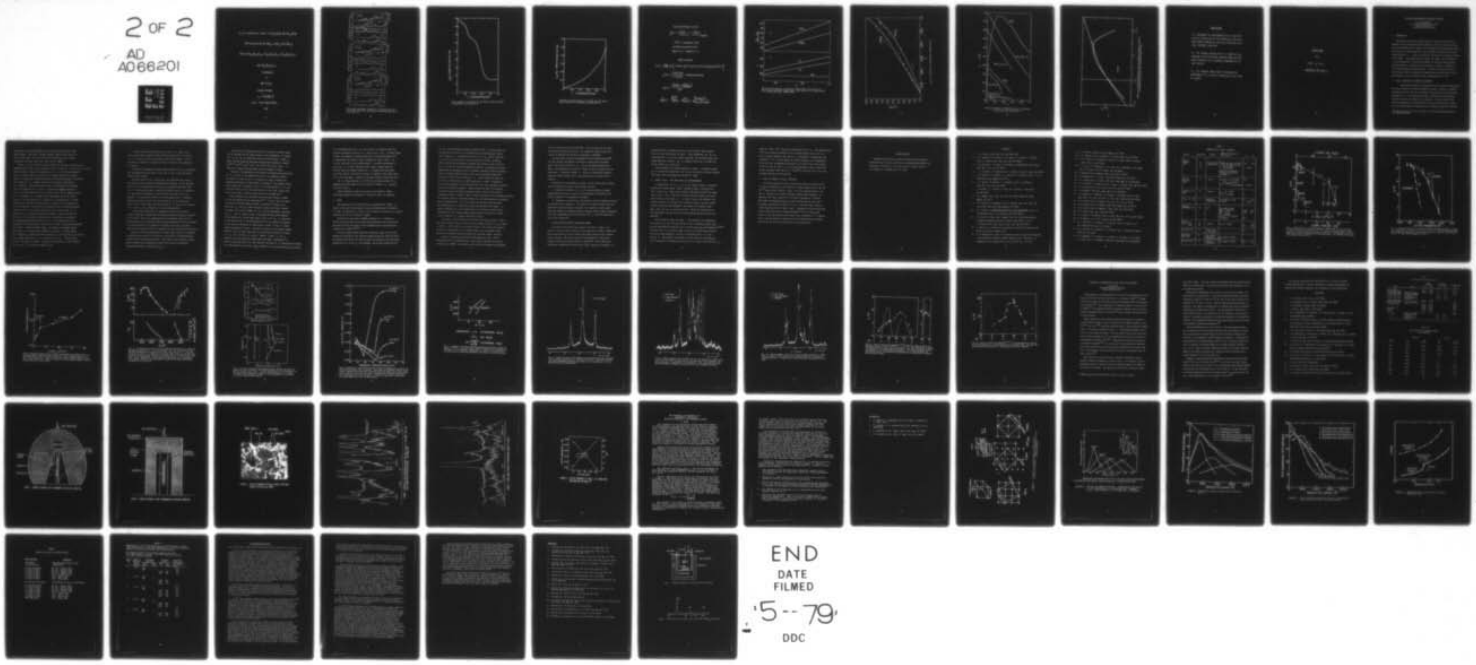

END
DATE
FILMED
5-79
DDC

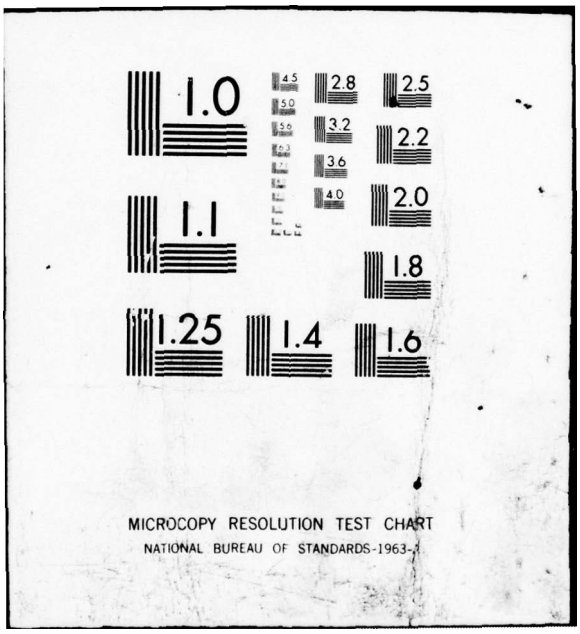
1.0
1.1
1.25
1.4
1.6
1.8
2.0
2.2
2.5
2.8
3.2
3.6
4.0
4.5
5.0
5.6
6.3
7.1
MICROCOPY RESOLUTION TEST CHART
NATIONAL BUREAU OF STANDARDS-1963-A

T_c AS A FUNCTION OF X AND Y IN $Pd_{1-Y}Ag_YH_X$ AND $Pd_{1-Y}Rh_YH_X$

APW CALCULATIONS FOR $PdH_{1.0}$, $AgH_{1.0}$ AND $RhH_{1.0}$

VCA FOR $Pd_{0.7}Ag_{0.3}H_{1.0}$, $Pd_{0.5}Ag_{0.5}H_{1.0}$, $Pd_{0.9}Rh_{0.1}H_{1.0}$

AND $Pd_{0.5}Rh_{0.5}H_{1.0}$

ℓ-COMPONENTS

OF

DOS $n_\ell^A(E_F)$

GASPARI-GYORFFY

$\eta_A = F(n_\ell^A, N_\ell^A, \delta_\ell^A)$

$\eta_A(x)$: RIGID BAND APPROX.

CPA

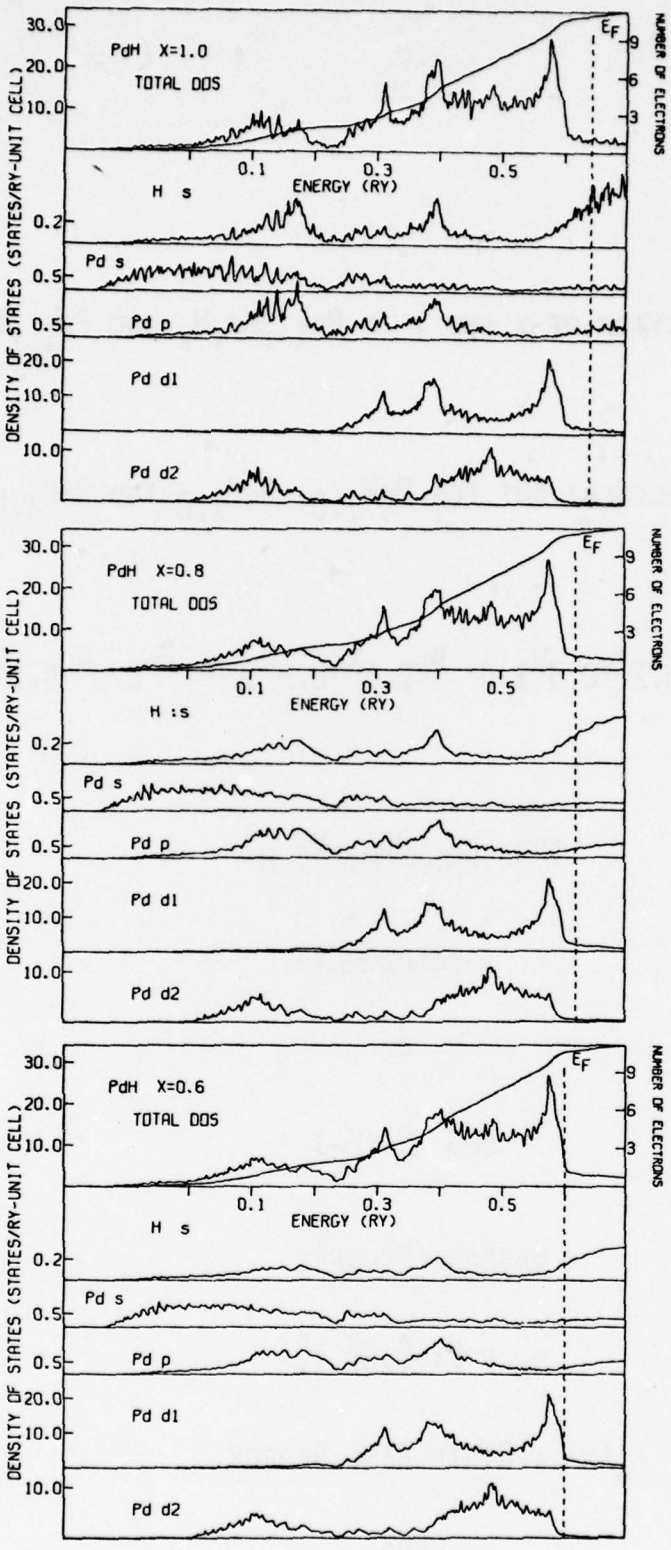

Total and component densities of states plotted vs energy for three hydrogen concentrations x=1.0, 0.8, and 0.6.

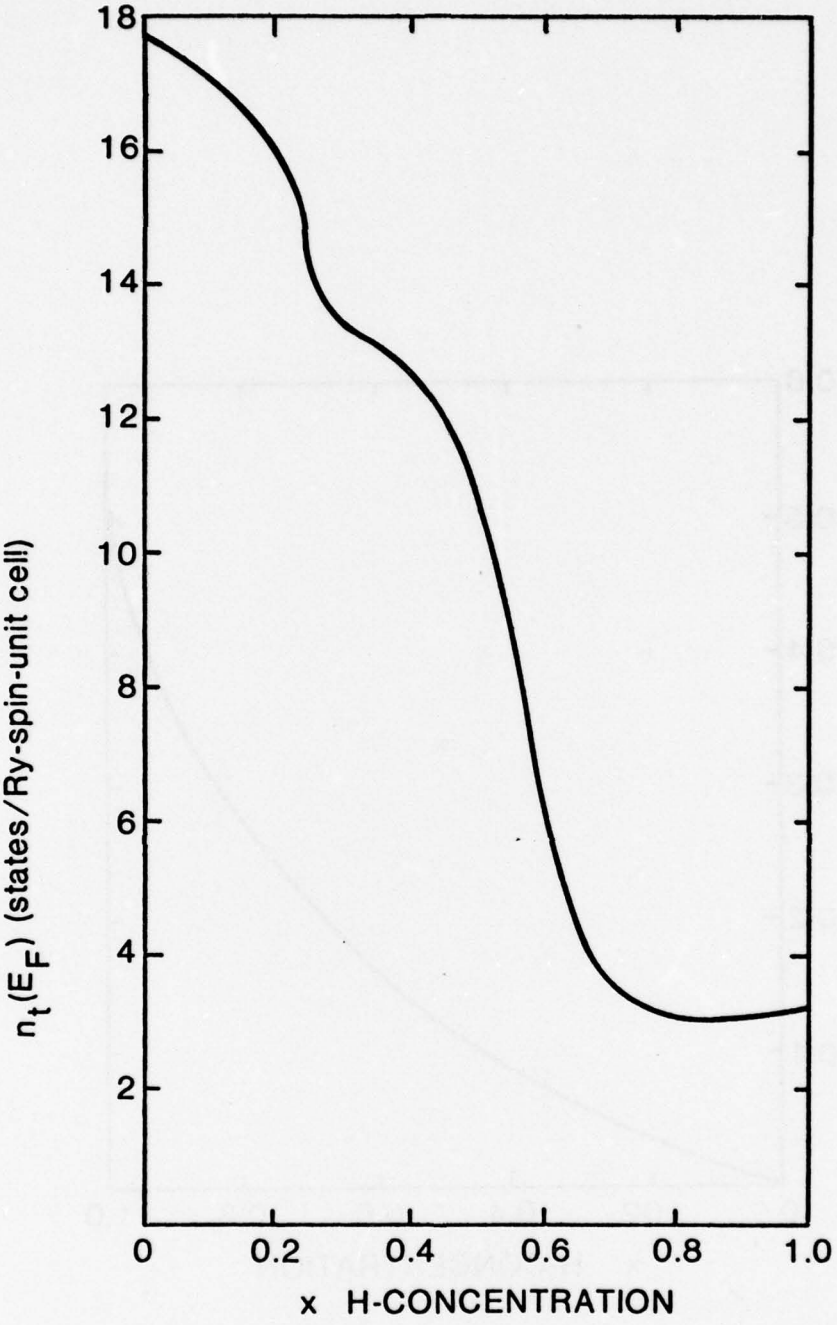

Total density of states at the Fermi level plotted vs hydrogen concentration.

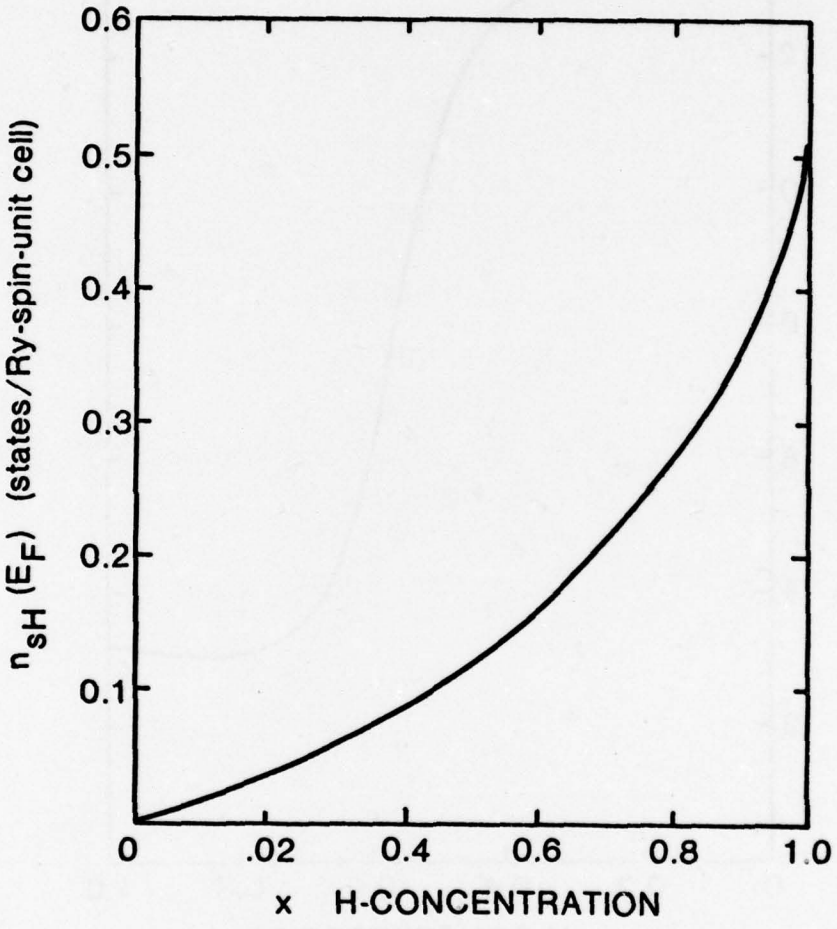

Hydrogen s-like density of states at the Fermi level plotted vs hydrogen concentration.

ELECTRON-PHONON COUPLING

$$\lambda(x) = \left(\frac{\eta(x)}{M\langle\omega^2\rangle} \right)_H + \left(\frac{\eta(x)}{M\langle\omega^2\rangle} \right)_{PD(AG)}$$

$\langle\omega^2\rangle$ = DETERMINED FROM

NEUTRON SCATTERING DATA

ROWE ET AL., RAHMAN ET AL.

McMILLAN-DYNES

$$T_c(x) = \frac{\langle\omega\rangle}{1.20} \exp\left[-1.04(1+\lambda(x))/(\lambda(x)-\mu^*(x)-0.62\lambda(x)\mu^*(x)) \right]$$

$$\mu^*(x) = \frac{0.26\, n_T(E_F)}{1 + n_T(E_F)} \quad \text{BENNEMANN-GARLAND}$$

$$\langle\omega\rangle = \frac{2\left[\alpha^2_H(x) + \alpha^2_{PD(AG)}(x)\right]}{\lambda(x)}$$

$$\alpha^2_H(x) = \frac{\eta_H(x)}{2M_H\omega_H} \quad , \alpha^{2(x)}_{PD(AG)} = \frac{\eta_{PD(AG)}(x)}{2M_{PD(AG)}\omega_{PD(AG)}}$$

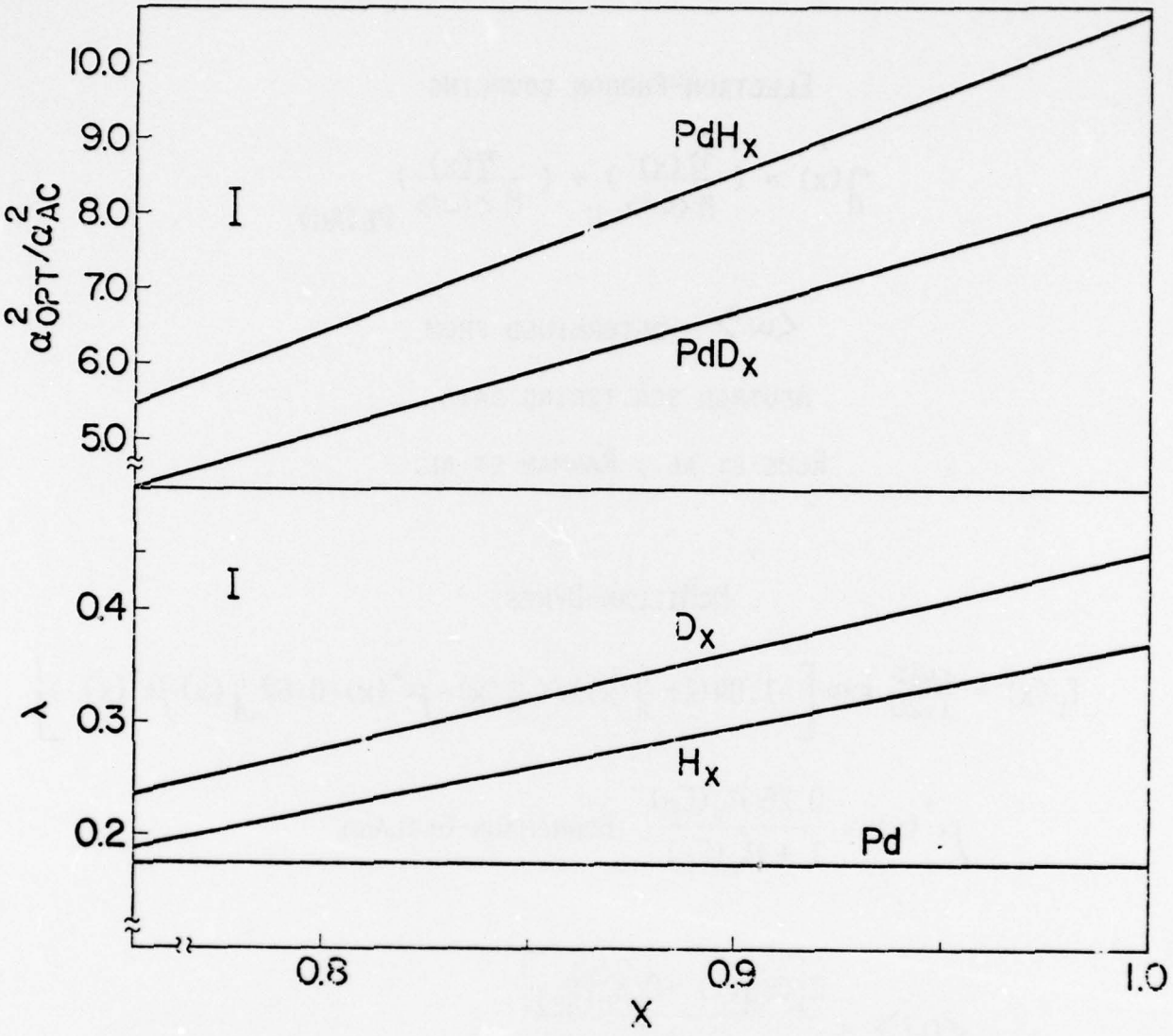

Ratios of the optical to acoustical phonon-mode contributions to the tunneling spectrum (upper panel), and values of λ_j (lower panel) vs x in PdH_x and PdD_x, respectively.

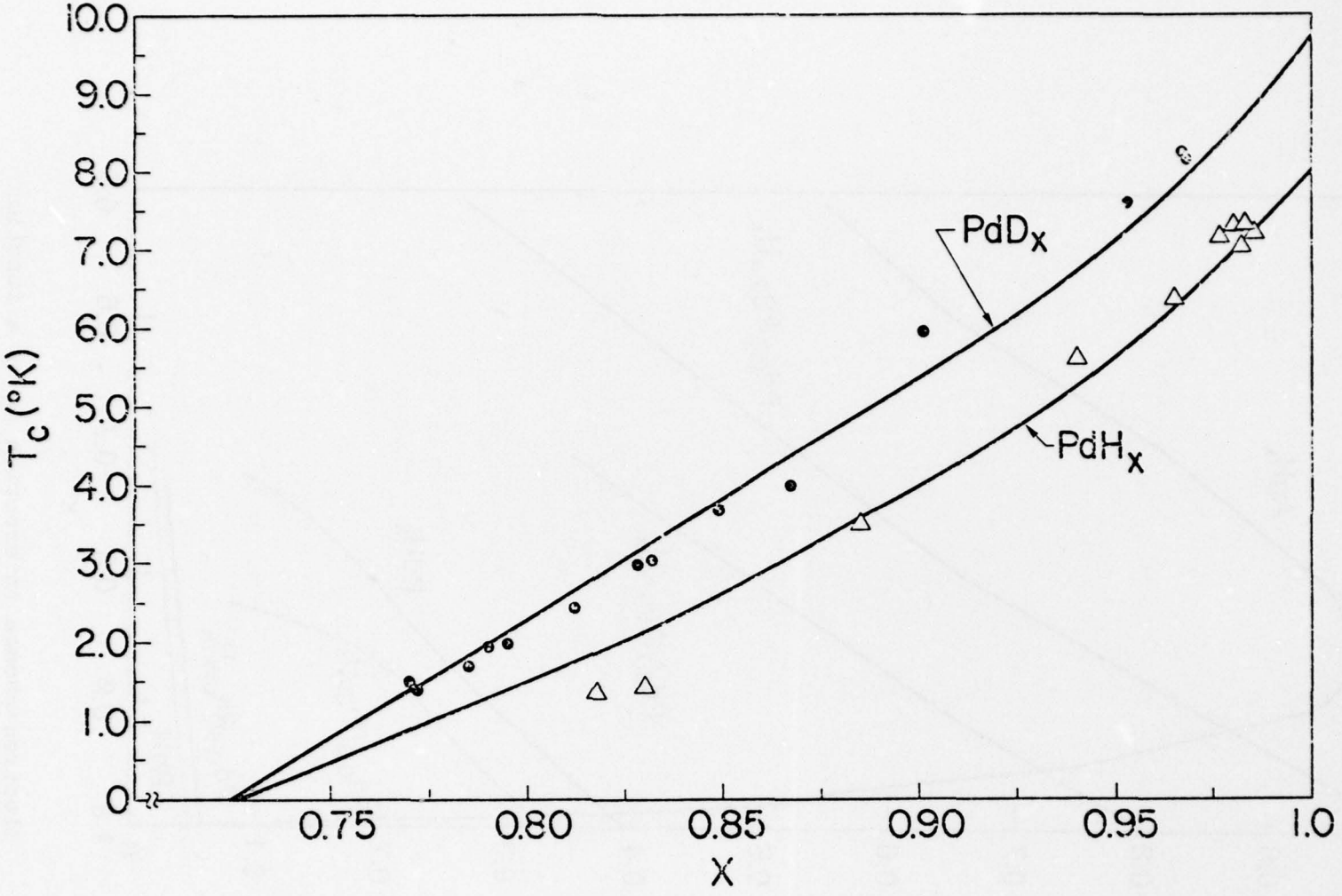

T_c as a function of hydrogen concentration.

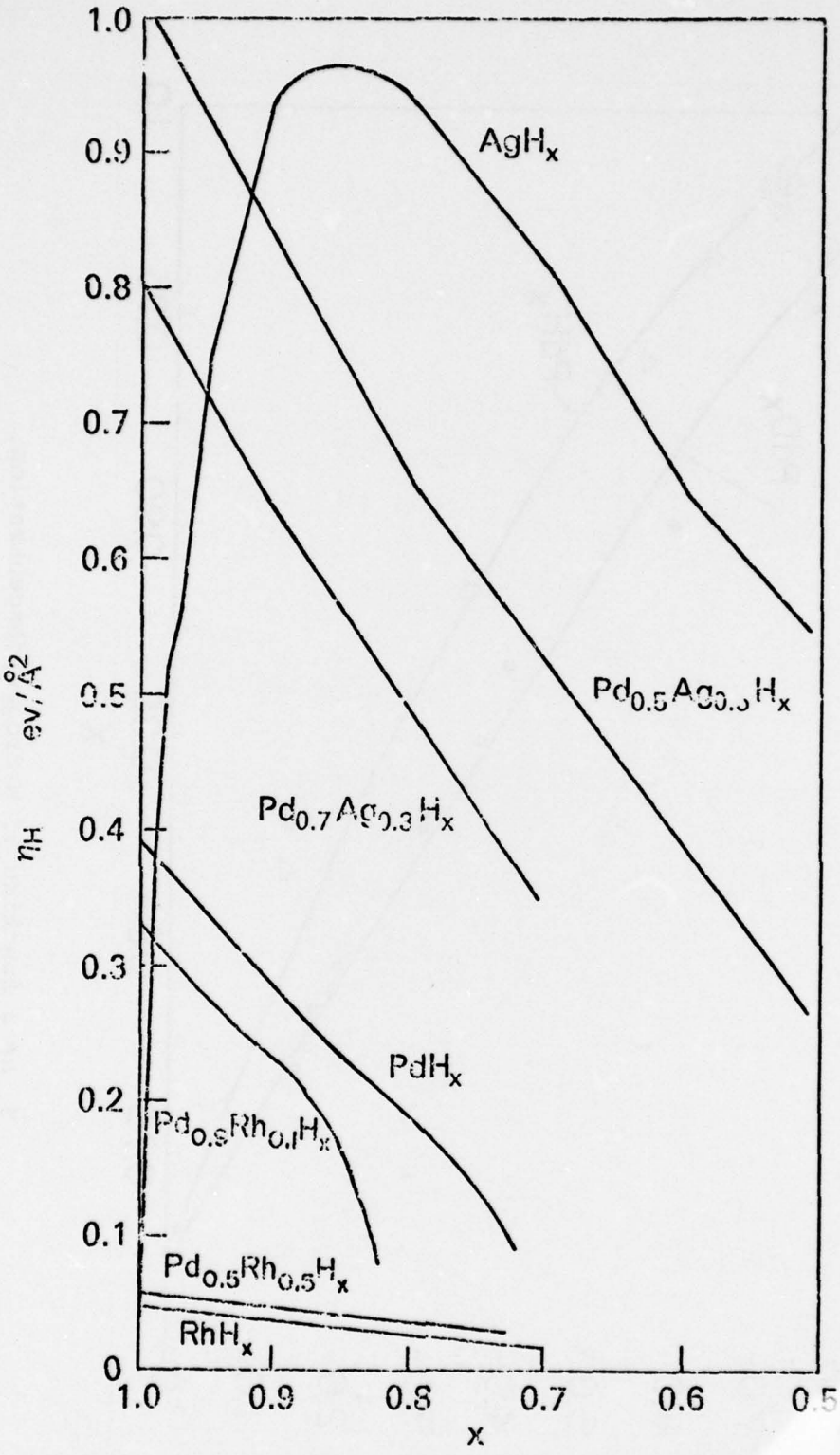

Electron-phonon interaction η_H as a function of hydrogen concentration x.

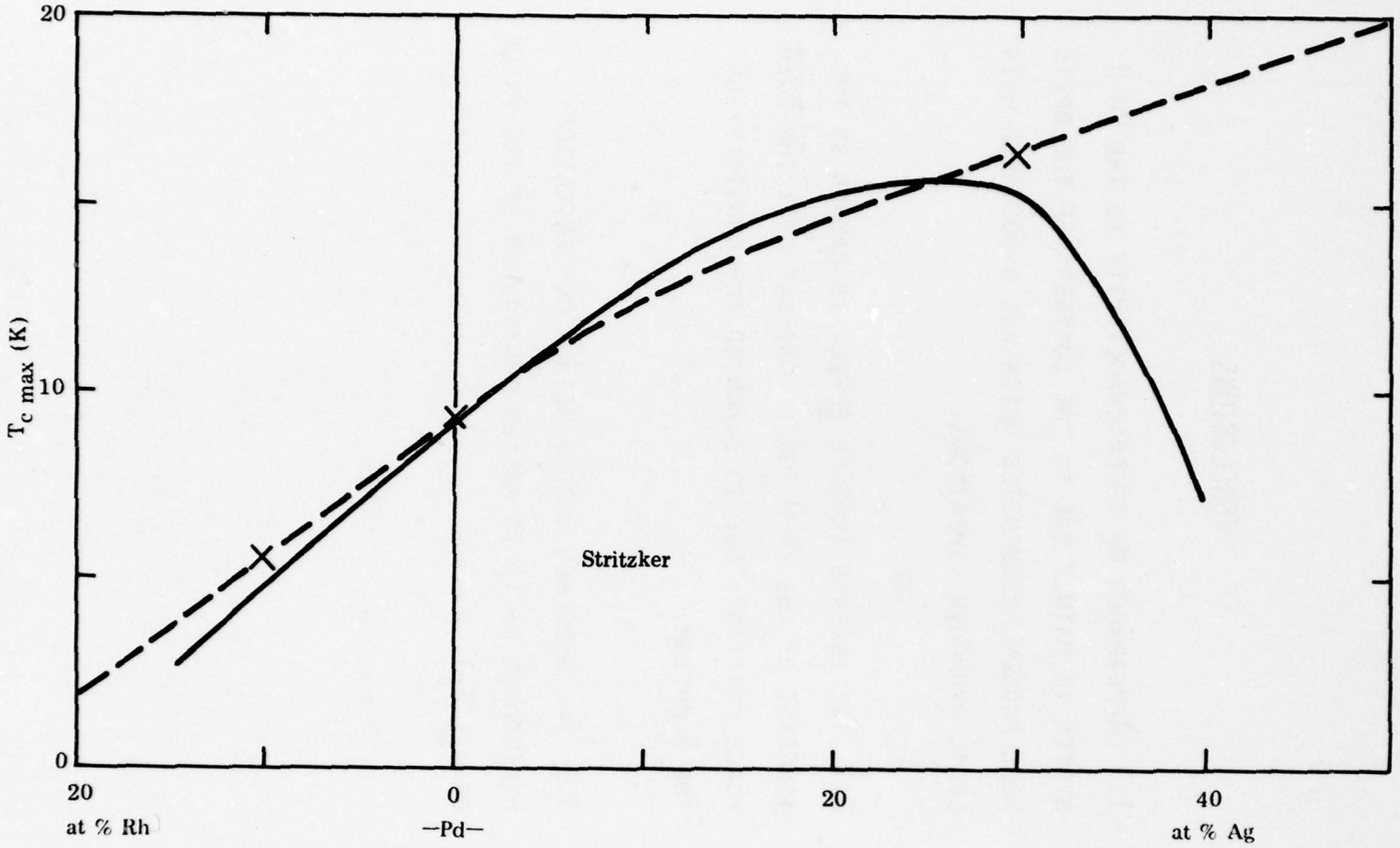

Maximum T_c in the Rh-Pd-Ag-H system. Solid line experiment by Stritzker. Dotted line our calculations with the optic phonon frequencies assumed constant.

CONCLUSIONS

1.) APPEARANCE OF SUPERCONDUCTIVITY IN THE Pa-H SYSTEM IS MAINLY DUE TO THE SOFTNESS OF THE OPTIC MODE PHONON FREQUENCIES WHICH ARE ASSOCIATED WITH LOCAL HYDROGEN VIBRATIONS.

2.) THE INVERSE ISOTOPE EFFECT IS CAUSED BY THE INCREASE OF THE Pa-H FORCE CONSTANT OVER THE Pa-D FORCE CONSTANT, DUE TO ENHANCED ANHARMONICITY OF THE H MOTION.

3.) THE HYDROGEN (NOBLE METAL) CONCENTRATION DEPENDANCE OF T_c IS MAINLY CONTROLLED BY THE VALUE OF $n_{SH}(E_F)$.

PREDICTIONS

Pt-H

Pt-(Cu, Ag, Au)-H

CANDIDATES FOR HIGH T_c

THIN FILM SUPERCONDUCTING MATERIALS RESEARCH

R. H. Hammond*
W. W. Hansen Laboratory of Physics
Stanford University
Stanford, California 94305

1. INTRODUCTION

This paper will discuss a limited number of topics that relate to the synthesis of thin film superconducting materials. These include a discussion of recent published work on Nb_3Ge, and the suggestion of an important impurity that results in a wide divergence in the conditions of formation for optimum superconducting T_c. This is followed by a discussion of the phase stability of A15 Nb_3Si. Concluding that both Nb_3Ge and Nb_3Si are very sensitive to certain impurities, in particular hydrogen, an alternate solution using epitaxial growth to stabilize the A15 structure is reviewed. Speculation on other A15's of potential interest follows. Finally, some recent results on the different types of microstructures obtained using a three source electron beam evaporator, and the critical current pinning found, are noted.

2. Nb_3Ge - VARIABILITY IN RESULTS AND METHODS

Starting with Gavaler,[1] sputtering, CVD, and electron-beam evaporation have been successful in synthesizing high-T_c material. However, it remains a disturbing fact that there is no agreement on the conditions for the optimum performance, i.e., each experimenter finds a different set of experimental parameters that are successful for his apparatus. Can the effects of the method of preparation be separated from the intrinsic properties of Nb_3Ge? Two recent publications both demonstrate the variability and offer a possible

*Supported in part by the Air Force Office of Scientific Research Contract No. F49620-78-C-0009.

explanation: The amount hydrogen in the lattice during formation is the main parameter. The papers: Lanford, Schmidt, Rowell, Poate, Dynes, and Dernier, Appl. Phys. Lett. 32, 339 (1978),[2] and Buitrago, Toth, Goldman, Schwanebeck, and Dayan, Appl. Phys. Lett. 32, 341 (1978).[3]

Figure 1, 2, and 3 taken from several figures in the paper by Lanford et al., summarize their results on two experiments (Curve (1) and (2)). Curve (1), Fig. 1,2,and 3 shows the dramatic effect that hydrogen has on T_c and the lattice parameter when a film with a high-T_c is dipped into a $HF:H_2O$ solution for varying amounts of time, giving a uniform distribution of hydrogen throughout the specimen. The lowering of T_c is roughly linear with the hydrogen concentration, $\Delta T_c \sim 1°K/at.\%H$. Next, they analyzed a series of samples made at differing substrate temperature for T_c and H concentration (without dipping in acid). The results, shown in curve (2) of Fig. 1, also show the apparent effect of H on lowering T_c , although for some unexplained reason the initial slope is $\sim$ 50 times greater, $\Delta T_c \sim 46°K/at.\%$ H, as compared with H doping . Unfortunately, the lattice constants were not shown for these specimens, so it isn't known how it compares with the behavior found on the doped specimens. As shown in Fig. 2, the relation between the lattice constant and T_c is different for H doping as compared with changes in composition, curve (3). This curve is for specimens of differing Ge concentration, resulting in an expanded single phase A15 lattice as the Ge is reduced from its 3:1 composition (as discussed later, the data is for Nb-Ge electron-beam deposited onto Nb-Ir). Radiation damaged Nb_3Ge also exhibits an expanded lattice and reduced T_c: typically these data fit on curve (3). The main feature of H doping is to expand the lattice initially at a fast rate (Fig.2 and 3) with only a slight reduction in T_c as a function of the a_o . Another feature is that it is nearly reversible. Annealing for 10 minutes at $\sim$ 600°C restores the T_c and a_o to nearly the original values.

It should be noted that the effects seen with H in Nb_3Ge have earlier been seen in Nb_3Sn,[4] the main difference being that it is easier for H to pass in and out of the sample in the case of Nb_3Ge. This is presumably a function of the degree to which the oxide at the surface acts as a barrier.

We wish now to compare the results found by Lanford et al., in particular the "as-deposited" results shown in curve (2) in Fig. 1, with the results found by other workers.

The data from curve (2) is replotted on the right-hand side of Fig. 4, now, however, with the substrate temperature the abscissa. On the left-hand side of Fig. 4 is plotted the data from the second paper[3] (Buitrago, Toth, et al.). Their apparatus gave a completely different result, T_c maximizing at a low substrate temperature. Also plotted in the lower left is the measured O_2 concentration (H has not yet been analyzed for). A possible conclusion from these data is that the presence of O_2 has reduced the effect of H_2 in the sample, and thus the rise in T_c is due to the decrease of H , and H , not T_s (substrate), is the primary parameter.

J. Rowell had earlier made the suggestion that this is the effect in those cases where "doping" gases are purposely admitted during the formation of the films.[5] Here we are suggesting that the underlying reasons for the wide diversity in the reported optimum substrate temperature and other parameters is actually related to the variability in hydrogen, and oxygen, and other impurities that cancel the effect of hydrogen, in each of the different apparatus.

Gavaler et al.[6] has proposed that the Nb_3Ge phase stability is dependent on impurities that result in an initially enlarged lattice (thermodynamically stable) due to interstitial impurities. This occurs at the substrate; further growth proceeds via a homoepitaxial process, with the lattice gradually contracting and with a resulting rise in T_c .

We note that the impurities could be the formation of stable "traps" for the hydrogen that is always present in these experiments. It appears that O_2 and N_2 in niobium form stable O-H and N-H bonds.[7] High T_c Nb_3Ge has been formed by admitting as doping gases (during the growth) O_2,[8,9,10] N_2,[8,10] Cl_2,[9] air,[8] and Si[10] in the form of SiH_4. It remains to be shown that these form traps for hydrogen in Nb_3Ge.

Because of the high mobility and probable low equilibrium concentration of H in Nb-Ge at the temperatures used for its formation (>500°C), the concept of traps for the H is necessary in order to explain the subsequent measurement of large amounts of hydrogen.[2] The trapping concept would require that in addition to the H, the other partner (O, N, etc) would also show up, unless structural defects in the Nb-Ge itself could act as traps (under conditions where these can not anneal out).[2]

These conclusions are consistent with the results found by a number of electron beam-evaporation experiments.[8,9,11] In Fig. 5 and 6 are shown the results of Hallak, Hammond, Geballe, and Zubeck,[9] in which it was shown that O_2 (and Cl_2) added during the formation of Nb_3Ge extends the region of A15 towards higher Ge and toward stoichiometry, increasing the T_c. The T_c begins to show an increase when the partial pressure of the admitted O_2 becomes about equal to that of the H_2. As indicated in the bottom of Fig. 5, the effectiveness of the O_2 addition is lessened as the substrate temperature is lowered below $\sim$ 750°C. In Fig. 6 is shown another manifestation of this: the lattice constant of the A15 phase remains constant in the two phase region when the conditions are optimum for high-T_c i.e. $T_s > 750$, and with O_2 present. However, at lower T_s the a_o suddenly rises upon leaving the single phase A15 region. Measurements by Lanford on specimens made in the same apparatus show that the H concentration is a factor of ten times higher in the two phase region (compared to the single phase) for a T_s of 700°C.

It is interesting that the Δa_o seen in Fig. 6 is consistent with the measured concentration and the Δa_o shown in Fig. 3 (i.e. H doped Nb_3Ge). However, this apparent correlation must await an actual measurement (The H measurements were made on Nb_3Ge deposited on Nb_3Ir films: 2 to 5 at.%H was found in the two-phase region. It would be interesting to see if the a_o in these "epitaxial grown" Nb_3Ge remains constant). Thus for some still unknown reasons the H is higher and concentrated in the A15 regions in the mixed two phase, as compared to the single phase A15, in the same sample. Perhaps the two-phase structure forms traps for H.

The T_c change observed in the 700°C and two-phase specimens is in agreement with that found for the "as grown" at different T_s material, curve (2) of Fig. 1.

Before discussing a final recent paper on the growth of Nb_3Ge, the present situation concerning the synthesis of Nb_3Si is discussed.

3. Nb_3Si

The purpose here is to review the efforts to synthesize A15 Nb_3Si in order to see if any of the lessons we may have learned about the formation of Nb_3Ge are applicable to Nb_3Si, and to establish if possible the stability conditions for the A15 structure in Nb_3Si.

The work of S. Hazra and R. Hammond, working at U. C. Berkeley in 1970-71, using multiple source electron beam evaporation are reviewed first. The details of this work have not been published before, appearing mostly in Hazra's M.S. thesis.[12,13,14]

A series of phase spread (typically covering the range 11-36 at %Si) depositions were made at five substrate temperatures between 100°C and 530°C. A15 structure was found over a limited range of composition, which increased towards more Si as the T_s was increased. The A2 phase bounded the low

Si side, and an amorphous component bounded the high Si side (see Fig. 7). The sharpest A15 structure (as determined by X-ray diffractometer traces) and the highest T_c was observed at 21% Si and a T_s = 530°C, where the T_c = 9.3°K, and 19 lines gave a lattice constant of 5.17 Å. At 25% and 530°C, both A15 and the amorphous component were present as seen in Fig. 8. The T_c was 9.1 K. The main emphasis was then put on annealing the various samples with the expectation that the amorphous component would by nucleation from the already existing A15 phase order into an atomically ordered A15 structure at 25% Si with a much higher T_c. Figure 9 shows the result of a 24 hours at 720°C anneal of a 200°C deposition, at 25%Si. As-deposited it was mostly amorphous; it now showed A15 plus the Ti_3P tetragonal structure, and still an amorphous component. Figure 10 shows the result of annealing a deposition with broad A15 plus amorphous phase: much more A15 and less tetragonal structure resulted. Figure 7 shows the summary of the annealing experiment: the amorphous component transformed mostly into the high temperature equilibrium phase (tetragonal Ti_3P). It is not certain how much of the A15 came from the amorphous phase, as compared to coming from disordered A15 regions. It appears (although this is not certain) that the A15 phase is stable against transforming to the tetragonal phase during an anneal at 720°C for 24 hours. In no case did the T_c increase above the 9.3 value.

In summary, it was found that the A15 phase was stable at least to 720°C. The range of composition over which it existed changes from very Si poor (11%) at 100°C to $\sim$ 21% at 530°C on the A15-A2 boundary. The silicon rich boundary is less well established, as it gradually merges into an amorphous region. Annealing the amorphous material produced the tetragonal Nb_3Si structure.

A number of methods have synthesized A15 Nb_3Si since 1971. Table I summarizes most of the published work. Some of these indicate that the A15 is stable up to 1000°C. An exception is the CVD work of Kawamura and Tachikawa

(1975), in which the limit was 900-950°C. Also noteworthy was the region over which the A15 phase was found. The composition range resembled that of Hazra and Hammond, but shifted in temperature to 800-900°C.

The most recent results of Dew-Hughes,[23] and of Somekh and Evetts[20] are very exciting, and lead us to continue to believe that eventually Nb_3Si will set the record for T_c. Just as was found previously for Nb_3Ge, the variability in results for Nb_3Si lead us to suspect that the same factor is important, namely H. This is to some extent evident in Somekh and Evetts results, and is certainly found in our recent work at Stanford.

The history of the synthesis of Nb_3Ge, and the recent work on Nb_3Si, point out the need for better characterization of the:

a. Synthesis conditions, i.e., in situ characterization of sample composition and structure, as well as the temperature of deposition, and impurity elements in the synthesis environment.

b. Composition and structure of the material while the specimen is cooled, and removed from the apparatus. For example, all transition metal alloy and compounds are good adsorbers of hydrogen; it is usually an oxide surface layer that prevents an immediate uptake of hydrogen from the ambient atmosphere. Structural transformations may occur between the T_s and room temperature, and at lower temperature.

4. EPITAXIAL STABILIZATION OF METASTABLE PHASES

An alternate solution that has worked in the case of Nb_3Ge, and appears to not be nearly so sensitive to the impurities, consist of depositing the desired material on top of another more stable structure with a similar lattice constant. This was successfully accomplished by A. Dayem (Bell Telephone Lab) and the Stanford group, at Stanford.[24] First niobium and iridium were co-deposited to form the A15 Nb_3Ir phase with a spread in Ir

composition and a consequent spread in lattice constant, which roughly but not exactly matched that of Nb_3Ge . Then, immediately, the Ge was substituted for Ir , and the Nb_3Ge deposited. The resulting Nb_3Ge was single phase A15 to 26% Ge , the T_c peaked at 25% Ge ($T_c \sim 22.5°K$), all without adding O_2 or other gas.

This technique is of course applicable to Nb_3Si . A number of groups are in the process of attempting to use Ti_3Au as the A15 with a lattice constant that comes close to matching that expected for Nb_3Si .

5. BEYOND Nb_3Si — ARE THERE OTHER A15 SUPERCONDUCTORS?

(1) Empirically, the T_c vs a_o of the Nb_3X A15 follow a remarkably smooth curve through Nb_3Sn , Nb_3Al , $Nb_3(AlGe)$, Nb_3Ga , and Nb_3Ge (See Fig. 4 in Ref. 14). These occur in order of decreasing values of the atomic radii of the X atom. Thus other elements with still smaller radii would seem to offer a still higher T_c . In order to keep on the maximum in the density of states it is though to be necessary to keep to the same columns (3 and 4) that have been successful — this leads us to consider Nb_3B , Nb_3C , V_3B , and V_3C in the A15 structure. These will certainly be at best metastable, and thus the techniques and problems discussed earlier are pertinent.

(2) A15 based on Mo_3X and Re_3X . The motivation for considering A15's based on the Mo of the 4d and Re of the 5 d transition metals comes from the experimental behavior of the 4 d and 5d series when made amorphous.[25,26,27] As seen in Fig. 11, T_c reaches a peak at an e/a of 6.3 when alloys of Mo-Ru or Mo-Re are made amorphous. For the 5 d the peak occurs at $\sim$ 7 or Re. See Fig. 12. This behavior is believed to be the result of a smoothing out of the variation as a function of e/a of some of the factors that determine T_c .

These are $N(0)$, $\langle\omega^2\rangle$, and the pre-exponential factor ω_D . The remaining term, $\langle I^2\rangle$, has recently been shown[28] to have a peaked behavior near to Mo for the 4 d series, similar to that seen in T_c (amorphous). Assuming that the variation of $\langle I^2\rangle$ will be similar in the A15 structure as it is apparently in the bcc, hcp, and amorphous structures, it is valid to look for a high-T_c in the Mo and Re A15's. It is of course desirable to have a large $N(0)$ as well (although recent work by C. C. Tsuei[29] has indicated that a very high or peaked $N(0)$ may not be necessary).

6. STUDY OF PINNING IN Nb_3Sn STRUCTURES

It has been possible to make an interesting variety of microstructures in Nb_3Sn by depositing a third element or compound along with the Nb and Sn.[30] Using an inert material, Al_2O_3 , the usual columnar growth of Nb and Sn instead is now a 500 Å (and less) equiaxal grain composite. In addition, each Nb_3Sn grain has $\sim$ 25 Å voids, separated by $\sim$ 75-100 Å . When copper is codeposited again very small equiaxed grains result when the copper concentration is small ($\sim$ 7% vol.). When the copper volume is $\sim$ 60%, long narrow rods of Nb_3Sn result. Transmission electron microscope views of these structures are being published,[31,32] as are the initial results of the high magnetic field pinning force measurements.[33] It appears that it will be possible to produce structural configurations for pinning that can be used for model calculations of the pinning force.

ACKNOWLEDGEMENTS

Although they should not be held responsible for the opinions expressed above, the author would like to acknowledge discussions with Professors T. H. Geballe, L. E. Toth, and M. M. Collver, and Drs. J. M. Rowell, R. E. Somekh, and A. H. Dayem.

REFERENCES

1. J. R. Gavaler, Appl. Phys. Lett. 23, 480 (1973).
2. W. A. Lanford, P. H. Schmidt, J. M. Rowell, J. M. Poate, R. C. Dynes, and P. D. Dernier, Appl. Phys. Lett. 32, 339 (1978).
3. R. H. Buitrago, L. E. Toth, A. M. Goldman, J. Schwanebeck, and M. Dayan, Appl. Phys. Lett. 32, 341 (1978).
4. L. J. Vieland, A. W. Wicklund, and J. G. White, Phys. Rev. B 11, 3311 (1975).
5. J. M. Rowell, P. H. Schmidt, E. C. Spencer, P. D. Dernier, and D. C. Joy, IEEE Trans. Magn. MAG-13, 644 (1977).
6. J. R. Gavaler, M. Ashkin, A. I. Braginski, and A. T. Santhanam, Appl. Phys. Lett. 33, 359 (1978).
7. J. Bottiger, S. T. Pieraux, N. Rud, and T. Laursen, J. Appl. Phys. 48, 920 (1977).
8. R. A. Sigsbee, Appl. Phys. Lett. 29, 211 (1976); IEEE Trans. Magn. MAG-13, 307 (1977).
9. A. B. Hallak, R. H. Hammond, and T. H. Geballe, Appl. Phys. Lett. 29, 314 (1976); IEEE Trans. Magn. MAG-13, 311 (1977).
10. J. R. Gavaler, in Superconductivity in d- and f-Band Metals, (Proc. of 2nd Rochester Conf., D. H. Douglass, Ed.), 421 (1976).
11. Y. Tarutani, M. Kudo, and S. Taguchi, Proc. of the 5th International Cryogenics Engineering Conference, Kyoto, Japan (1974), p. 477; Y. Tarutani and M. Kudo, Japan J. Appl. Phys. 16, 509 (1977).
12. S. Hazra, M. Sc. Dissertation, University of California, Berkeley, LBL-Report No. LBL-433, December 1971.
13. R. H. Hammond and S. Hazra in Proceedings of 13th International Conference on Low Temperature Physics, Boulder, Colorado, 1972. Edited by K. D. Timmerhaus et al. (Plenum Press, New York, 1974) vol. 3, p. 465.

14. R. H. Hammond, IEEE Trans. Magn. MAG-11, 201 (1975).

15. G. R. Johnson and D. H. Douglass, J. Low Temp. Phys. 14, 575 (1974).

16. L. R. Testardi, J. H. Wernick, W. Royer, D. D. Bacon, and A. R. Storm, J. Appl. Phys. 45, 446 (1974).

17. V. H. Pan, V. P. Aleksuvskii, A. G. Popov, Yu. I. Beletskii, L. M. Yupko, and V. V. Yarosh, J.E.T.P. Letters, 21, 228 (1975).

18. H. Kawamura and K. Tachikawa, Phys. Lett. 55A, 65 (1975).

19. R. E. Somekh and J. E. Evetts, Solid State Commun. 24, 733 (1977).

20. R. E. Somekh and J. E. Evetts, IEEE Trans. Magn. MAG (to be published).

21. L. R. Testardi, T. Wakiyama, and W. A. Boyer, J. of Appl. Phys. 48, 2055 (1977).

22. M. T. Clapp and R. M. Rose, Appl. Phys. Lett. 33, 205 (1978).

23. D. Dew-Hughes, IEEE Trans. Magn. MAG (to be published).

24. A. H. Dayem, T. H. Geballe, R. B. Zubeck, A. B. Hallak, and G. W. Hull, Appl. Phys. Lett. 30, 541 (1977); J. Phys. Chem. Solids, 39, 529 (1978).

25. M. M. Collver and R. H. Hammond, Phys. Rev. Lett. 30, 92 (1973).

26. M. M. Collver and R. H. Hammond, Solid State Commun. 22, 55 (1977).

27. M. M. Collver and R. H. Hammond, J. Appl. Phys. 49, 2422 (1978).

28. W. H. Butler, Phys. Rev. B 15, 5267 (1977).

29. C. C. Tsuei, S. Von Molnar, and J. M. Coey, Phys. Rev. Lett. 41, 664 (1978).

30. R. H. Hammond, J. Vac. Sci. Technol. 15, 382 (1978).

31. B. E. Jacobson, R. H. Hammond, T. H. Geballe, and J. R. Salem, J. of Less Common Metals, 62, xxx (in press).

32. B. E. Jacobson, R. H. Hammond, T. H. Geballe, and J. R. Salem, Thin Solid Films, 54, 243 (1978).

33. R. H. Hammond, B. E. Jacobson, T. H. Geballe, J. Talvacchio, J. R. Salem, H. C. Pohl, and A. I. Braginski, IEEE Trans. Magn. MAG (to be published).

TABLE I

SUMMARY OF A15 Nb_3Si SYNTHESIS

Authors	Reference	Method	Range of Occurance of A15 Structure	T_c	a_o
Hazra, Hammond 1971	12 13 14	Electron Beam Evaporation	Stable at Least to 720°C Low Si Boundary (A2-A15): 11% at 100°C 21% at 530°C High Si A15 boundary: Gradual merging into amorphous	9.3 21% Si	5.17
Johnson Douglass 1974	15	Sputter	T_s=750°C, A15 15-25%Si (+A2 + tetragonal) A15 $\xrightarrow{1000°C}$ A2+tetragonal	6.9 24% Si	
Testardi et al. 1974	16	Sputter	T_s = 700 - 900°C A15 + tetragonal	9	
Pan et al. 1975	17	Explosive Compression	A15 stable at least at 650°C	19 23% Si	5.03
Kawamura Tachikawa 1975	18	CVD	A15 single phase: 800°C : 9-14 % Si 850 :11-17 900 :16-23 A15 $\xrightarrow{900-950°C}$ A2+FCC+ tetragonal	8.05 11%Si 6 23%	5.16 23%
Somekh Evetts 1977, 1978	19 20	Sputter	A15 at ∿ 1000°C	14 17.1	5.18 5.185
Testardi 1977	21	Pushed Heat of Amorphous		12	
Clapp and Rose 1978	22	Ion Implant-Epitaxial Recrystallization	A15 stable at 980°C		
Dew-Huges 1978	23	Explosive Compression	A15 stable at 600°C	18.2	5.15

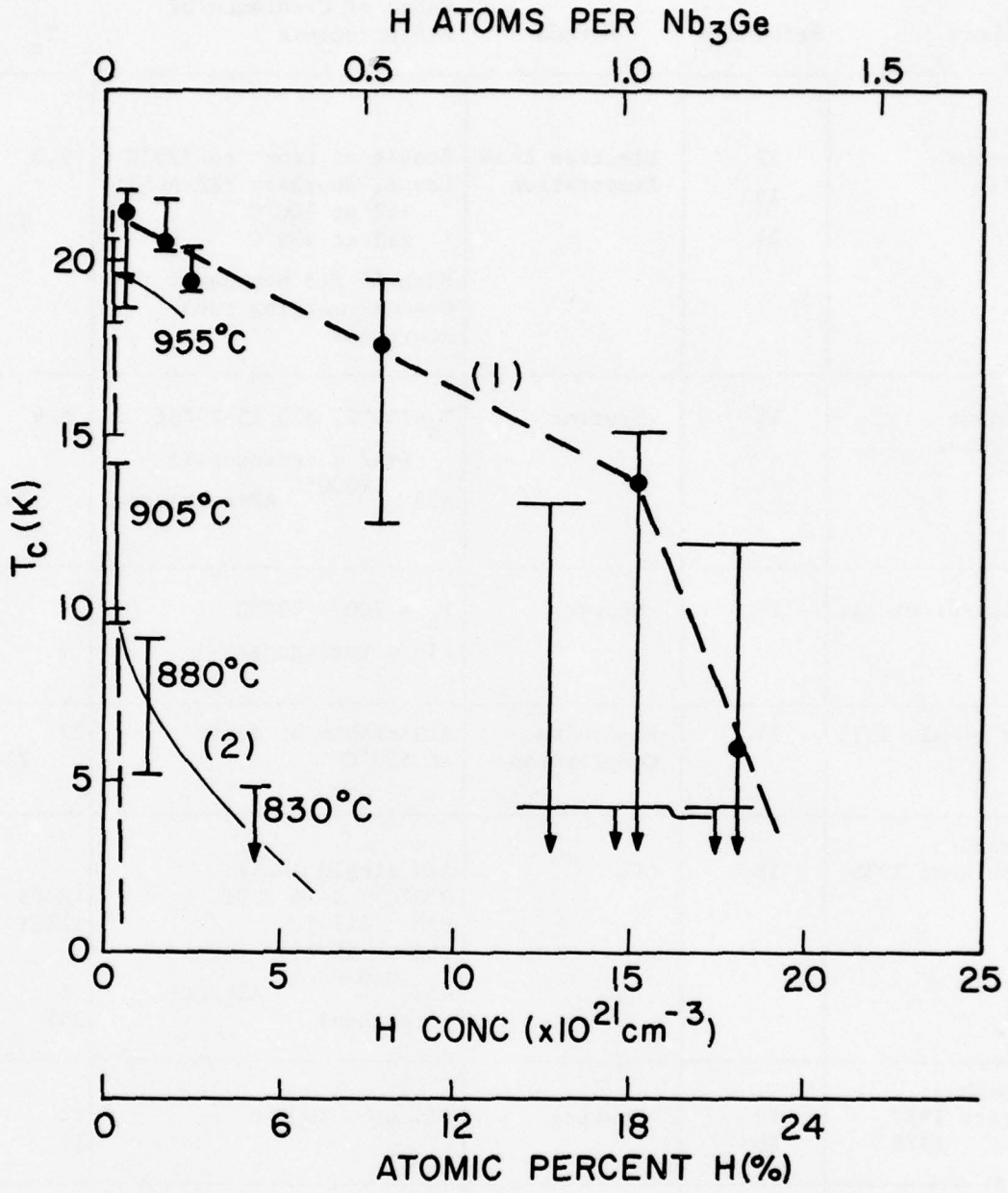

Fig. 1 - Reduction in T_c of sputtered Nb_3Ge, summarizing the data contained in several figures from Lanford et. al.[2] Curve (1) shows the effect of doping with H by dipping high-T_c specimens into $HF:H_2O$. In comparison, curve (2) shows the T_c and H concentration in specimens made at the temperature indicated (not purposely doped with H).

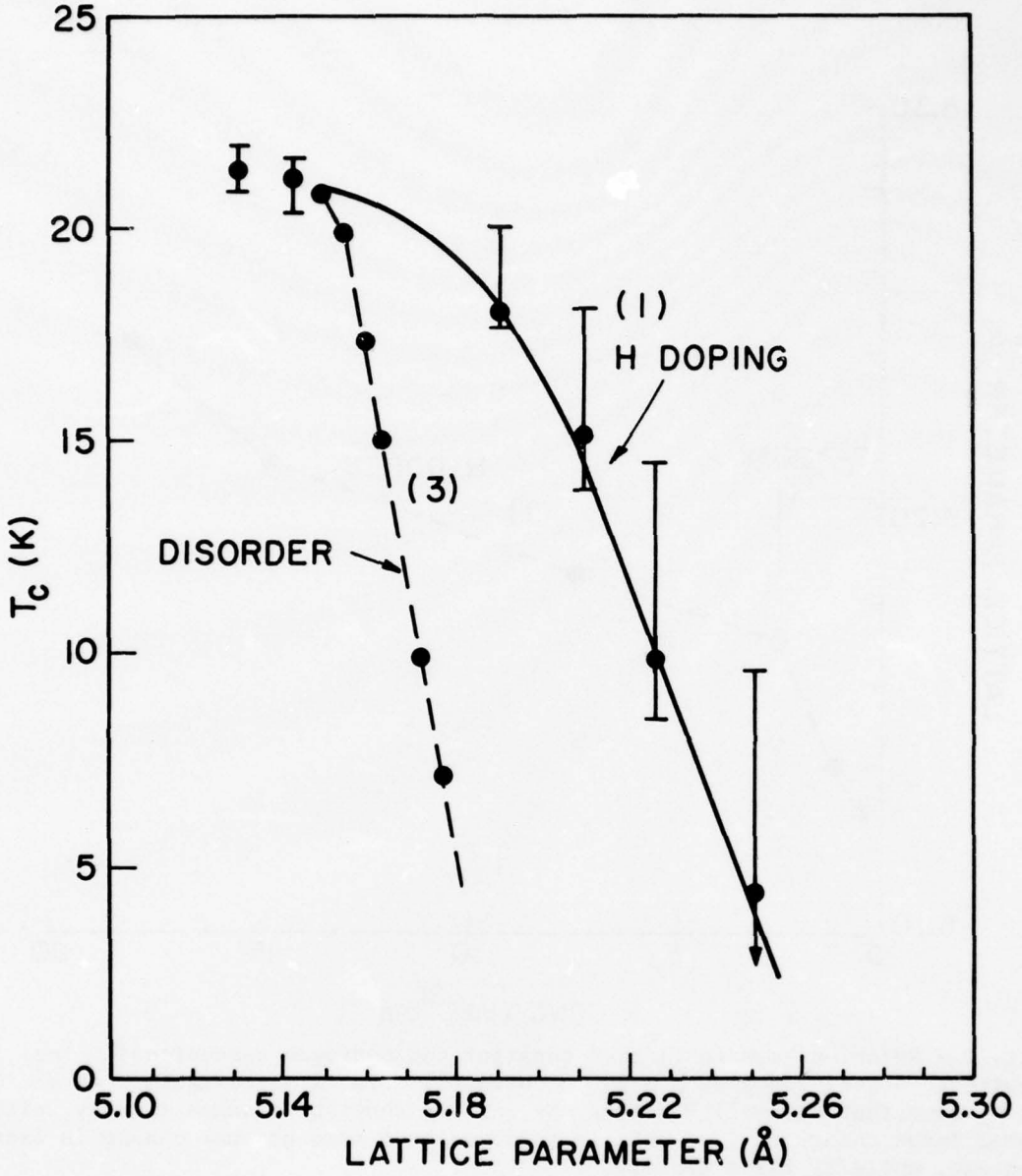

Fig. 2 - Relation between T_c and lattice constant for sputtered Nb_3Ge in curve (1), doped with H as in Fig. 1 curve (1), and for electron beam deposited Nb_3Ge made at various compositions and disorder, curve (3). Curve (1) from Lanford et al. [2]; curve (3) from Dayem et al. [24]

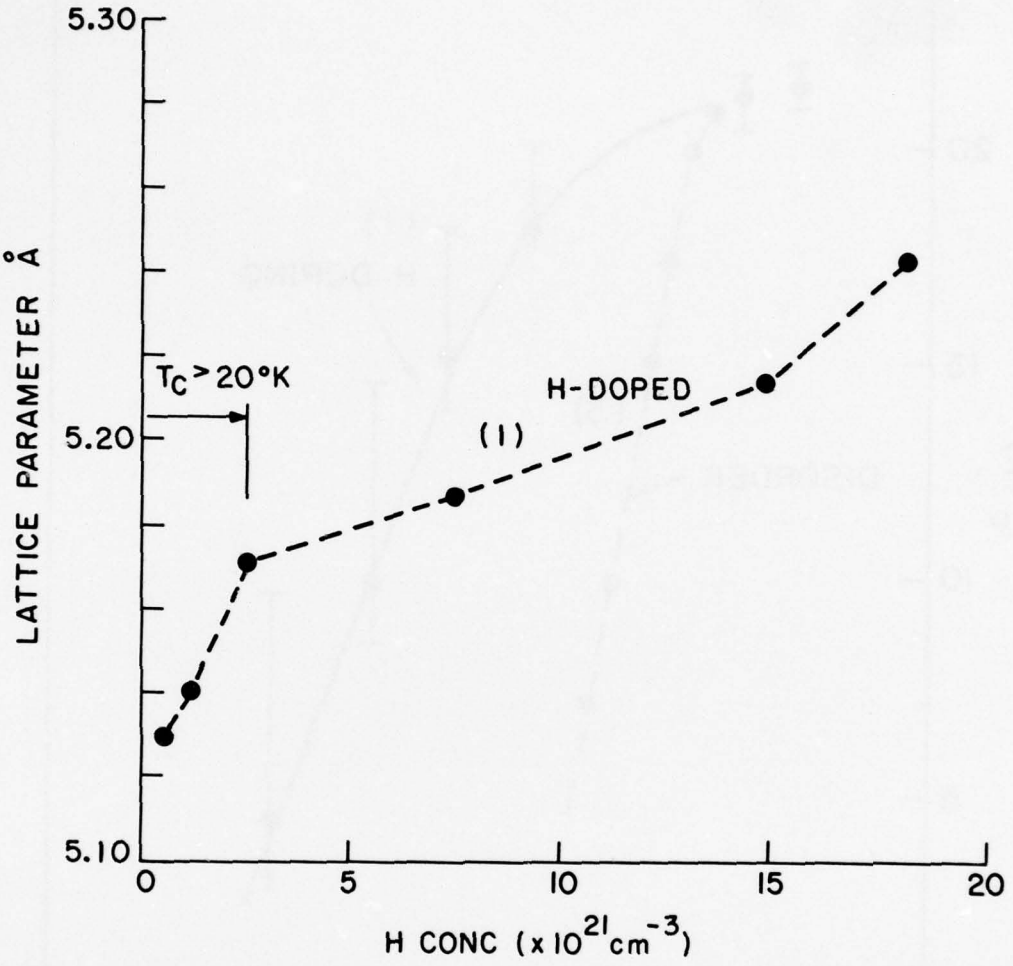

Fig. 3 - Relation between lattice constant and hydrogen concentration for sputtered Nb_3Ge, doped with H as in curve (1), Fig. 1 (from Lanford et al.[2]). This shows that at small H doping the lattice constant changes rapidly, without a large change in T_c. This is followed by a more gradual change in lattice contant, while T_c falls rapidly.

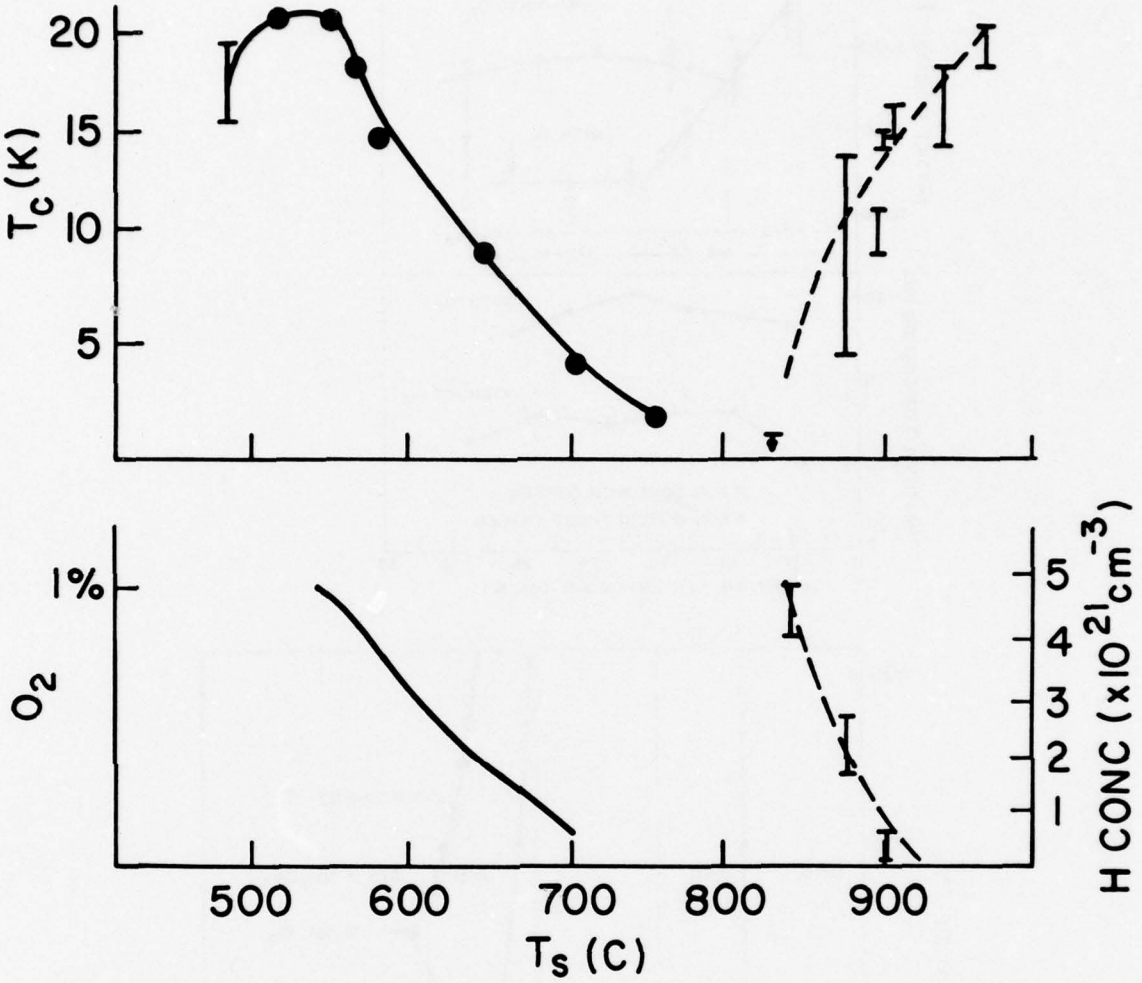

Fig. 4 _ The variation of the T_c with the substrate temperature, T_s, comparing the data of Lanford et al., [2] and Buitrago et al. [3] Also shown are the measured impurities of H (Lanford et al.) and O (Buitrago et al.). The data of curve (2), Fig. 1, is replotted in the upper right, with the substrate temperature now the abscissa. The data of Bruitrago et al. is shown on the upper left. The H concentration is also shown for the Lanford et al. specimens (lower right), while the O_2 concentration estimated from Auger measurements are shown on the lower left.

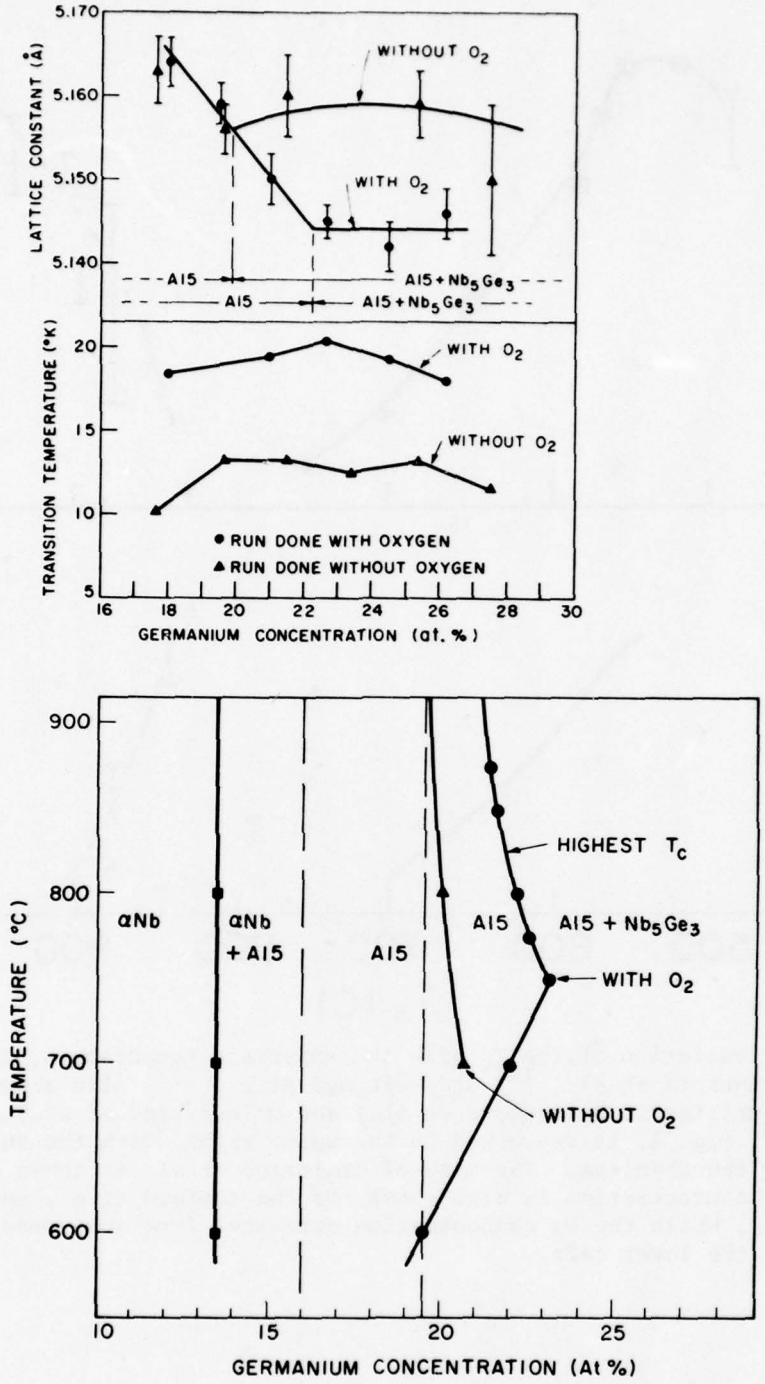

Fig. 5 - Data for electron beam evaporated Nb_3Ge, showing the effect of depositing with O_2 present. The upper figures show the variation of the lattice constant and of the T_c with Ge concentration at a T_s of 800°C. The lower figure summarizes a number of such measurements at different T_s, giving a pseudo-phase diagram.

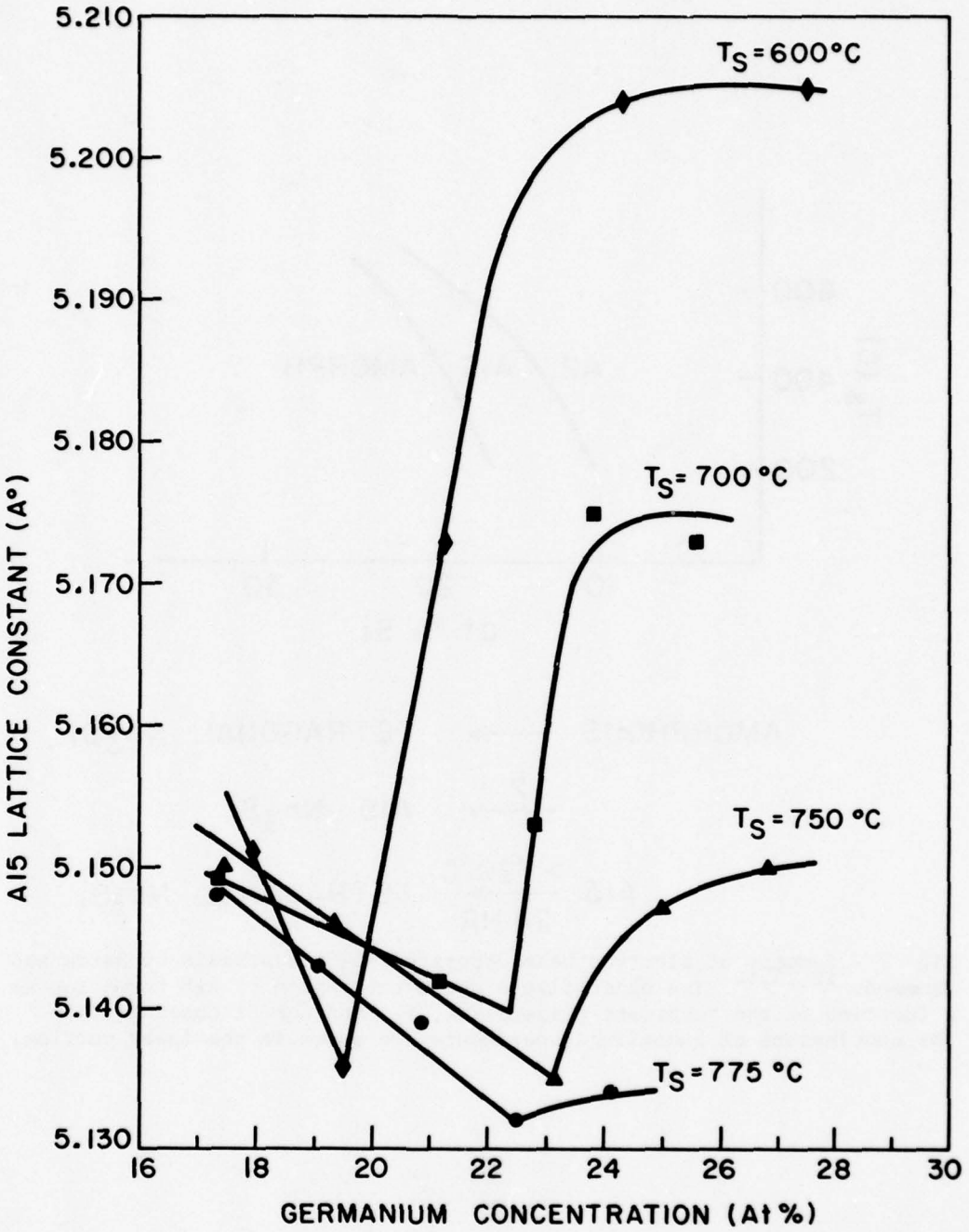

Fig. 6 - Variation of the lattice constant versus Ge concentration for electron beam deposited Nb_3Ge, with O_2 present. This shows the anomalous increase in the lattice constant upon going from the single phase A15 region into the two phase region, when the T_s is less than 800°C. Measurements on similar specimens of the H concentration show an increase of an order of magnitude in going from the single phase A15 to the two phase region.

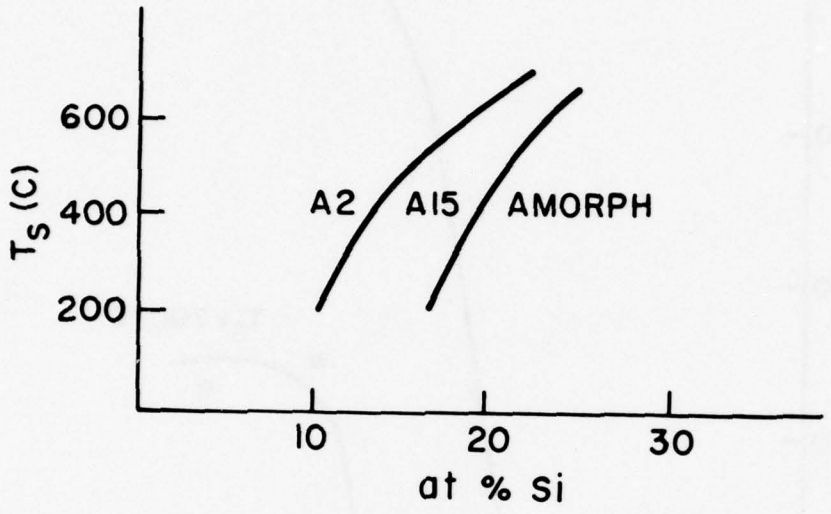

AMORPHOUS $\longrightarrow$ TETRAGONAL Nb_3Si

$\xrightarrow{?}$ A15 Nb_3Si

A15 $\xrightarrow[24\ HR]{>720°C}$ TETRAGONAL Nb_3Si

Fig. 7 - Summary of electron beam deposited Nb_3Si synthesis by Hazra and Hammond.[12,13,14] The upper figure shows the region of A15 formation as a function of the substrate temperature, T_s, and the Si concentration. The conclusions of annealing experiments are shown in the lower portion.

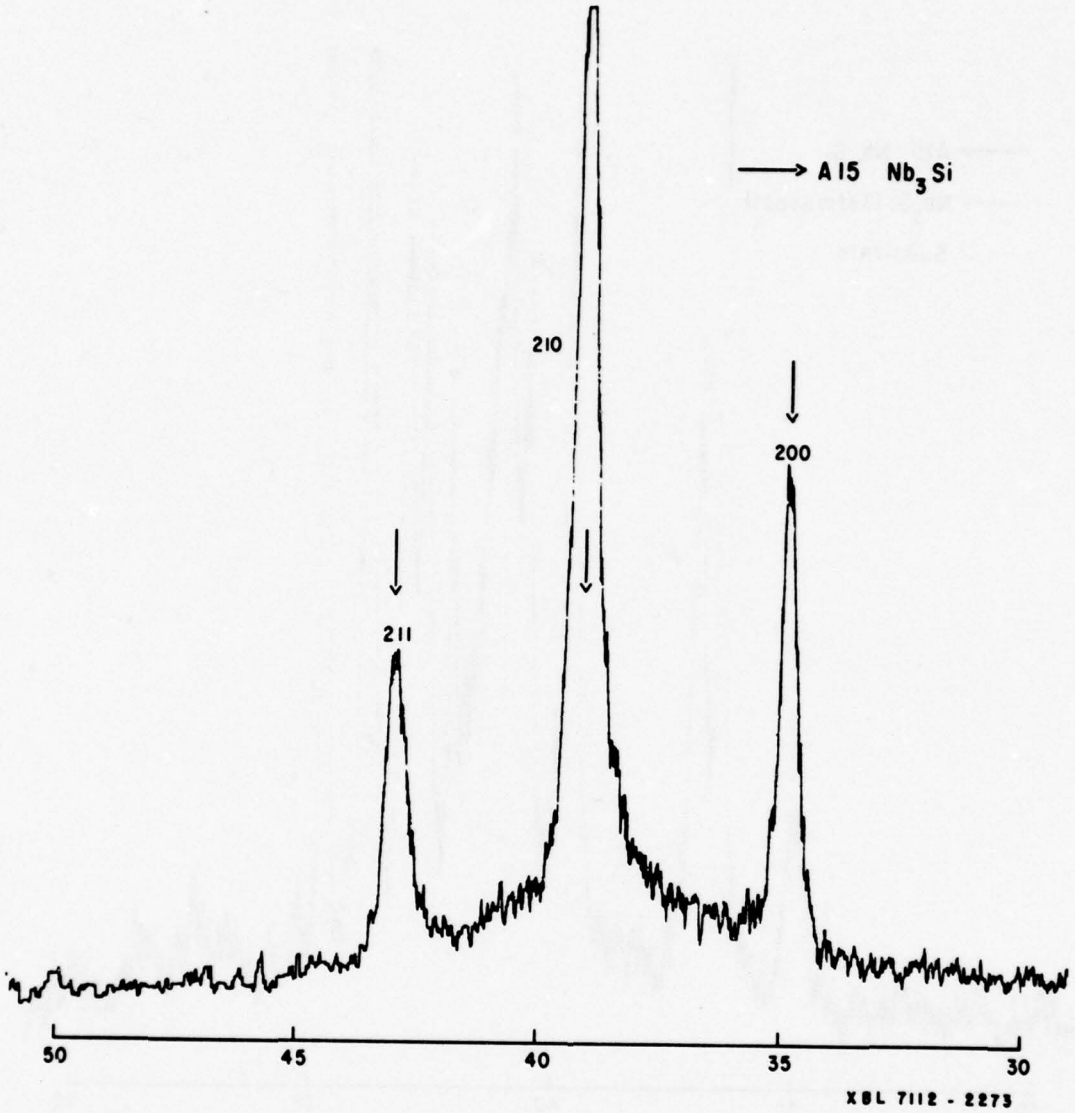

Fig. 8 - Portion of X-ray diffractometer traces showing the three strongest lines of Nb_3Si deposited at $T_s = 530^oC$ and at 25% Si. Both the A15 structure and an amorphous component are found at this concentration. The T_c was 9.1^oK for this concentration.

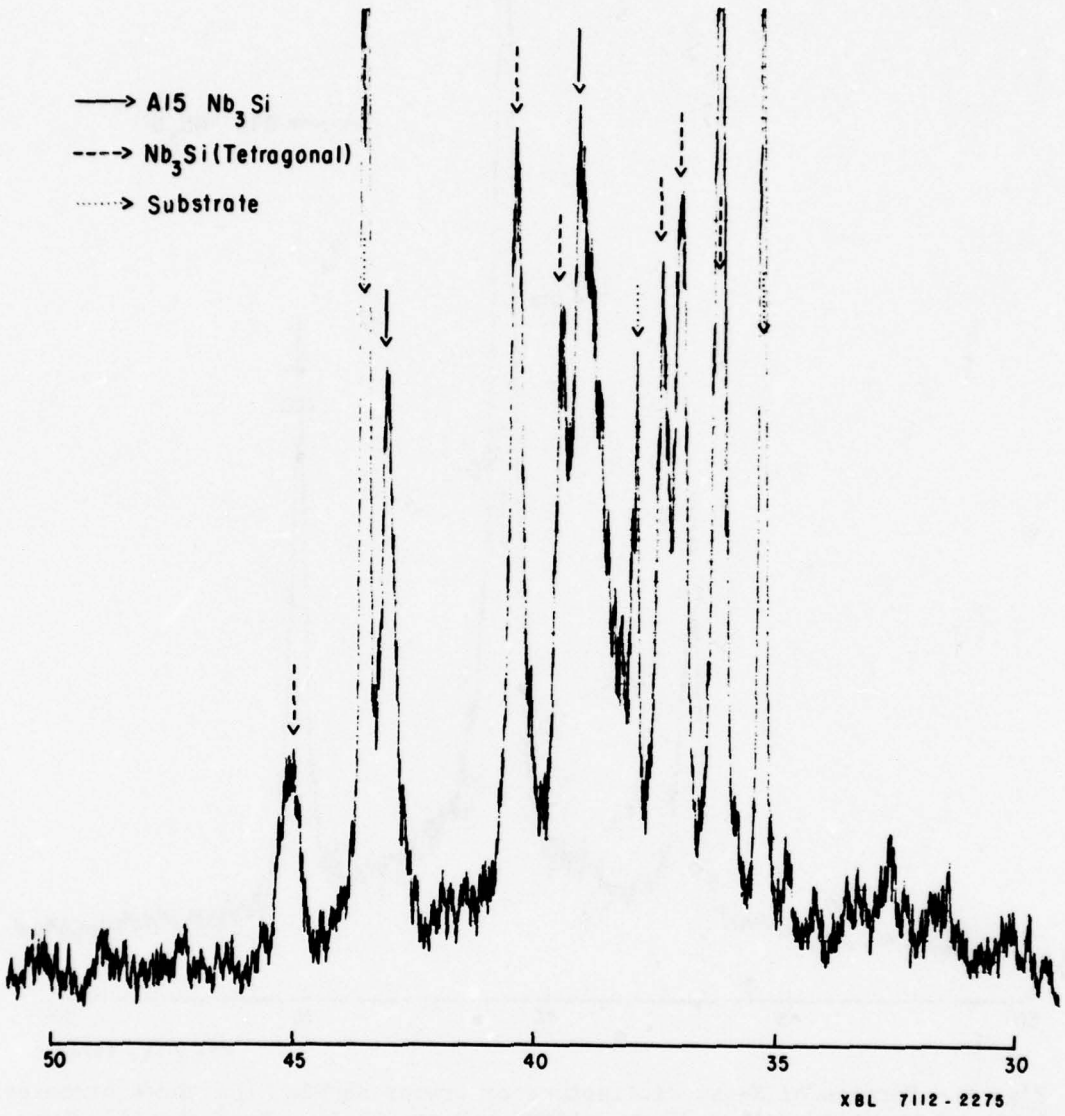

Fig. 9 - Diffractrometer trace of Nb_3Si (25 at.% Si) deposited at 220°C, after a 720°C 24 hour anneal showing some A15 and much more of the tetragonal Ti_3P type structures. As deposited it was amorphous. This illustrates the idea that the amorphous component anneals mostly to the tetragonal structure.

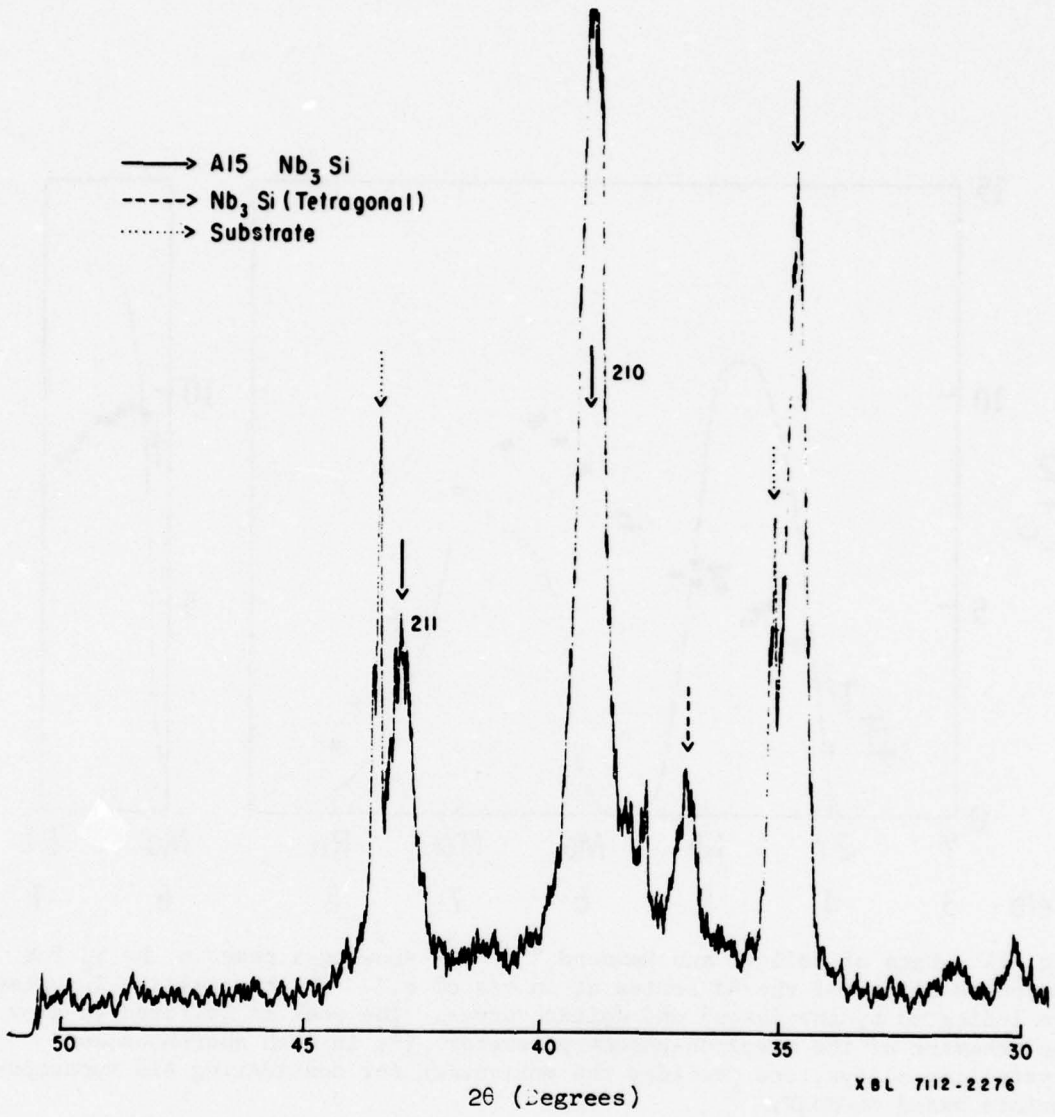

Fig. 10 - Diffractrometer traces of a 25 at.% Si Nb_3Si deposited at 450°C, after an anneal at 720°C for 24 hours, showing mostly A15, with some tetragonal structure. As deposited it showed broad A15 plus amorphous struture.

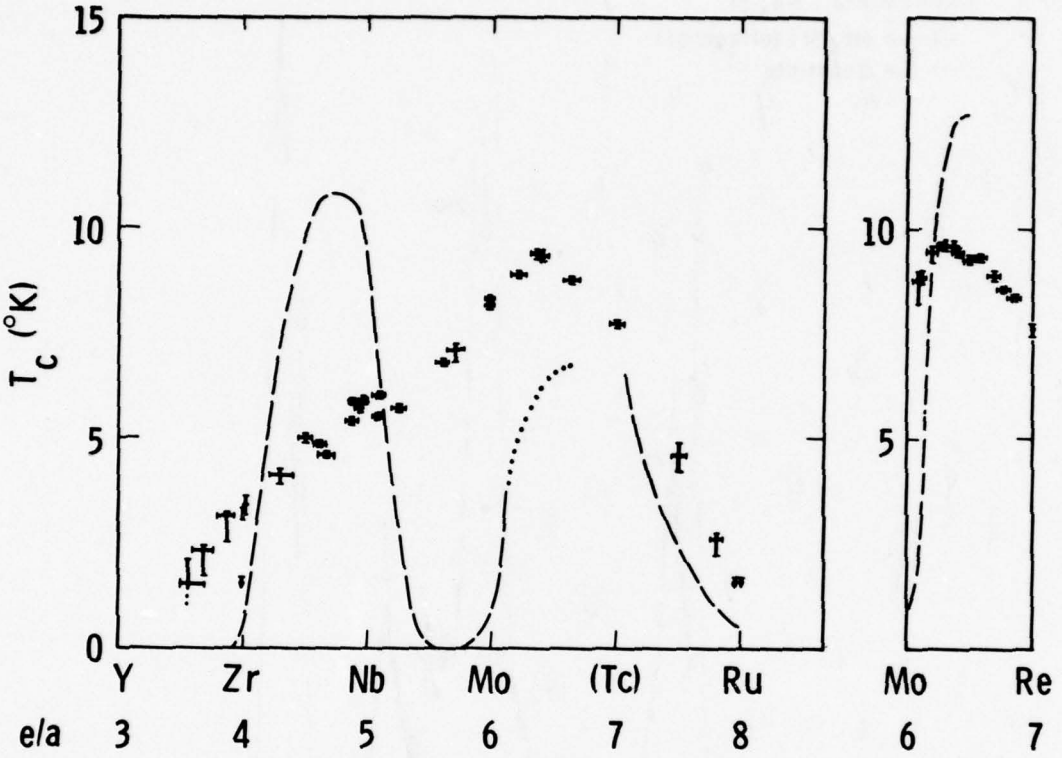

Fig. 11 - Data of Collver and Hammond [25,26,27] showing a peak in the T_c for amorphous alloys of the 4d series at an e/a of 6.3. The crystalline T_c values are indicated by the dashed and dotted curves. The peak is believed to show the behavior of the electron-phonon parameter $\langle I^2 \rangle$ in both amorphous and crystalline alloys, and provides the motivation for considering A15 superconductors based on Mo_3X.

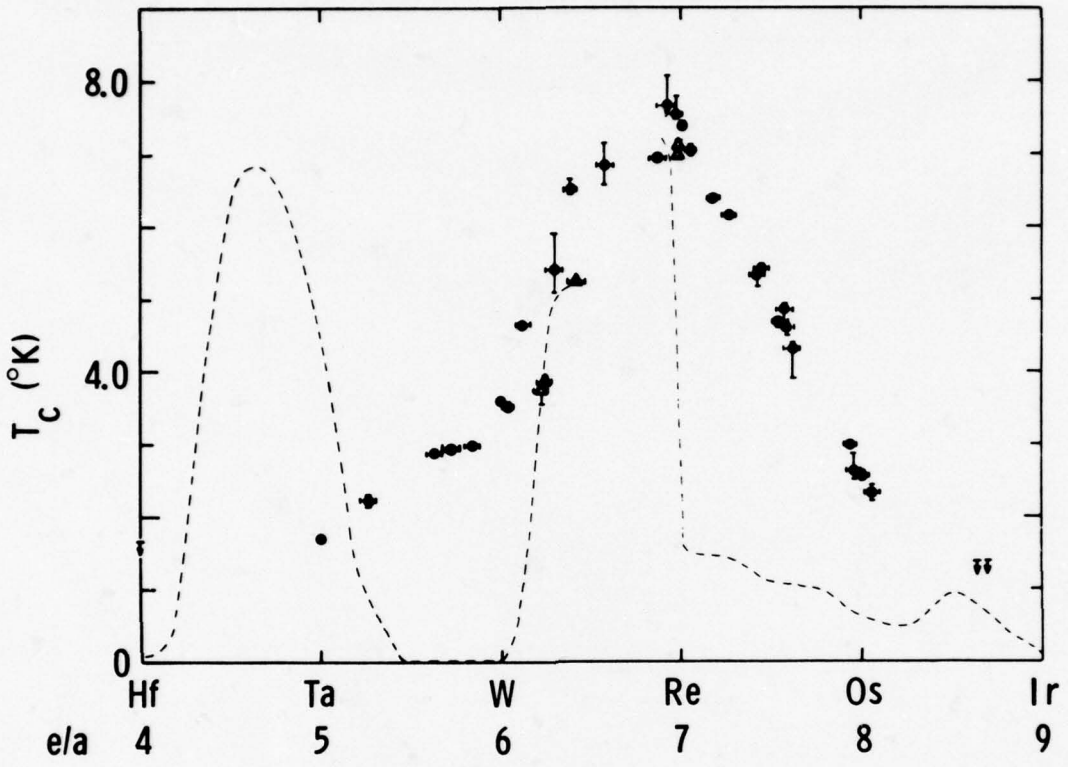

Fig. 12 - Data of Collver and Hammond[25,26,27] for the amorphous 5-d alloys, with the crystalline T_c values indicated by the dashed curve. The peak near Re provides the motivation for considering the A15 Re_3X compounds.

SYNTHESIS OF SUPERCONDUCTING Nb_3Si USING HIGH PRESSURES*

D. Dew-Hughes
Brookhaven National Laboratory
Upton, New York 11973

Extrapolations of superconducting data on known A15 compounds predict that Nb_3Si with the A15 structure should have a T_c (variously 25-38K[1-4]) higher than that for Nb_3Ge. The A15 phase with Nb_3Si stoichiometry has the tetragonal, Ti_3P structure.[6] Static compression of elemental powders to 70 kbar and up to 2000°C,[7] of sputtered metastable bcc Nb_3Si to 100 kbar, and of high temperature tetragonal Nb_3Si up to 60 kbar,[8] fails to produce any material with the A15 structure.

Higher pressures are more readily achieved by detonation of explosives. Superconducting A15 Nb_3Si has been synthesized from elemental powders in this way.[9] Pan et al.[10] subjected tetragonal Nb_3Si to shock pressures exceeding 1 Mbar in the manner illustrated in Fig. 1. A superconducting phase, with an onset T_c of 19.5-19K, was formed. This they claim to have the A15 structure, with a lattice parameter a_o=5.03 Å, considerably less than that predicted for stoichiometric A15 Nb_3Si, 5.08 Å[11] Subsequently A15 Ta_3Si was produced by an identical technique.[12] Pan claims that he has repeated this experiment many times, and that for success the starting compound must not deviate from the 3:1 stoichiometry, and the detonation velocity of the explosive must exceed 7,300 m/s.[13]

Pan's results have been essentially confirmed at Brookhaven, using a slightly different arrangement, as shown in Fig. 2. The explosive used has a detonation velocity of 7100 m/s giving an estimated pressure of 0.9 Mbar, at the center of the sample. The sample was converted into a mixture of powder

* Work performed under the auspices of the U.S. Dept. of Energy.

and friable flakes. The larger flakes were separated from the powder which was shaken on a 80 mesh sieve. The material which did not pass through the sieve was ground and resieved.

Metallographic examinations were carried out on some of the flakes. The microstructure is shown in Fig. 3. Microprobe analysis indicated the overall composition to be 76.5 $^{a}/_{o}$ Nb, 23.5 $^{a}/_{o}$ Si; that of the purple areas was consistently 77.5 $^{a}/_{o}$ Nb, 22.5 $^{a}/_{o}$ Si. Critical temperatures were measured inductively. The results, including those for annealing and neutron irradiation experiments, are summarized in Table I. The low temperature transition is niobium solid solution. The reduction in T_c on irradiation, and its partial recovery on subsequent annealing, is the behavior expected of a metastable A15 compound. The intermediate transition in the ground sample could be A15 material degraded by mechanical deformation.[14]

Positive identification of the structure of the high temperature phase was not possible, as x-ray diffraction patterns were complicated by the presance of untransformed tetragonal Nb_3Si, Nb solid solution, and Nb_5Si_3 which can exist in two tetragonal, and one hexagonal, structures. A comparison between portions of the diffractometer trace for one of the powder samples and that of a mixture of tetragonal Nb_3Si, Nb, and Nb_5Si_3 powders is shown in Fig. 4 and 5. There are clearly reflections present in the former, which are absent in the latter, and which can be indexed to the A15 structure with a lattice parameter of 5.12 Å (see Table II).

Hammond, by electron-beam vapor deposition has produced A15 Nb_3Si films with 21 $^{a}/_{o}$ Si, a_o=5.17 Å and T_c=9.3K.[15] On a plot of a_o versus silicon content, the value of 5.12 Å for 22.5 $^{a}/_{o}$ Si interpolates well between Hammond's value and that of 5.08 Å deduced for 25 $^{a}/_{o}$ Si (Fig. 6). On the same figure are plotted Hammond's, Pan's and the present values of T_c versus silicon content. This extrapolates to a T_c of 28K for 25 $^{a}/_{o}$ Si.[16]

The explosive compression was carried out by V. D. Linse at Battelle-Columbus Laboratories; J. Hattayer performed the optical metallography, R. Sabatini the microprobe analysis, and O. Kammerer the x-ray diffraction.

REFERENCES

1. L. Gold, Phys. Stat. Sol. 4, 261 (1964).
2. D. Dew-Hughes and V. G. Rivlin, Nature 250, 723 (1974).
3. D. Dew-Hughes, Cryogenics 15, 475 (1975).
4. S. Geller, Appl. Phys. 7, 321 (1975).
5. D. K. Deardorff, R. E. Siemens, P. A. Romans, and R. A. McCune, J. Less Common Metals 18, 11 (1969).
6. V. M. Pan, V. V. Pet'kov, and O. G. Kulik, "Physics and Metallurgy of Superconductors", Moscow (1965-1961), E. M. Savitskii and V. V. Baron (Eds) Consultants Bureau, New York (1970).
7. J-M. Léger and H. T. Hall, J. Less Common Metals 32, 181 (1973).
8. R. M. Waterstrat, F. Haenssler, J. Müller, S. D. Dahlgren, and J. O. Willis, J. Appl. Phys. 49, 1143 (1978).
9. G. H. Otto, U. Roy, and D. Y. Reece, J. Less Common Metals 32 355 (1973).
10. V. M. Pan, V. P. Alekseevskii, A. G. Popov, Yu. I. Beletskii, L. M. Yupko, and V. V. Yarosh, JETP Letters 21, 228 (1975).
11. Y. Tarutani and M. Kudo, J. Less Common Metals 55, 221 (1977).
12. V. M. Pan, A. G. Popov, V. P. Alekseevskii, O. G. Kulik, and V. V. Yarosh, Fizika Nizkich Temperatur, 3, 801 (1977).
13. V. M. Pan, private communication.
14. M. Rohr and P. Muller, Phys. Stat. Sol. B42, 477 (1977).
15. R. H. Hammond, Trans. IEEE MAG-11, 201 (1975).
16. D. Dew-Hughes, Applied Superconductivity Conference, Pittsburgh (1978).

TABLE I

Superconducting Transition Temperatures

Sample	Treatment	High Temperature Onset	High Temperature Mid Pt.	Intermediate Temperature Onset	Intermediate Temperature Mid Pt.	Low Temperature Onset
-80 Mesh Powder		18.1 K	15.9 K			8.1 K
-80 Mesh Ground Powder		18.2 K	16.3 K	13.1 K	11.9 K	8.0 K
-80 Mesh Ground Powder	Annealed 44 hrs 600°C	17.7 K	14.0 K			
-80 Mesh Ground Powder	Irradiated 9.4×10^{18} nvt					8.0 K
-80 Mesh Ground Powder	Irradiated, Annealed 20 hrs 500°C			11.55K	8.95K	
-80 Mesh Ground Powder	Irradiated, Annealed 50 hrs 600°C			11.0 K	9.0 K	
+80 Mesh Ground Powder		18.1 K	15.6 K			7.95K
+80 Mesh Ground Powder	Annealed 44 hrs 600°C	17.1 K	15.0 K			
+80 Mesh Ground Powder	Irradiated 9.4×10^{18} nvt					8.0 K
Flakes (Various) 1		18.3 K	13.7 K			8.0 K
2		17.9 K	15.4 K			7.8 K
3		17.85K	15.8 K			8.0 K
(H_{c2} Sample) 4		17.7 K	15.2 K			7.7 K
(Microprobe Sample) 5		17.5 K	15.9 K			7.6 K
6		16.8 K	15.8 K			7.9 K
Flakes 3 & 4	Irradiated 9.4×10^{18} nvt					8.1 K
3 & 4	Irradiated, Annealed 5 hrs 600°C			11.4 K	8.25K	
3 & 4	Irradiated, Annealed 10 hrs 600°C			12.1 K	8.9 K	

Table II.

X-RAY DATA ON TWO EXPLODED SAMPLES
CuKα RADIATION

	Sample 2		Sample 3	
Line	2θ°	a_o (Å)	2θ°	a_o (Å)
200	35.45	5.06	35.15	5.11
210	39.2	5.13	39.15	5.14
211	43.4	5.11	43.45	5.10
220	50.85	5.08	--	--
310	56.25	5.17	--	--
320	65.85	5.11	65.7	5.12
321	68.0	5.16	67.7	5.18
400	74.2	5.11	74.1	5.12
440	117.0	5.11	116.9	5.12

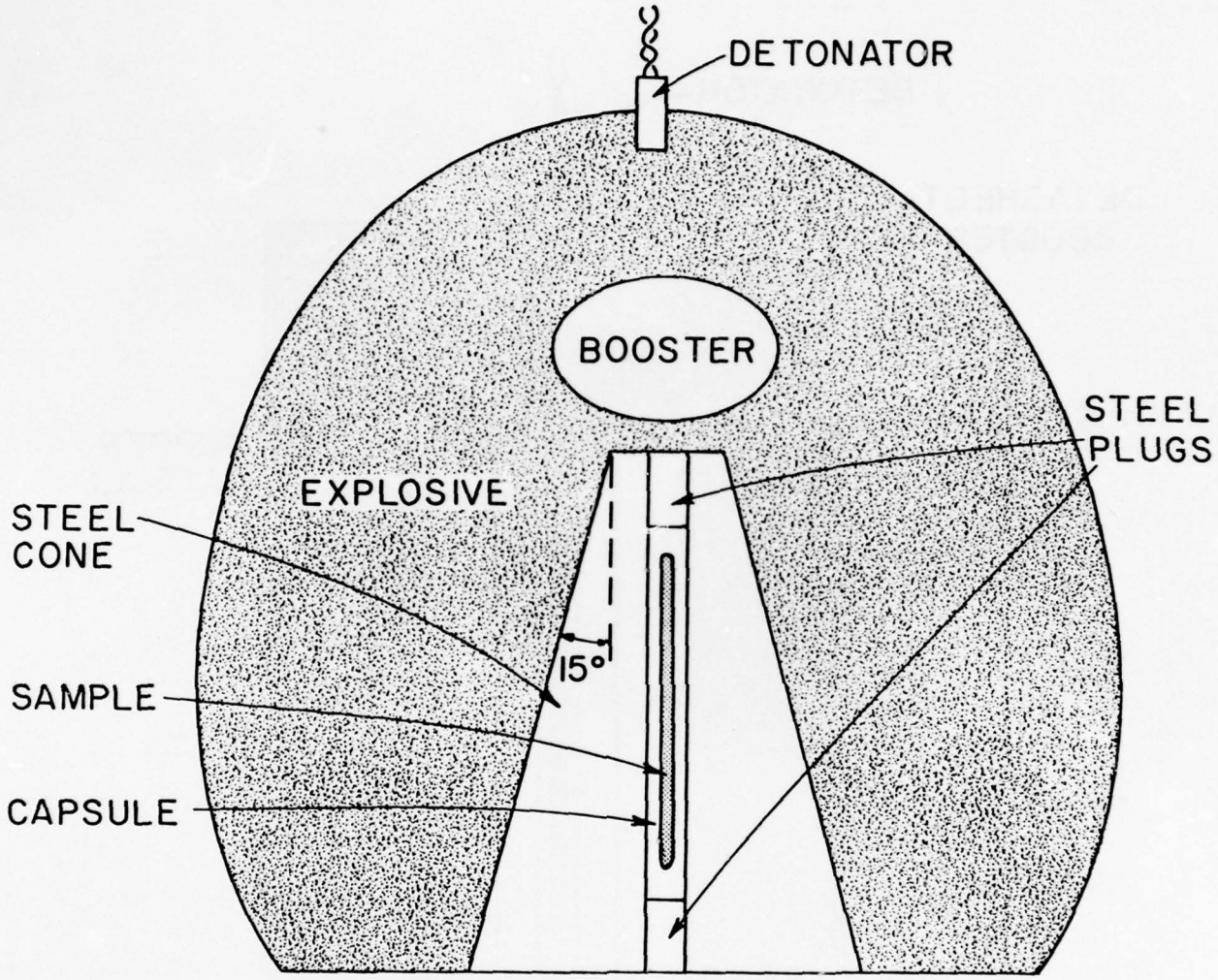

FIGURE 1. SCHEMATIC DIAGRAM OF PAN'S ARRANGEMENT FOR EXPLOSIVE COMPACTION.

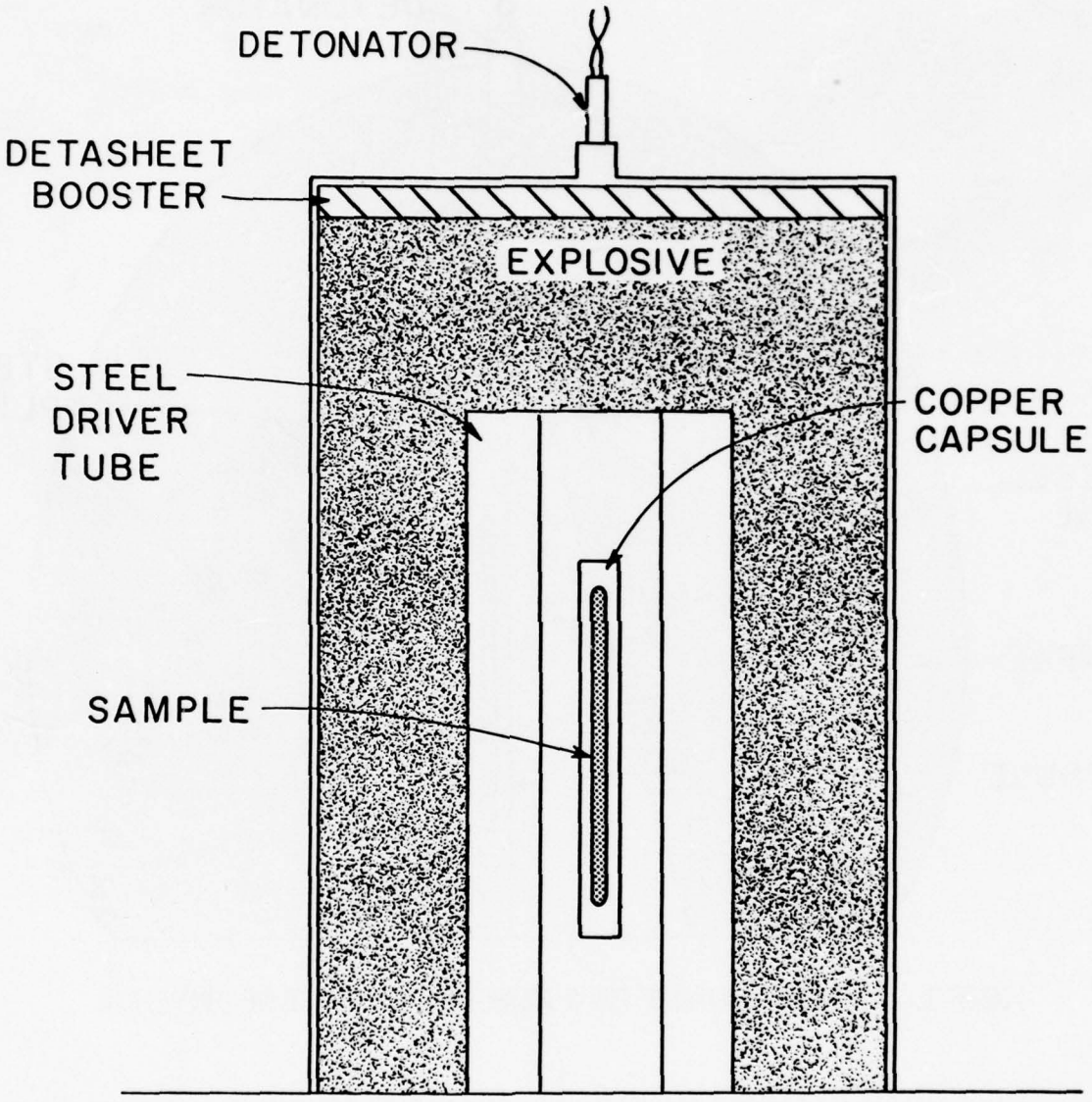

FIGURE 2. SCHEMATIC DIAGRAM OF LINSE'S ARRANGEMENT FOR EXPLOSIVE COMPACTION.

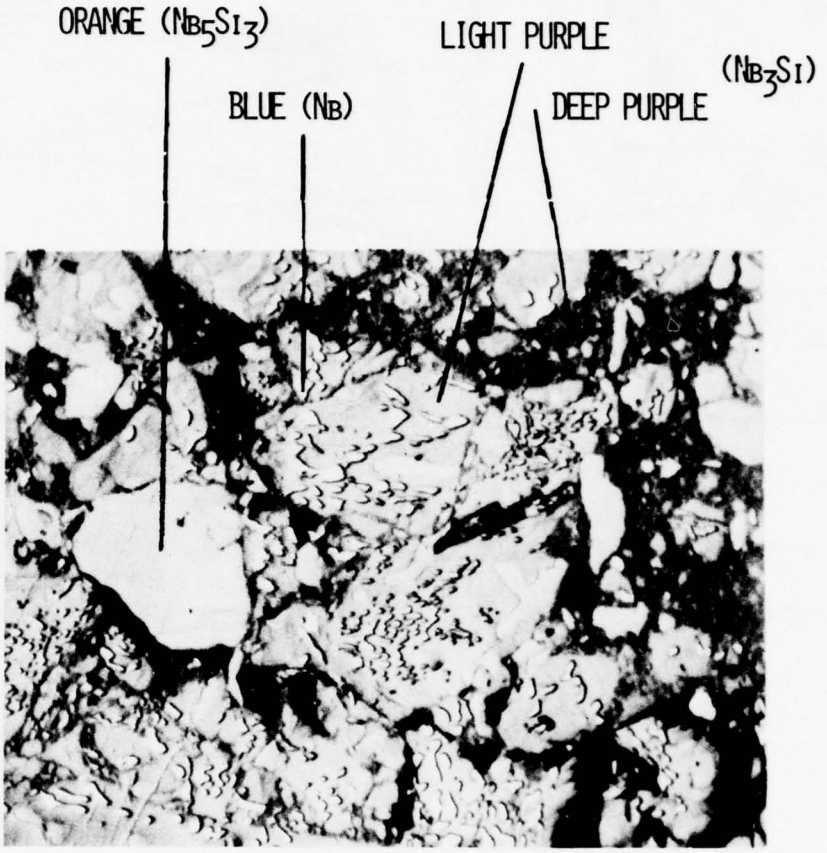

FIGURE 3. OPTICAL MICROGRAPH OF Nb_3Si FLAKES, AFTER ANODIZING IN CITRIC ACID (x500).

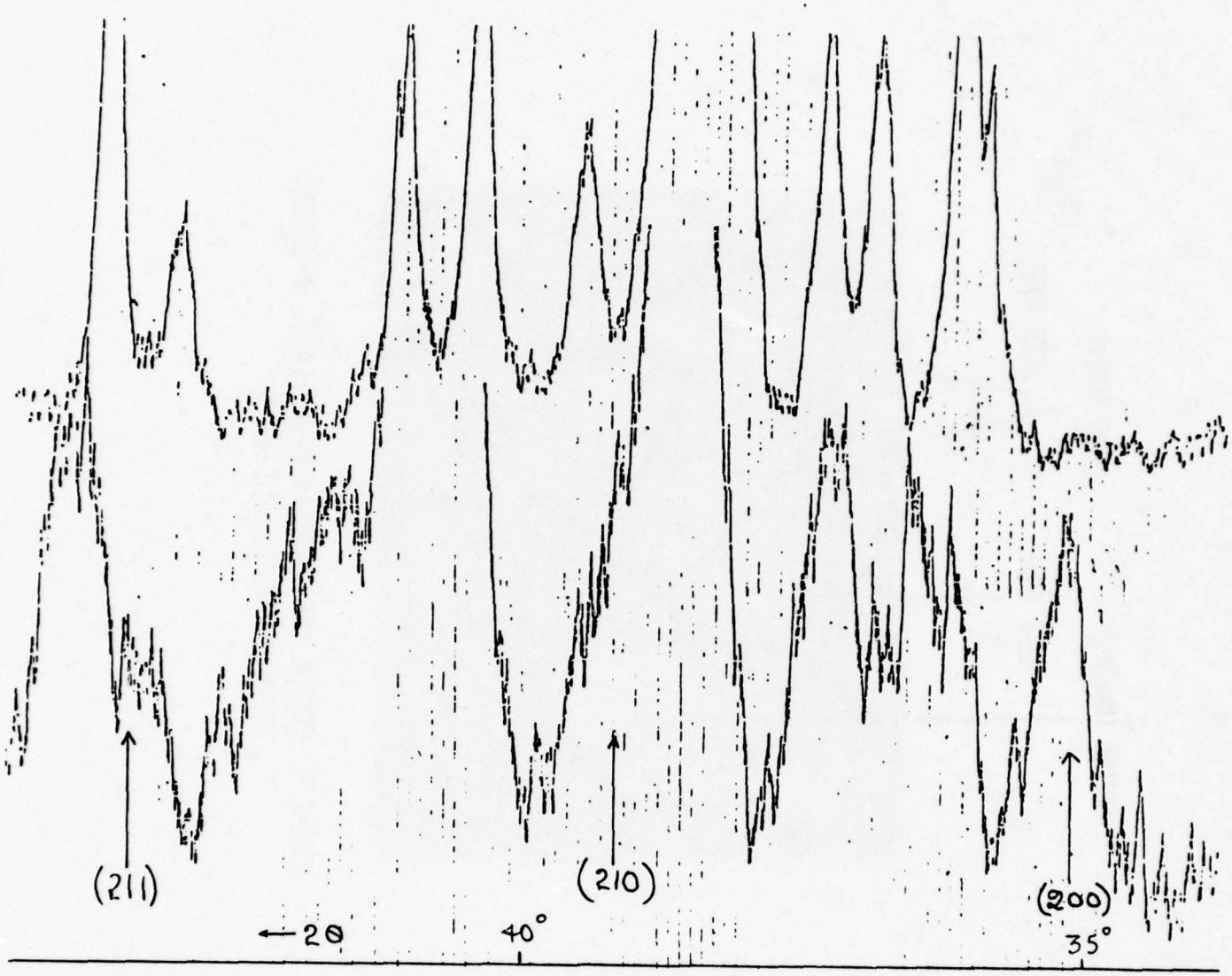

FIGURE 4. PORTION OF X-RAY DIFFRACTOMETER TRACES FROM Nb_3Si + Nb_5Si_3 + Nb POWDER (TOP) AND Nb_3Si POWDER AFTER EXPLOSION (BOTTOM). CuKα RADIATION.

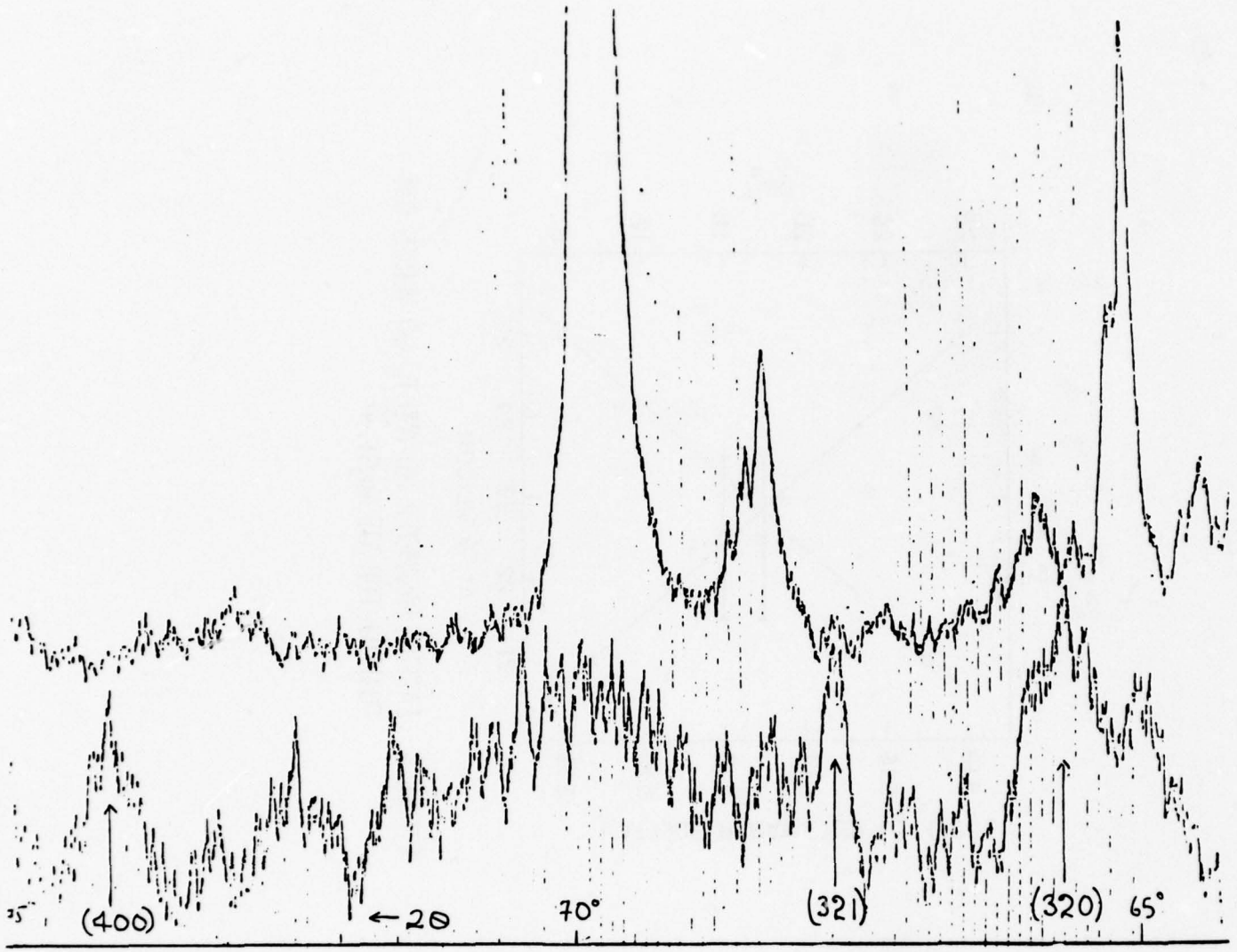

FIGURE 5. HIGHER ANGLE PORTION OF DIFFRACTOMETER TRACES OF FIGURE 4.

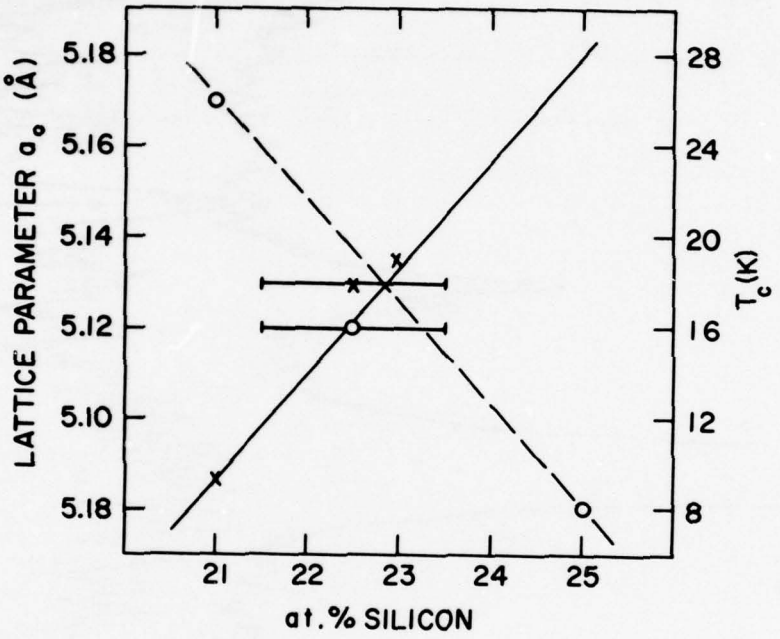

FIGURE 6. LATTICE PARAMETER (O) AND T_c (X) VERSUS COMPOSITION FOR A15 Nb_3Si.[16]

THE SYNTHESIS OF UNSTABLE A-15 COMPOUNDS BY EPITAXIAL RECRYSTALLIZATION OF ION IMPLANTED LAYERS

R. Rose

The formation of A-15 diffusion layers from solid phases or vapor appears to be characterized in many cases by orientation relationships between the A-15 layer and the bcc substrate (1,2). Figure 1 (from Reference 1) shows the correspondence (or coincidence sites) implied by the orientation relationship in the V(Ga)-V_3Ga diffusion couple. For Nb_3Sn layers grown on Nb single crystals in Sn vapor, the relationship is different, but more striking (2). There is also evidence indicating the possibility of A-15 to A-15 epitaxy: Dayem et al. (3) find that the range of stability and Tc of A-15 Nb_3Ge is enhanced when the material is made by coevaporation on an Nb_3Ir substrate. The latter was chosen on the basis of lattice parameter matching.

Because of the many structural similarities between the A-15 and competing Ti_3P structure (and also other Nb-Si phases of the sigma family), a selective method of enhancing the stability of the A-15 relative to the other phases appeared necessary. Epitaxy offers such a possibility, and epitaxial growth of a heavily ion-implanted layer presented other possible advantages as well. For semiconductor systems at least, the epitaxy is strong; reordering of the disordered implanted layer is known to occur at the interface between the implanted layer and the substrate; and reordering occurs at temperatures so low that solute redistribution probably does not occur (3,4) on any scale above a few interatomic distances.

Our substrate was $Nb_3Al_{0.9}Si_{0.1}$. The lattice parameter of this material as a well-ordered A-15 phase is 5.174 Å, which is with 2% of the predicted (Geller) lattice parameter for Nb_3Si, ca. 5.09 Å.

Typical composition profiles for ion implantation are shown in Figure 2. The profiles are approximately gaussian; both the mean depth and the distribution width depend on incident kinetic energy as well as the masses of the species involved. (Of course, channeling will have dramatic effects on the penetration.) In principle, almost any kind of dopant profile may be obtained by appropriate superimposition of various implantation conditions. We chose, as our intial goal, a gradual rather than sharp compositional change. In particular, the aluminum can be depleted at a carefully prepared surface by annealing in vacuum. The resulting diffusion profile is

$$C(x,t) = Co\ \mathrm{erf}\left[\frac{x}{2\sqrt{Dt}}\right].$$

For instance, 1-1/2 hours at 1050°C produces a depleted region ca. 2000 Å deep. Since the gaussian is the integrand of the error function, the evaporated aluminum can be (in principle) precisely replaced by appropriately sweeping the incident kinetic energy during implantation.

As Figure 3 shows, using only the three energies should replenish the deficiency, with the exception of the outer 400 (ca.) Å. The actual results shown in Figure 4 are somewhat better, probably due to sputtering off of the surface during implantation. The composition as a function of depth was determined by ion microprobe, with a depth resolution ca. 10 Å.

The structure of the specimens was determined by reflection electron diffraction, because the implanted layer was too thin for X-ray diffraction and too thick for LEED or similar techniques. (The RED method typically samples 50-100 Å deep.) The disadvantage of RED is that lattice parameters cannot be determined with precision. A special hot stage was designed for the RED apparatus so that heat treatments up to 1000°C could be done directly in the chamber of the RED apparatus without removing the specimen. Using this method, it was found that proper surface preparation of the substrate resulted in fine continuous diffraction rings corresponding to the A-15 structure; depletion of Al from the surface collapsed the A-15 into bcc structure; implantation disordered the bcc (the rings became diffuse), but did not create an amorphous layer; annealing at temperatures from 800°C to 980°C (upper limit of temperature capability) recrystallized the bcc layer into an A-15 structure. Table I summarizes the results of the structural investigations.

Transition temperatures were measured by a transverse four-point probe technique. Typical data are shown in Figure 5. Table II presents the results to date of such measurements. Several of these results are of interest.

1. The extremely high implanted dose undoubtedly caused a very high defect density but apparently there was little enhancement of diffusion.

2. There was no large redistribution of Si due to the annealing; apparently the Si distribution is controllable.

3. The A-15 structure collapsed into a bcc structure when depleted of Al, and this structure remained crystalline during implantation, in contrast to the behavior of semiconductors. (Not unexpected!)

4. The implanted layer remained A-15 at temperatures up to (and possibly beyond) 980°C.

5. The Tc of the implanted layer was low and insensitive to annealing temperature. This can be due to (among other things) poor stoichiometry, persistent epitaxial defects, or intrinsic properties of the compound itself.

REFERENCES

1. K. Togano, K. Tachikawa and R. M. Rose, to appear in J. Appl. Phys.

2. V. Diadiuk, J. L. Bostock and M.L.A. MacVicar, to be published.

3. L. Csepregi et al., Appl. Phys. Lett. 29, 92 (1976).

4. J. W. Mayer et al., Can. K. Phys. 46, 663 (1968).

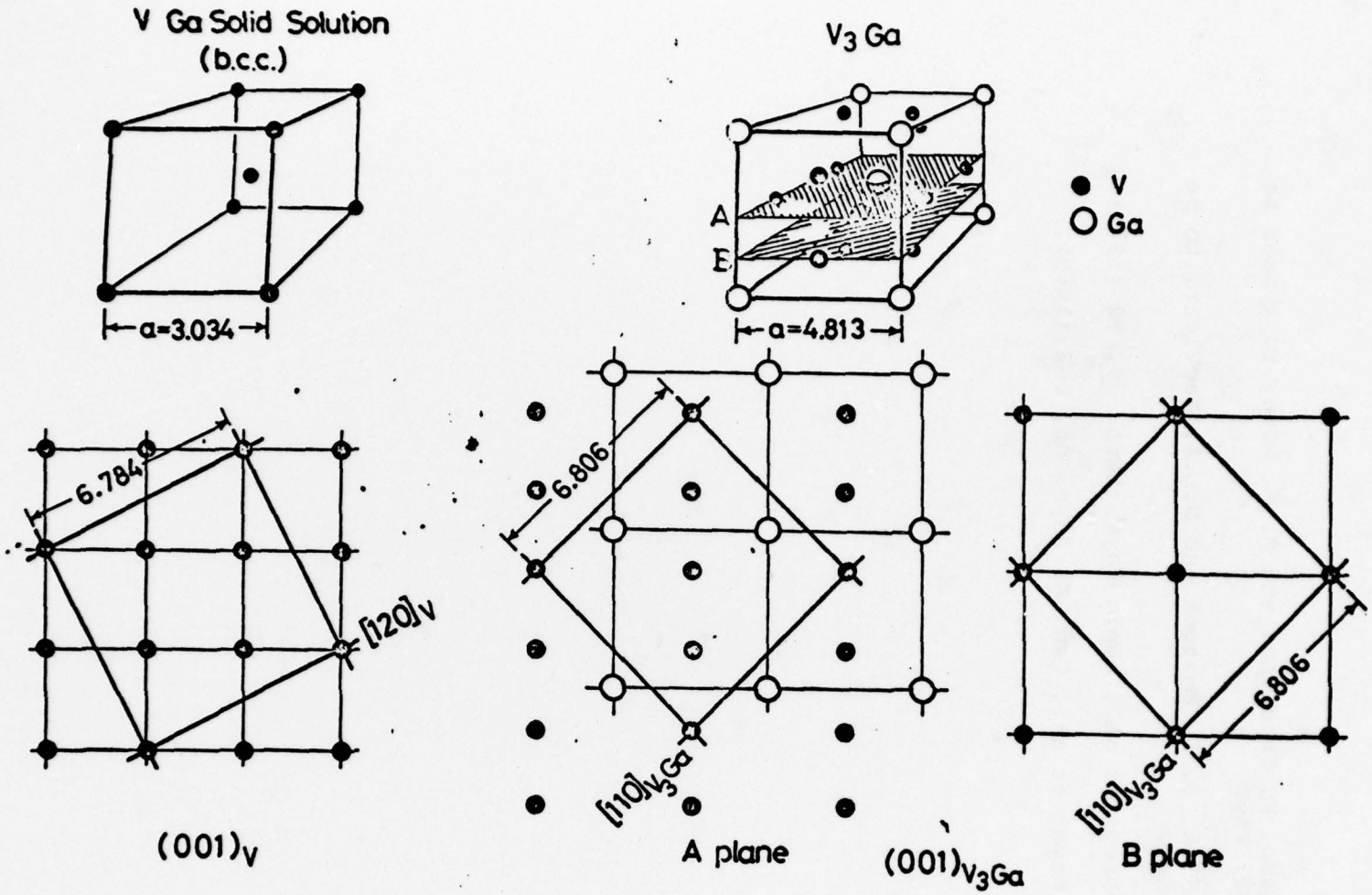

Figure 1. A model for crystallographic registry across an A15-bcc interface. (Togano, Tachikawa and Rose, to be published.)

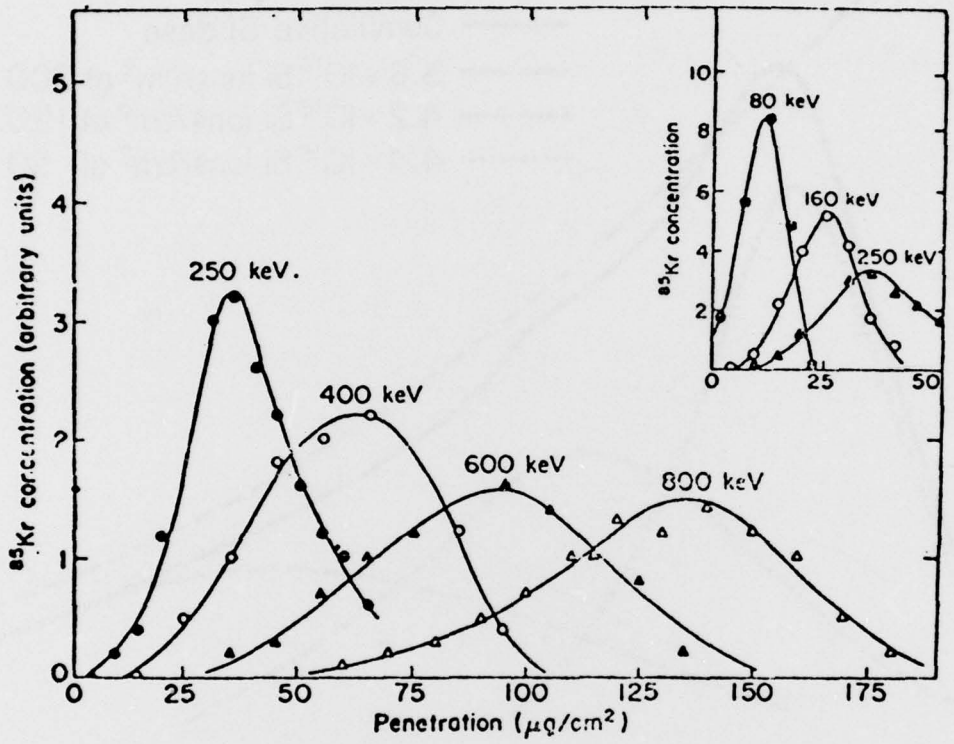

Differential range distributions for ^{85}Kr in amorphous Al_2O_3. (From Jespersgard and Davies.[24]) In Al_2O_3, 1 $\mu g/cm^2$ is equivalent to approximately 30 Å.

Figure 2. Typical ion dopant profiles. (Jespersgard and Davies, in "Ion Implantation in Semiconductors" (Academic Press, 1976) edited by J. W. Mayer and L. Eriksson.)

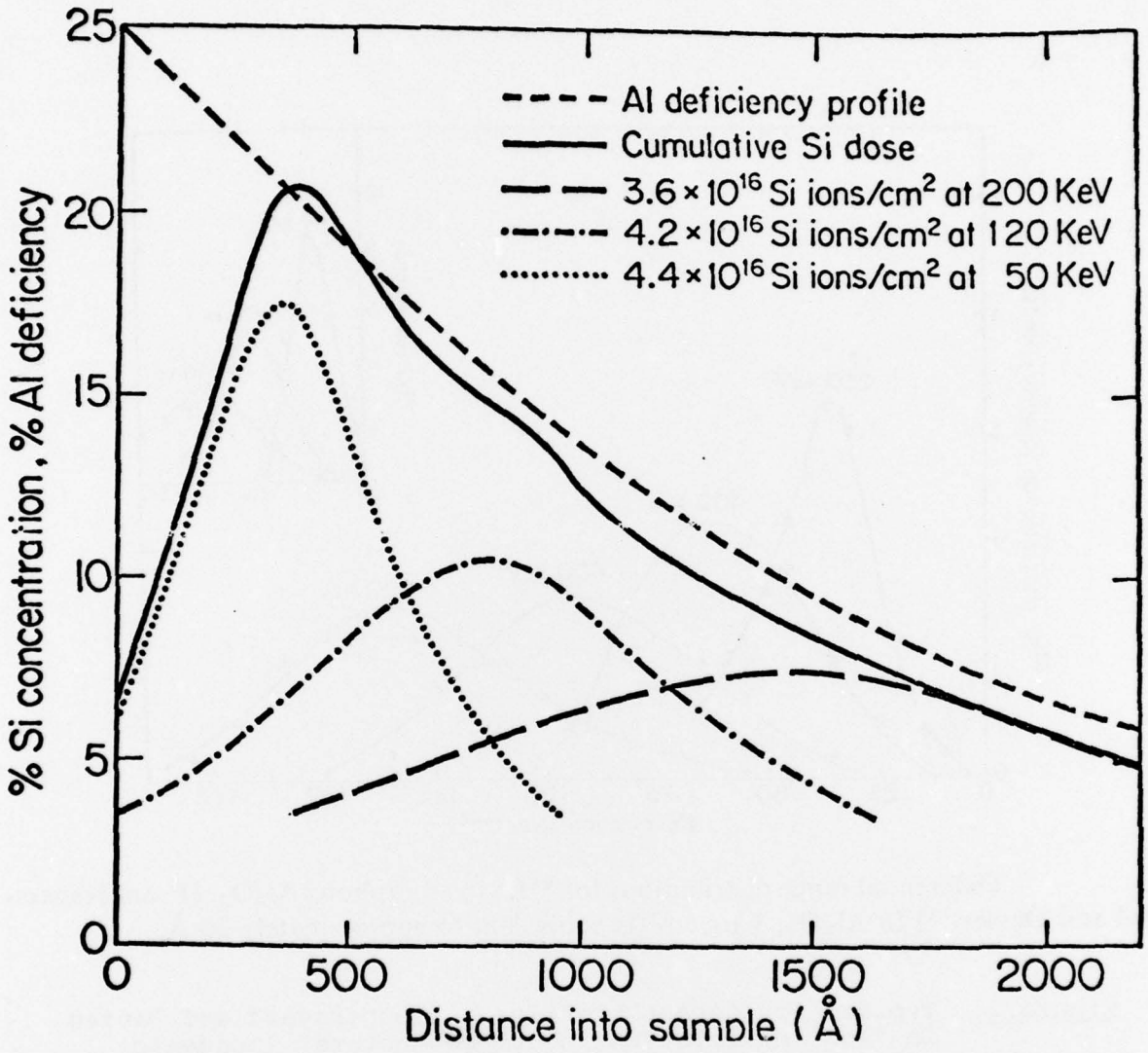

Figure 3. Theoretical Si dopant profile and Al deficiency profile.

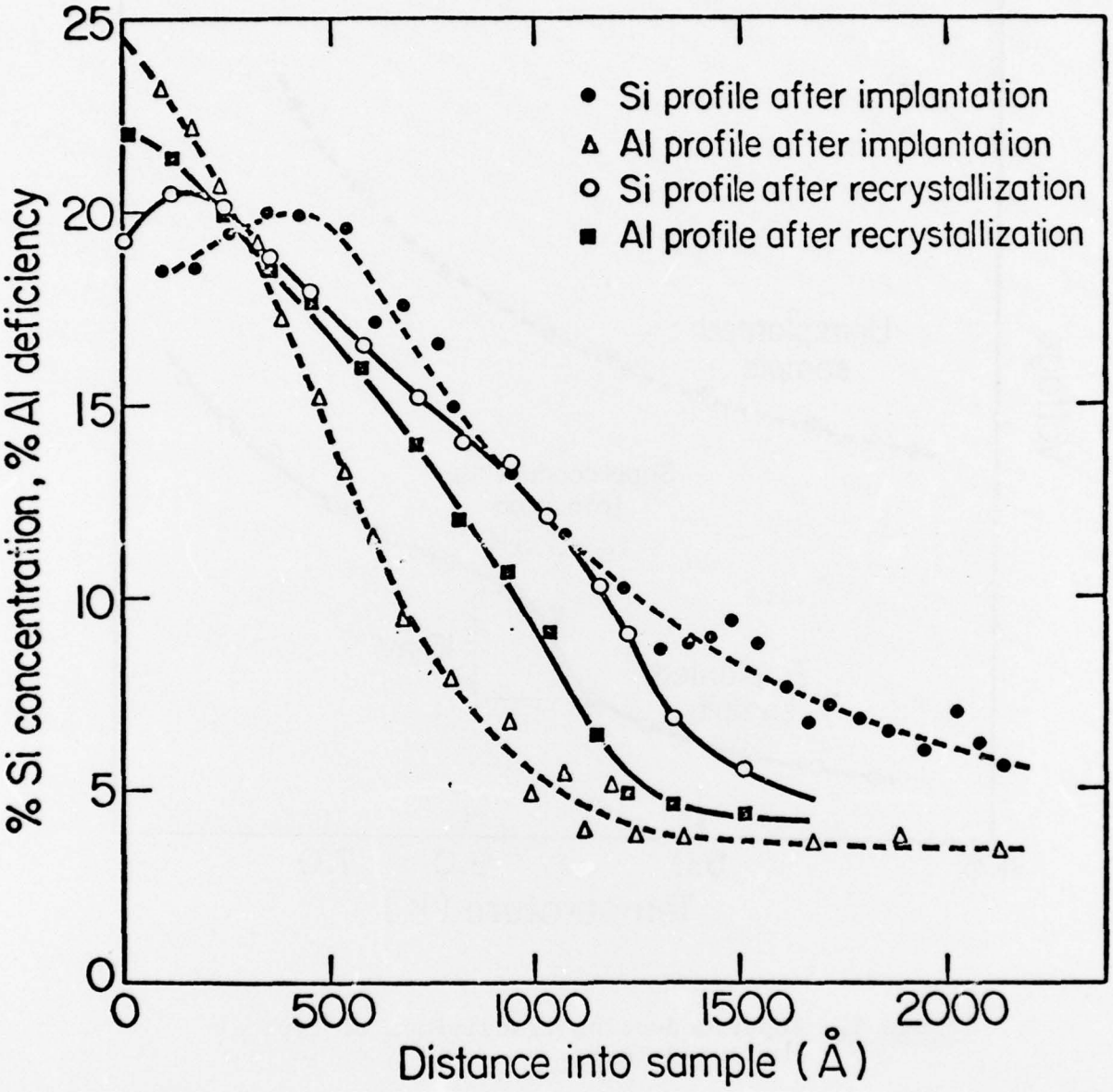

Figure 4. Ion microprobe analysis of Si and Al (deficiency) after implantation and recrystallization.

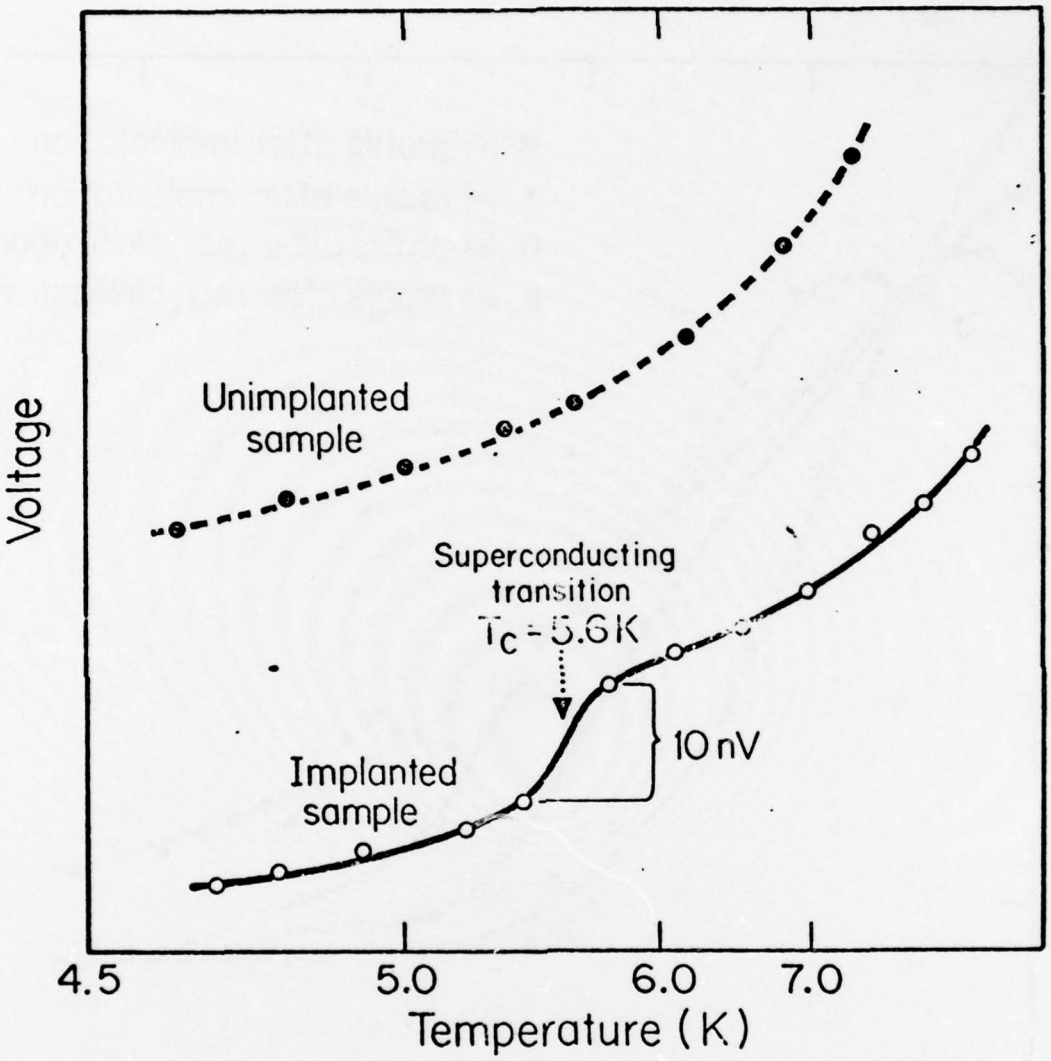

Figure 5. Superconducting transitions of typical implanted layer.

TABLE I

Surface Structures of Implanted Layers

Heat Treatment	Structure
(in dynamic vacuum furnace)	(from RED photos taken at room temperature)
at room temperature	Nb. bcc - diffuse rings
+ 1 hour at 650°C	Nb. bcc - diffuse rings
+ 1 hour at 700°C	Nb. bcc - diffuse rings
+ 1 hour at 750°C	Nb. bcc - diffuse rings
+ 1 hour at 800°C	A-15 - diffuse rings
+ 1 hour at 850°C	A-15 - sharp rings
+ 1 hour at 900°C	A-15 - sharp rings
(in electron microscope)	(from RED photos taken at temperature)
at room temperature	Nb. bcc - diffuse rings
+ 5 mins at 360°C	Nb. bcc - diffuse rings
+ 5 mins at 550°C	Nb. bcc - diffuse rings
+ 10 mins at 750°C	Nb. bcc - sharper rings
+ 5 mins at 850°C	A-15 - difuse rings
+ 10 mins at 930°C	A-15 - diffuse rings
+ 15 mins at 980°C	A-15 - sharp rings
room temperature	A-15 - sharp rings

TABLE II

Implantation of Si ions into $Nb_3Al_{0.9}Si_{0.1}$ substrates having a surface layer depleted of Al. Transition temperatures as a function of diffusion anneals, recrystallization anneals and ordering anneals.

All samples subjectd to the following sequential Si doses:
3.6×10^{16} ions/cm^2 at 200 KeV; 4.2×10^{16} ions/cm^2 at 120 KeV;
4.4×10^{16} ions/cm^2 at 50 KeV.

Sample No.	Length of Diffusion Anneal (hours)	Recrystallization Anneal Temp. C	Recrystallization Time hours	Ordering Anneal Temp. C	Ordering Anneal Time hours	Transition Temperature of Implanted Layer K
1	1-1/2	R.T.				<4.5
		850	1			5.6
				+575	100	5.4
				+675	100	5.5
2	1-1/2	R.T.				
		900	1			
				+500	106	
				+610	120	
				+675	64	5.4
3	1-1/2	R.T.				<4.3
		900	1			5.1
				+500	100	5.0
				+575	100	5.1
				+675	100	5.1
				+725	50	5.0
4	1-1/2	R.T.				
		980	1/4			
				+500	106	
				+610	120	
				+675	64	5.2
5	2-1/2	R.T.				<4.5
		900	1			5.0
				+575	100	5.1
				+675	100	5.0

The Sputtering of Nb_3Si

R.E. Somekh, Dept. of Metallurgy and Materials Science, Pembroke St., Cambridge, U.K.

The aim of this contribution is to discuss DC sputtering as a technique for preparing the 'metastable' high T_c A15 superconductors. Our recent work on the preparation of Nb_3Si is discussed in the context of a parallel study of the formation of high T_c Nb_3Ge. A wide variety of sputtering techniques[1,2,3] have been reported by different workers. The variability of the performance of the different systems reflects the difficulties associated with the technique and the many system dependent parameters that play a role in the attainment of high T_c's. The most significant of these parameters appear to be composition, deposition temperature, the sputtering pressure voltage and current, cleanliness of the vacuum system and background impurities. The latter two are important due to inherent slowness of the film growth. In principle the faster technique of RF sputtering should be better than the DC technique on these grounds though in practice RF sputtering suffers from the rather energetic particles produced which apparently damage the films as they grow[4]. The two more commercially viable techniques of co-evaporation[5] and chemical vapour deposition (CVD) have in the past never quite attained the high T_c values for Nb_3Ge that are found with sputtering; though recent CVD work[7] shows that this is probably again a question of controlling the many specific growth parameters associated with these techniques.

In our work we have placed emphasis on three main areas: cleanliness and a high degree of control of the impurity background pressures[8]; isolation of specific variables such as composition and deposition temperature, and finally detection of factors which have been hitherto disregarded such as orientation and texture of the films[8] and convection effects in the sputtering gas[9]. This work has led to a general understanding of the formation conditions for high T_c Nb_3Ge in a DC sputtering system.

Two DC getter sputtering systems have been used and are described elsewhere[10]. (See Fig. 1). The dirtier of the two systems has a background pressure of around 10^{-8} torr and its inner nitrogen-cooled can is not isolated from the outer vacuum whereas the clean system, capable of 10^{-10} torr (with the heater strip at $\sim 1000^{o}C$), has an inner chamber which can be completely isolated. Our earlier work used a DC voltage of around 550V and a sputtering pressure of $\sim$ 300 mtorr whilst our more recent and more promising results have been achieved with a voltage of $\sim$ 200V and pressure $\sim$ 750 mtorr. The high degree of cleanliness has allowed us to control the level of background impurities which though relatively easy in a co-evaporation system is more difficult to attain in sputtering systems in which little active pumping occurs during sputtering and one relies on the passive gettering of reactive species.

We have been able to produce high T_c Nb_3Ge in our MkI system, the best sample had a 0.1% onset of 23.5K & 1% onset of 23.2K, though several samples have shown an onset of over 23K. These optimised samples show very small amounts of other phases ($\lesssim 2\%$). The important preparation parameters are the deposition temperature T_D of $\sim 800^{o}C$ and also high sputtering pressure. Also they have all been made with $\sim$ 40 ppm of O_2 added to the sputtering gas which we estimate gives about 4 ppm O_2 in the inner can. At present the exact role of oxygen is still not fully understood[11], though this level compares well with other workers using co-evaporation[5,12] except in our case the rate of deposition is considerably lower. Other features of these high T_c samples which we believe to be relevant, are the pronounced variably orientated textures found in the films and the occurrence of the hexagonal form of Nb_5Ge_3 as the main competing phase[8]. It has been observed

that textures orientated away from (200) and towards (211) seem in some way to be correlated with higher T_c's. At this stage we are not certain of the exact origin of these observations, the interaction of the T_D and observed convection effects are considered to be important.

Alongside these improvements of T_c in the Nb_3Ge system we have seen similar increases in T_c onsets in Nb_3Si (1% onset up to 17.6K). Though we have some reservations about the high T_c's of the Nb_3Si films mentioned below, we consider the similarities found between the two systems give credence to the idea that the high T_c originates from the A15 Nb_3Si.

The main similarity overall is that the same sputtering conditions of high sputtering pressure and target-substrate geometry are required for both Nb_3Ge and Nb_3Si to produce the highest T_c's and, in the case of Nb_3Si, to produce significant amounts of the A15 phase. The deposition temperatures for Nb_3Si are in the range 880°C - 920°C slightly higher than that for Nb_3Ge as one would expect from a general comparison between the germanides and silicides in the A15 series. The X-ray traces for Nb_3Si show a strong set of A15 lines (Fig. 2) and for the best samples less than 5% of a competing phase. The lattice parameters obtained are of about 5.18 - 5.19Å much expanded over that expected from the Geller radii (5.1 Å), but reasonable when it was found from some Rutherford backscattering data[13] that the composition of the films was off-stoichiometry and in the region of 15 - 20 at% Si. The X-ray traces also show a similarly orientated texture, away from (200) and towards(211) especially in the best material, which suggests a similar optimisation process found in Nb_3Ge. We also have evidence for the effects of convection in the sputtering gas and the growth morphology as indicated by surface markings playing the same role in giving the highest T_c's for both Nb_3Ge and Nb_3Si.

One major difference in the formation of Nb_3Si has been that no impurities have been added to the sputtering gas and the inner can has been completely isolated. Whether or not any trace impurities are in the structure, stabilising it to some extent is uncertain at present.

In a DC resistance measurement of a transition there is always a problem of identifying what and how much of the film is superconductive. Rutherford backscattering data[13] indicates that there is an apparent reaction layer between the film and substrate, we thought this could be producing superconducting Nb_3Al. We believe the above comparison with Nb_3Ge rules out this possibility, the most important factor being that the more of the A15 phase there is the higher the transition temperature. The possible explanation for the 'reaction' layer observed in the Rutherford backscattering data lies in the roughness of the surface. A further substantial indication that it is the A15 phase that is producing the high T_c in Nb_3Si is that any heat treatment at around or above T_D has the effect of reducing T_c and if such heat treatments are prolonged the A15 phase completely disappears and the samples cease to be superconducting. Possibly the best direct evidence for superconductivity in the film only and none in a 'reaction' layer is from an ion beam milling experiment, in which a 3000Å "Nb_3Si" film (T_c midpoint 15.9K) was progressively thinned. Over all regions of the film the T_c midpoint was seen to drop to below 4K after the removal of 70% of the film. However until we have raised the T_c above 19K or prepared the A15 Nb_3Si on a different substrate this problem will not be completely resolved.

However there is an overriding problem arising from the lattice parameter a_o with its large observed value. There are at least three possibilities to account for this. (a) There is a small proportion of material with a small lattice parameter occurring on a small scale within the microstructure, which we know from EM measurements is only just crystalline with some regions of amorphous phase present. (b) The A15 phase "Nb_3Si" is in some way impurity stabilised with an expanded lattice. (c) That with this very metastable A15 phase there is a tendency for a_o to be variable due to defects of one sort or another. There is some evidence for this from Nb_3Ge in that a large range of a_o has been reported in the literature for a given T_c onset e.g. for a T_c onset of 18°K. There is a range of .05Å (0.07Å if data for hydrogen inclusion is taken into account[14]). This sort of variability easily accounts for the differences that are found between our a_o, Dew Hughes' data[15] and some of the early work using different preparation units[16,17] and suggests other factors are important other than just forming an A15 phase in attaining a high T_c, (c.f. recent CVD work[18]).

We conclude that "Nb_3Si" shows great potential and believe that 'near to stoichiometric' "Nb_3Si" may be formed with a suitable addition of an impurity as in the case of Nb_3Ge. We speculate that further avenues of research be in the realm of the lighter element A15's e.g. Nb_3C and V_3C though the stability difficulties with these materials are likely to be even worse than those found with Nb_3Si and Nb_3Ge, again the hope is that a suitable impurity may be found to stabilise the A15 phase in such a way that a high T_c is achieved.

References

1. Gavaler,J.R., Janocko,M.A., and Jones C.K., J.A.P. 45, 3009, 1974.

2. Testardi,L.R., Meek,R.L., Poate,J.M., Royer,W.A., Storm,A.R., and Wernick,J.H., Phys. Rev. B, 11, 4304, 1975.

3. Kammerdiner,L., Wu,C.T., and Luo,H.L., J. Low Temp. Phys. 24, 111, 1976.

4. Cadieu,F.J., and Chencinski,N., I.E.E.E. Trans. Magn. Mag., 11, 227, 1975.

5. Hammond, R.H., Hallak,A.B., Geballe,T.H., and Zubeck,T., I.E.E.E. Trans. Magn. Mag. 13, 311, 1977.

6. Engelhardt,J.J., and Webb, G.W., Sol. Stat. Comm., 18, 837, 1976.

7. Paidassi,S., Spitz.J., and Besson,J., Appl. Phys. Lett. 33, 105, 1978.

8. Somekh, R.E., LT15, J de Physique 39 Suppl. 8 C6 - 398, 1978.

9. Evetts, J.E., and Somekh,R.E., Applied Superconductivity (Pittsburgh) 1978 to be published.

10. Somekh, R.E., Phil. Mag. B, 37, 713, 1978.

11. Gavaler,J.R., Ashkin,M., Braginski,A.I., and Santhanam A.T., LT15, Je de Physique, 39, Suppl.8, C6 - 400, 1978.

12. Sigsbee,R.E., I.E.E.E. Trans. Magn. Mag. 13, 307, 1977.

13. Testardi,L.R., (Private Communication).

14. Lanford,W.A., Schmidt,P.H. Rowell,J.M., Poate,J.M., Dynes,R.C., and Dernier,P.D. Appl. Phys. Lett. 32, 339, 1978.

15. Dew-Hughes,D., and Linse,V.D., to be published.

16. Johnson,G.R., and Douglass,D.H., J. Low Temp. Phys. 14, 575, 1974.

17. Hammond, R.H., and Harza,S., LT13 (Plenum, New York 1963).

18. Paidassi,S., and Spitz.J., J. of Less. Comm. Metals 1978, to be published.

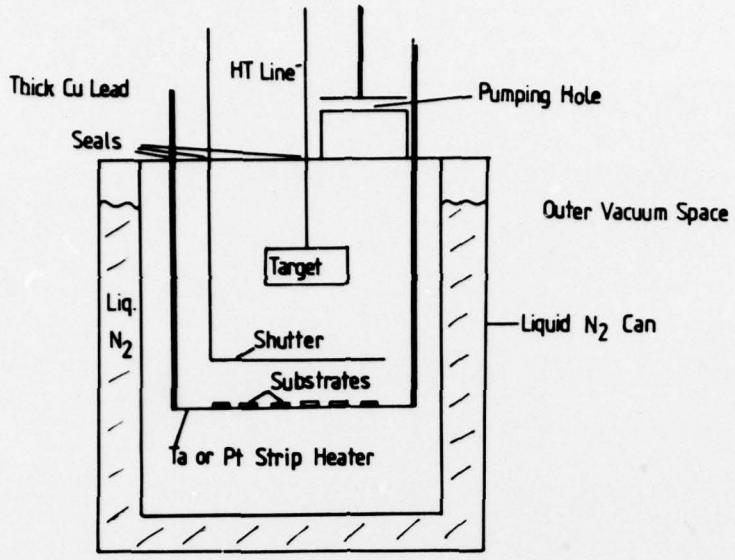

Fig.1. Schematic diagram of getter sputtering chamber.

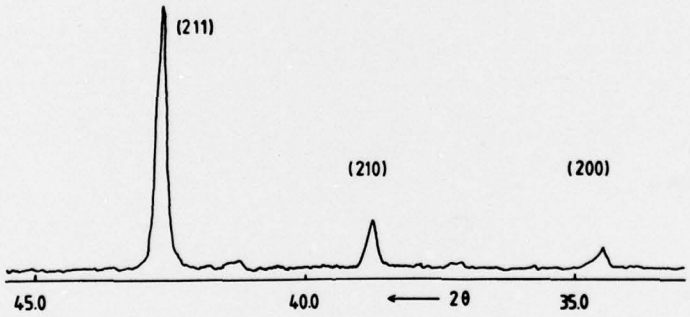

Fig.2. X-ray trace of low angle lines of A15 "Nb Si" ($Cu_{K\alpha}$ radiation).